Table 5: Areas and volumetric analysis per stent (excluding overlapping segments) at 13 months follow-up

58 patients **72 lesions** **107 stents**	ZES 30 patients 36 lesions 50 stents	EES 28 patients 36 lesions 57 stents	**p-value**
Stent length (mm)	18.7 (9.3)	18.6 (8.6)	0.959
MLA (mm^2)	5.45 (2.39)	5.35 (2.45)	0.845
Mean lumen Area (mm^2)	6.89 (2.52)	6.68 (2.75)	0.681
Lumen volume (mm^3)	130.1 (80.4)	123.2 (73.0)	0.641
Min stent area (mm^2)	6.37 (2.41)	6.47 (2.42)	0.831
Mean stent area (mm^2)	7.70 (2.38)	7.64 (2.59)	0.902
Stent volume (mm^3)	145.2 (85.1)	140.8 (77.2)	0.777
% frames with ISA	5.10 (9.84)	3.18 (7.00)	0.255
Max ISA area (mm^2)	0.39 (0.76)	0.49 (1.56)	0.666
ISA volume (mm^3)	0.79 (1.80)	1.08 (3.90)	0.615
ISA volume (% of stent volume)	0.58 (1.39)	0.66 (2.27)	0.835
Max NIH area (mm^2)	1.73 (0.82)	1.88 (0.87)	0.367
NIH volume (mm^3)	15.9 (11.6)	18.7 (14.4)	0.274
NIH volume obstruction (%)	12.5 (7.9)	15.0 (10.7)	0.157

Data presented as mean(SD).

EES: everolimus-eluting stent; ISA: Incomplete stent apposition; MLA: Minimal lumen area; NIH : Neointimal hyperplasia; ZES: Zotarolimus-eluting stent.

There were no significant differences in the proportion of non-covered struts or in the mean thickness of coverage between the treatment groups in multilevel analysis. Introducing the variables with imbalanced distribution (serum creatinine, ejection fraction,) in the regression model as covariates, did not translate into any significant variation in the differences of coverage.

Figure 4 shows the spread-out-vessel graphics of the 109 stents and corresponding overlaps.

DISCUSSION

The main finding of this study is that OCT did not detect any significant difference between ZES and EES in tissue coverage at 13 months. Both DES have durable polymers, but with different properties. The BioLinx polymer on ZES is an amphiphilic blend of 3 different polymers, with a hydrophilic surface in contact with the blood or the vessel wall. Conversely, the poly(vinylidene fluoride-co-hexafluoropropylene) on EES, offers a hydrophobic fluorinated surface, that might induce fluoropassivation. Hydrophilicity (ZES) and fluoropassivation (EES) improve both the biocompatibility of the corresponding intracoronary device, as previously

Table 6: Areas and volumetric analysis of overlapping segments at 13 months follow-up.

19 patients **21 lesions** **28 overlaps**	ZES 8 patients 9 lesions 11 overlaps	EES 11 patients 12 lesions 17 overlaps	**p-value**
Overlap length (mm)	2.4 (2.4)	2.1 (2.7)	0.771
MLA (mm^2)	5.37 (2.09)	6.67 (2.89)	0.208
Mean lumen Area (mm^2)	5.61 (2.14)	6.93 (2.97)	0.213
Lumen volume (mm^3)	14.1 (16.2)	16.1 (22.8)	0.805
Min stent area (mm^2)	6.15 (1.70)	7.89 (3.02)	0.095
Mean stent area (mm^2)	6.50 (1.68)	8.20 (3.00)	0.100
Stent volume (mm^3)	15.7 (17.3)	18.5 (26.2)	0.760
% frames with ISA	3.03 (10.05)	2.94 (12.13)	0.984
Max ISA area (mm^2)	0.02 (0.08)	0.02 (0.07)	0.821
ISA volume (mm^3)	0.01 (0.04)	0.01 (0.04)	0.892
ISA volume (% of stent volume)	0.10 (0.34)	0.24 (0.99)	0.601
Max NIH area (mm^2)	1.16 (0.56)	1.50 (0.94)	0.297
NIH volume (mm^3)	1.7 (1.5)	2.5 (3.6)	0.433
NIH volume obstruction (%)	16.0 (12.3)	17.0 (11.8)	0.835

Data presented as mean(SD).

EES: everolimus-eluting stent; ISA: Incomplete stent apposition; MLA: Minimal lumen area; NIH : Neointimal hyperplasia; ZES: Zotarolimus-eluting stent.

discussed. No significant differences were found in mean thickness of coverage, although it tended to be thinner in ZES. Likewise, there were no significant differences regarding the proportion of covered struts, a possible surrogate for completeness of neointimal coverage. In view of these results a hydrophilic polymer coating does not seem to translate into any clear advantage in terms of neointimal coverage with respect to a hydrophobic fluoropolymer coating. Beyond the hydrophilicity of the polymer surface, other factors like the different antiproliferative drugs (with different inhibitory potency and dose), the kinetics of release (more sustained release in ZES, prolonged up to 180 days), mechanical characteristics of the stent platform and the polymer itself, play certainly a role in determining the neointimal coverage after stenting. Interestingly, the proportion of uncovered struts in ZES in our study is higher than in previous OCT studies on another zotarolimus-eluting stent with a phosphorylcholine polymer and different kinetics of release[18,35]. This could be the consequence of the sustained drug-elution, although the absolute proportions in these studies cannot be directly compared due to small methodological differences in the asssessment.

Since no significant differences in ISA were found between the treatment groups, an eventual confounding effect of ISA on the coverage can be ruled out.

Because the number of patients in the OCT substudy was modest compared to the large numbers in the main trial, and a sizeable number of control variables were tested, some dif-

Table 7: Analysis of apposition and coverage per strut at 13 months follow-up.

All struts **58 patients** **72 lesions** **107 stents** **23197 struts**		ZES 30 patients 36 lesions 50 stents 11930 struts	EES 28 patients 36 lesions 57 stents 11267 struts		Estimate	95% CI Low	 Up	p-val
Apposition	**Apposition category**							
	Well-apposed	11624 (97.4%)	10989 (97.5%)	OR	0.96	0.52	1.76	0.898
	ISA	216 (1.8%)	161 (1.4%)	OR	1.27	0.56	2.91	0.569
	NASB	90 (0.8%)	117 (1.0%)	OR	0.72	0.41	1.29	0.271
Coverage	Thickness of coverage (μm)	116 (99)	142 (113)	Difference	-11.4	-42.4	19.65	0.466
	Coverage category							
	Covered	11043 (92.6%)	10613 (94.2%)	OR	0.77	0.43	1.38	0.378
	Uncovered	887 (7.4%)	654 (5.8%)	OR	1.30	0.72	2.33	
Overlapping segments **19 patients** **21 lesions** **28 overlaps** **1251 struts**		8 patients 9 lesions 11 overlaps 629 struts	11 patients 12 lesions 17 overlaps 622 struts					
Apposition	**Apposition category**							
	Well-apposed	626 (99.5%)	618 (99.4%)	OR	1.35	0.14	13.50	0.798
	ISA	3 (0.5%)	1 (0.2%)	OR	2.98	0.19	47.83	0.441
	NASB	0 (0.0%)	3 (0.5%)	OR	—	—	—	NA
Coverage	Thickness of coverage (μm)	129 (98)	171 (125)	Difference	-47.97	-159.37	63.44	0.376
	Coverage category							
	Covered	588 (93.5%)	600 (96.5%)	OR	0.53	0.24	1.16	0.111
	Uncovered	41 (6.5%)	22 (3.5%)	OR	1.89	0.86	4.17	

EES: everolimus-eluting stent; ISA: Incomplete stent apposition; NASB: Non-apposed side branch; ZES: Zotarolimus-eluting stent.

ferences appeared by chance between treatment groups in spite of randomization. In order to control potential confusion, an additional sensitivity analysis was performed, introducing the variables with imbalanced distribution as covariates in the multilevel regression models, but the results did not change with respect to the prespecified analysis.

The results about OCT coverage seem consistent with the clinical findings of the RESOLUTE All Comers trial[31], in which ZES proved to be non-inferior to EES for target-lesion failure. Furthermore, on the basis of this OCT substudy, differences in coverage cannot be advocated to explain the ambiguous clinical results regarding stent thrombosis. The correlation between OCT substudies and the clinical outcome of large prospective trials can contribute to understand the predictive value of OCT. In the LEADERS trial the OCT substudy detected an advantage in coverage in one of the stents at 9 months[16], but no differences in thrombosis rates have been reported hitherto[20]. Likewise, HORIZONS-AMI found worse coverage in DES than in BMS after primary PCI[36], but no significant difference in thrombosis[37]. In RESOLUTE-all comers

there was a non-significant trend to lower stent thrombosis in the EES group, although most of the events occurred in the first 30 days when neointimal healing is still unlikely to play a role[31]. The results of this OCT substudy could be interpreted as reassuring that factors other than differences in coverage are the key for these clinical results, but the potential of OCT coverage to predict future thrombotic events must be still properly understood.

The "spread-out-vessel" summary in Figure 5 may be the best possible graphic representation for the clustering and spatial distribution of non-coverage. It clearly shows, without the need of complex statistics, that the type of stent is not the only factor determining coverage: concentration of uncovered struts in some patients or in some stents within a patient or in some regions within a stent points out clearly the relevance of individual, mechanical and loco-regional factors, respectively. Among them, diabetes[38], levels of circulating endothelial progenitor cells[39] or regional shear-stress[40,41] are known to play a role in neointimal healing after stenting.

Limitations

The unequal distribution of some control variables in the randomization has been previously addressed.

Some caution should be advised about using OCT tissue coverage as surrogate of neointimal healing. Although biologically plausible and intuitively accepted by the scientific community, this approach cannot be fully supported by current evidence. OCT tissue coverage correlates with histological neointimal healing and endothelialization after stenting in animal models[12-14], but its sensitivity and specificity in human atherosclerotic vessels are still unknown. OCT is not able to detect thin layers of endothelium, below its 10-20 μm axial resolution, and cannot discern between neointima and other material, like fibrin or thrombus. The analysis of optical density might be useful in the future to discern between neointima and fibrin[15].

Per strut quantitative analysis was performed at 1mm longitudinal intervals. Although this methodology has been experimentally validated for the assessment of coverage[14] and showed excellent reproducibility[34], it might have different sensitivity to detect uncovered struts than shorter longitudinal intervals. The results from studies using different longitudinal segmentation might not be directly comparable.

Finally, the OCT substudy of RESOLUTE All Comers did not follow a non-inferiority design, as was done in the main trial. Therefore the conclusion cannot be the absence of significant differences between the compared stents, in spite of not having found them. The possibility of an underpowered design cannot be strictly ruled out, although the lack of any clear trend between the groups makes it very unlikely.

CONCLUSION

No significant differences in tissue coverage, malapposition or lumen/stent areas and volumes were detected by OCT between the hydrophilic-polymer coated ZES and the fluoropolymer-coated EES at 13 months follow-up.

ACKNOWLEDGEMENTS

Dick Goedhart (senior statistician), Peter Jüni (Institute of Social and Preventive Medicine, University of Bern, CH) and Gerritt-Anne van Es (Cardialysis BV, Rotterdam, NL) for their scientific advice.

FUNDING

Medtronic Inc., Santa Rosa, CA, USA

Conflict of interest: This study has been sponsored by Medtronic Inc., Santa Rosa, CA, USA. The core-lab and CRO responsible for the analysis (Cardialysis BV, Rotterdam) and the participating centres (except[5]) have received grants from the sponsor to run the trial. Serruys PW, Windecker S and Silber S have received speakers' fees from the sponsor.

REFERENCES

1. Garg S, Serruys PW. Coronary Stents: Current Status. *J Am Coll Cardiol* 2010;56:S1-S42.
2. Iakovou I, Schmidt T, Bonizzoni E, Ge L, Sangiorgi GM, Stankovic G, Airoldi F, Chieffo A, Montorfano M, Carlino M, Michev I, Corvaja N, Briguori C, Gerckens U, Grube E, Colombo A. Incidence, Predictors, and Outcome of Thrombosis After Successful Implantation of Drug-Eluting Stents. *JAMA* 2005;293:2126-2130.
3. Ong AT, McFadden EP, Regar E, de Jaegere PP, van Domburg RT, Serruys PW. Late angiographic stent thrombosis (LAST) events with drug-eluting stents. *J Am Coll Cardiol* 2005;45:2088-2092.
4. Pfisterer M, Brunner-La Rocca HP, Buser PT, Rickenbacher P, Hunziker P, Mueller C, Jeger R, Bader F, Osswald S, Kaiser C. Late clinical events after clopidogrel discontinuation may limit the benefit of drug-eluting stents: an observational study of drug-eluting versus bare-metal stents. *J Am Coll Cardiol* 2006;48:2584-2591.
5. Lagerqvist B, James SK, Stenestrand U, Lindback J, Nilsson T, Wallentin L, the SCAAR Study Group. Long-Term Outcomes with Drug-Eluting Stents versus Bare-Metal Stents in Sweden. *N Engl J Med* 2007;356:1009-1019.
6. Farb A, Heller PF, Shroff S, Cheng L, Kolodgie FD, Carter AJ, Scott DS, Froehlich J, Virmani R. Pathological Analysis of Local Delivery of Paclitaxel Via a Polymer-Coated Stent. *Circulation* 2001;104:473-479.
7. Farb AM, Burke APM, Kolodgie FDP, Virmani RM. Pathological Mechanisms of Fatal Late Coronary Stent Thrombosis in Humans. *Circulation* 2003;108:1701-1706.
8. Joner M, Finn AV, Farb A, Mont EK, Kolodgie FD, Ladich E, Kutys R, Skorija K, Gold HK, Virmani R. Pathology of Drug-Eluting Stents in Humans: Delayed Healing and Late Thrombotic Risk. *J Am Coll Cardiol* 2006;48:193-202.
9. Finn AV, Joner M, Nakazawa G, Kolodgie F, Newell J, John MC, Gold HK, Virmani R. Pathological Correlates of Late Drug-Eluting Stent Thrombosis: Strut Coverage as a Marker of Endothelialization. *Circulation* 2007;115:2435-2441.
10. Virmani R, Guagliumi G, Farb A, Musumeci G, Grieco N, Motta T, Mihalcsik L, Tespili M, Valsecchi O, Kolodgie FD. Localized Hypersensitivity and Late Coronary Thrombosis Secondary to a Sirolimus-Eluting Stent: Should We Be Cautious? *Circulation* 2004;109:701-705.
11. Duckers HJ, Soullie T, den HP, Rensing B, de Winter RJ, Rau M, Mudra H, Silber S, Benit E, Verheye S, Wijns W, Serruys PW. Accelerated vascular repair following percutaneous coronary intervention by capture of endothelial progenitor cells promotes regression of neointimal growth at long term follow-up: final results of the Healing II trial using an endothelial progenitor cell capturing stent (Genous R stent). *EuroIntervention* 2007;3:350-358.
12. Suzuki Y, Ikeno F, Koizumi T, Tio F, Yeung AC, Yock PG, Fitzgerald PJ, Fearon WF. In vivo comparison between optical coherence tomography and intravascular ultrasound for detecting small degrees of in-stent neointima after stent implantation. *JACC Cardiovasc Interv* 2008;1:168-173.
13. Prati F, Zimarino M, Stabile E, Pizzicannella G, Fouad T, Rabozzi R, Filippini A, Pizzicannella J, Cera M, De Caterina R. Does optical coherence tomography identify arterial healing after stenting? An in vivo comparison with histology, in a rabbit carotid model. *Heart* 2008;94:217-221.
14. Murata A, Wallace-Bradley D, Tellez A, Alviar C, Aboodi M, Sheehy A, Coleman L, Perkins L, Nakazawa G, Mintz G, Kaluza GL, Virmani R, Granada JF. Accuracy of optical coherence tomography in the evaluation of neointimal coverage after stent implantation. *JACC Cardiovasc Imaging* 2010;3:76-84.

15. Templin C, Meyer M, Muller MF, Djonov V, Hlushchuk R, Dimova I, Flueckiger S, Kronen P, Sidler M, Klein K, Nicholls F, Ghadri JR, Weber K, Paunovic D, Corti R, Hoerstrup SP, Luscher TF, Landmesser U. Coronary optical frequency domain imaging (OFDI) for in vivo evaluation of stent healing: comparison with light and electron microscopy. *Eur Heart J* 2010;31:1792-1801.
16. Barlis P, Regar E, Serruys PW, Dimopoulos K, van der Giessen WJ, van Geuns RJ, Ferrante G, Wandel S, Windecker S, Van Es GA, Eerdmans P, Juni P, di Mario C. An optical coherence tomography study of a biodegradable vs. durable polymer-coated limus-eluting stent: a LEADERS trial sub-study. *Eur Heart J* 2010;31:165-176.
17. Guagliumi G, Sirbu V, Musumeci G, Bezerra HG, Aprile A, Kyono H, Fiocca L, Matiashvili A, Lortkipanidze N, Vassileva A, Popma JJ, Allocco DJ, Dawkins KD, Valsecchi O, Costa MA. Strut coverage and vessel wall response to a new-generation paclitaxel-eluting stent with an ultrathin biodegradable abluminal polymer: Optical Coherence Tomography Drug-Eluting Stent Investigation (OCTDESI). *Circ Cardiovasc Interv* 2010;3:367-375.
18. Guagliumi G, Sirbu V, Bezerra H, Biondi-Zoccai G, Fiocca L, Musumeci G, Matiashvili A, Lortkipanidze N, Tahara S, Valsecchi O, Costa M. Strut coverage and vessel wall response to zotarolimus-eluting and bare-metal stents implanted in patients with ST-segment elevation myocardial infarction: the OCTAMI (Optical Coherence Tomography in Acute Myocardial Infarction) Study. *JACC Cardiovasc Interv* 2010;3:680-687.
19. Cook S, Ladich E, Nakazawa G, Eshtehardi P, Neidhart M, Vogel R, Togni M, Wenaweser P, Billinger M, Seiler C, Gay S, Meier B, Pichler WJ, Juni P, Virmani R, Windecker S. Correlation of Intravascular Ultrasound Findings With Histopathological Analysis of Thrombus Aspirates in Patients With Very Late Drug-Eluting Stent Thrombosis. *Circulation* 2009;120:391-399.
20. Windecker S, Serruys PW, Wandel S, Buszman P, Trznadel S, Linke A, Lenk K, Ischinger T, Klauss V, Eberli F, Corti R, Wijns W, Morice MC, Di MC, Davies S, van Geuns RJ, Eerdmans P, Van Es GA, Meier B, Juni P. Biolimus-eluting stent with biodegradable polymer versus sirolimus-eluting stent with durable polymer for coronary revascularisation (LEADERS): a randomised non-inferiority trial. *Lancet* 2008;372:1163-1173.
21. Udipi K, Melder RJ, Chen M, Cheng P, Hezi-Yamit A, Sullivan C, Wong J, Wilcox J. The next generation Endeavor Resolute Stent: role of the BioLinx Polymer System. *EuroIntervention* 2007;3:137-139.
22. Udipi K, Chen M, Cheng P, Jiang K, Judd D, Caceres A, Melder RJ, Wilcox JN. Development of a novel biocompatible polymer system for extended drug release in a next-generation drug-eluting stent. *J Biomed Mater Res A* 2008;85:1064-1071.
23. Hezi-Yamit A, Sullivan C, Wong J, David L, Chen M, Cheng P, Shumaker D, Wilcox JN, Udipi K. Impact of polymer hydrophilicity on biocompatibility: implication for DES polymer design. *J Biomed Mater Res A* 2009;90:133-141.
24. Rogers C, Welt FG, Karnovsky MJ, Edelman ER. Monocyte recruitment and neointimal hyperplasia in rabbits. Coupled inhibitory effects of heparin. *Arterioscler Thromb Vasc Biol* 1996;16:1312-1318.
25. Carter AJ, Melder RJ, Udipi K, Ozdil F, Virmani R, Wilcox J. In vivo performance of a novel co-polymer system for extended release of zotarolimus in a next generation drug-eluting stent. Presented at the Transcatheter Cardiovascular Therapeutics Annual Meeting, Washington DC . 2006.
26. Guidoin R, Marois Y, Zhang Z, King M, Martin L, Laroche G, Awad J. The benefits of fluoropassivation of polyester arterial prostheses as observed in a canine model. *ASAIO J* 1994;40:M870-M879.
27. Xie X, Guidoin R, Nutley M, Zhang Z. Fluoropassivation and gelatin sealing of polyester arterial prostheses to skip preclotting and constrain the chronic inflammatory response. *J Biomed Mater Res B Appl Biomater* 2010;93:497-509.

28. Meredith IT, Worthley S, Whitbourn R, Walters D, Popma J, Cutlip D, Fitzgerald P. The next-generation Endeavor Resolute stent: 4-month clinical and angiographic results from the Endeavor Resolute first-in-man trial. *EuroIntervention* 2007;3:50-53.
29. Meredith IT, Worthley S, Whitbourn R, Walters DL, McClean D, Horrigan M, Popma JJ, Cutlip DE, DePaoli A, Negoita M, Fitzgerald PJ. Clinical and angiographic results with the next-generation resolute stent system: a prospective, multicenter, first-in-human trial. *JACC Cardiovasc Interv* 2009;2:977-985.
30. Meredith IT, Worthley S, Whitbourn R, Walters D, McClean D, Ormiston J, Horrigan M, Wilkins GT, Hendriks R, Matsis P, Muller D, Cutlip D. Long-term clinical outcomes with the next-generation Resolute Stent System: a report of the two-year follow-up from the RESOLUTE clinical trial. *EuroIntervention* 2010;5:692-697.
31. Serruys PW, Silber S, Garg S, van Geuns RJ, Richardt G, Buszman PE, Kelbaek H, van Boven AJ, Hofma SH, Linke A, Klauss V, Wijns W, Macaya C, Garot P, DiMario C, Manoharan G, Kornowski R, Ischinger T, Bartorelli A, Ronden J, Bressers M, Gobbens P, Negoita M, van Leeuwen F, Windecker S. Comparison of Zotarolimus-Eluting and Everolimus-Eluting Coronary Stents. *New Engl J Med* 2010;363:136-146.
32. Ruygrok PN, Desaga M, Van Den BF, Rasmussen K, Suryapranata H, Dorange C, Veldhof S, Serruys PW. One year clinical follow-up of the XIENCE V Everolimus-eluting stent system in the treatment of patients with de novo native coronary artery lesions: the SPIRIT II study. *EuroIntervention* 2007;3:315-320.
33. Gonzalo N, Tearney GJ, Serruys PW, van Soest G, Okamura T, Garcia-Garcia HM, van Geuns RJ, van der Ent M, Ligthart JM, Bouma BE, Regar E. Second-generation optical coherence tomography in clinical practice. High-speed data acquisition is highly reproducible in patients undergoing percutaneous coronary intervention. *Rev Esp Cardiol* 2010;63:893-903.
34. Gonzalo N, Garcia-Garcia HM, Serruys PW, Commissaris KH, Bezerra H, Gobbens P, Costa M, Regar E. Reproducibility of quantitative optical coherence tomography for stent analysis. *EuroIntervention* 2009;5:224-232.
35. Guagliumi G, Musumeci G, Sirbu V, Bezerra HG, Suzuki N, Fiocca L, Matiashvili A, Lortkipanidze N, Trivisonno A, Valsecchi O, Biondi-Zoccai G, Costa MA. Optical coherence tomography assessment of in vivo vascular response after implantation of overlapping bare-metal and drug-eluting stents. *JACC Cardiovasc Interv* 2010;3:531-539.
36. Guagliumi G, Costa MA, Sirbu V, Musumeci G, Bezerra HG, Suzuki N, Matiashvili A, Lortkipanidze N, Mihalcsik L, Trivisonno A, Valsecchi O, Mintz GS, Dressler O, Parise H, Maehara A, Cristea E, Lansky AJ, Mehran R, Stone GW. Strut Coverage and Late Malapposition With Paclitaxel-Eluting Stents Compared With Bare Metal Stents in Acute Myocardial Infarction: Optical Coherence Tomography Substudy of the Harmonizing Outcomes With Revascularization and Stents in Acute Myocardial Infarction (HORIZONS-AMI) Trial. *Circulation* 2011;123:274-281.
37. Stone GW, Lansky AJ, Pocock SJ, Gersh BJ, Dangas G, Wong SC, Witzenbichler B, Guagliumi G, Peruga JZ, Brodie BR, Dudek D, M+Âckel M, Ochala A, Kellock A, Parise H, Mehran R. Paclitaxel-Eluting Stents versus Bare-Metal Stents in Acute Myocardial Infarction. *New England Journal of Medicine* 2009;360:1946-1959.
38. Tanaka N, Terashima M, Rathore S, Itoh T, Habara M, Nasu K, Kimura M, Itoh T, Kinoshita Y, Ehara M, Tsuchikane E, Asakura K, Asakura Y, Katoh O, Suzuki T. Different Patterns of Vascular Response Between Patients With or Without Diabetes Mellitus After Drug-Eluting Stent Implantation: Optical Coherence Tomographic Analysis. *JACC Cardiovasc Interv* 2010;3:1074-1079.

39. Duckers HJ, Silber S, de WR, den HP, Rensing B, Rau M, Mudra H, Benit E, Verheye S, Wijns W, Serruys PW. Circulating endothelial progenitor cells predict angiographic and intravascular ultrasound outcome following percutaneous coronary interventions in the HEALING-II trial: evaluation of an endothelial progenitor cell capturing stent. *EuroIntervention* 2007;3:67-75.
40. Wentzel JJ, Krams R, Schuurbiers JC, Oomen JA, Kloet J, van der Giessen WJ, Serruys PW, Slager CJ. Relationship between neointimal thickness and shear stress after Wallstent implantation in human coronary arteries. *Circulation* 2001;103:1740-1745.
41. Gijsen FJH, Oortman RM, Wentzel JJ, Schuurbiers JCH, Tanabe K, Degertekin M, Ligthart JM, Thury A, de Feyter PJ, Serruys PW, Slager CJ. Usefulness of shear stress pattern in predicting neointima distribution in sirolimus-eluting stents in coronary arteries. *Am J Cardiol* 2003;92:1325-1328.
42. Onuma Y, Serruys PW, Perkins LE, Okamura T, Gonzalo N, Garcia-Garcia HM, Regar E, Kamberi M, Powers JC, Rapoza R, van Beusekom H, van der Giessen WJ, Virmani R. Intracoronary Optical Coherence Tomography and Histology at 1 Month and 2, 3, and 4 Years After Implantation of Everolimus-Eluting Bioresorbable Vascular Scaffolds in a Porcine Coronary Artery Model. An Attempt to Decipher the Human Optical Coherence Tomography Images in the ABSORB Trial. *Circulation* 2010;122:2288-2300.

"One man that has a mind and knows it can always beat ten men who haven't and don't".

The Apple Cart

George Bernard Shaw

PART 6

METALLIC DRUG-ELUTING STENTS WITH BIODEGRADABLE POLYMERS

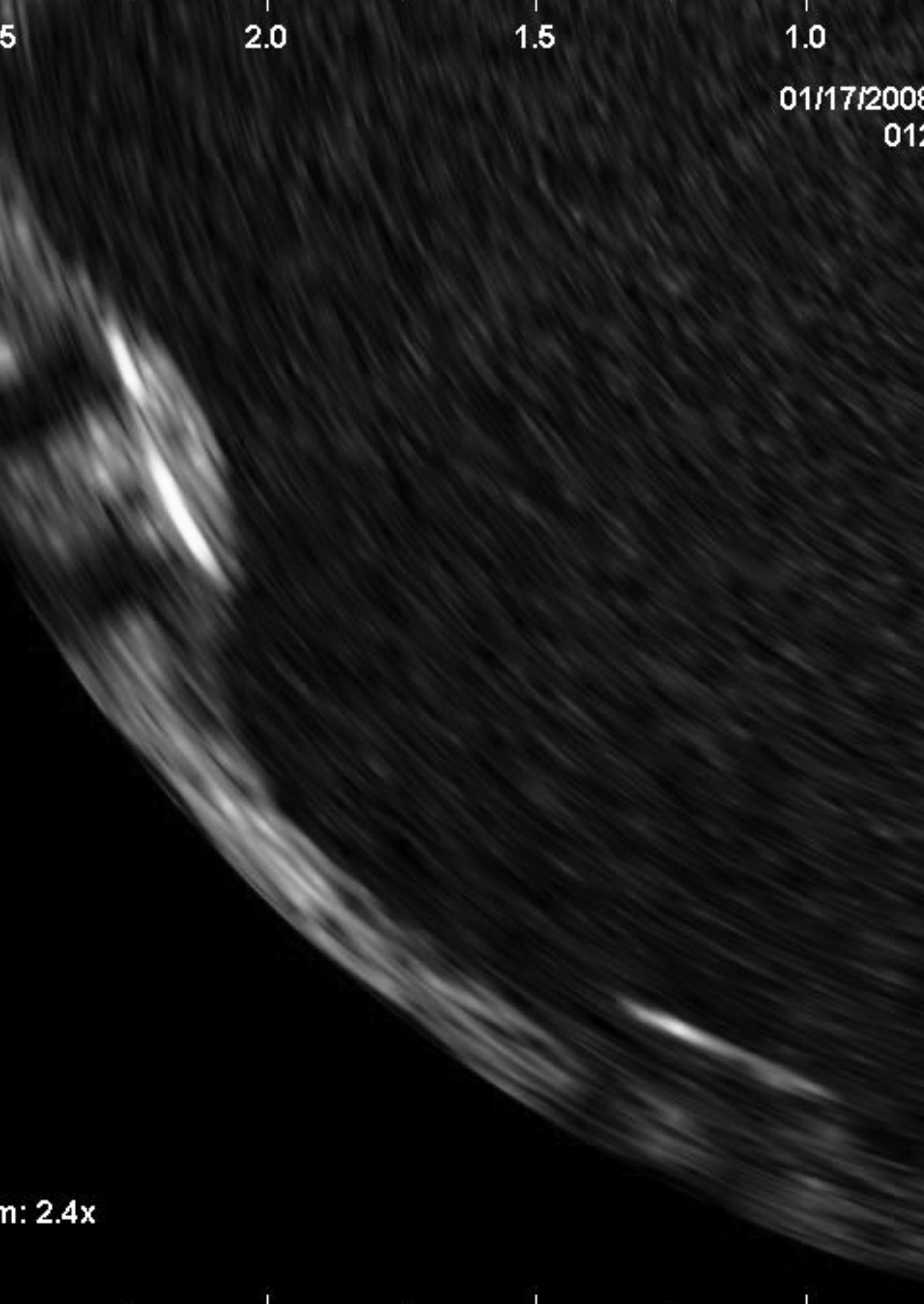
5
2.0
1.5
1.0
01/17/2008
01
m: 2.4x

CHAPTER 8

Polylactide biodegradable polymer in abluminal coating

Long term tissue coverage of a biodegradable polylactide polymer-coated biolimus-eluting stent: comparative sequential assessment with optical coherence tomography till complete resorption of the polymer.

Gutiérrez-Chico JL, Jüni P, García-García HM, Regar E, Nüesch E, Borgia F, van der Giessen WJ, Davies S, van Geuns RJ, Secco GG, Meis S, Windecker S, Serruys PW, di Mario C.

Am Heart J 2011;162:922-931.

STRUCTURED ABSTRACT

Background: Biolimus-eluting stents (BES) with biodegradable polymer in abluminal coating achieve more complete coverage at 9 months than sirolimus-eluting stents (SES) with durable polymer, as assessed by optical coherence tomography (OCT). Whether this advantage persists or augments after complete resorption of the polymer (>12 months) is unknown.
Methods: The LEADERS trial compared the performance of BES vs. SES. Patients were randomly allocated to sequential angiographic follow-up, including OCT in selected sites, at 9 and 24 months. Struts coverage was compared using Bayesian hierarchical models, as primary outcome for the OCT substudy.
Results: 56 patients (26 BES, 30 SES) were enrolled in the OCT substudy. 21 patients (10 BES, 11 SES) agreed to perform a second OCT follow-up at 24 months. Eleven lesions, 12 stents were analyzed sequentially in the BES group (2455 struts at 9 months, 2131 struts at 24 months) and 11 lesions, 18 stents in the SES group (3421 struts at 9 months, 4170 struts at 24 months). The previously reported advantage of BES over SES in terms of better strut coverage at 9 months was followed by improvement in coverage of the SES, resulting in identical coverage in both BES and SES at 24 months: 1.5 vs. 1.8% uncovered struts, difference -0.2%, 95% Credibility Interval -3.2 to 2.6%, p=0.84.
Conclusions: More complete strut coverage of BES as compared with SES at 9 months was followed by improvement of coverage in SES between 9-24 months and similar long-term coverage in both stent types at 24 months.
Key words: Tomography, optical coherence; poly(lactide); biolimus A9; sirolimus; drug-eluting stents; angioplasty, transluminal, percutaneous coronary.

ABBREVIATIONS

BES: biolimus-eluting stent
DES: drug-eluting stent.
ISA: incomplete stent apposition.
IVUS: intravascular ultrasound.
MLA: minimal lumen area.
NIH: neointimal hyperplasia.
OCT: optical coherence tomography.
PLA: Poly-lactic acid
QCA: quantitative coronary angiography
SES: sirolimus-eluting stent

INTRODUCTION

Drug-eluting stents (DES) have reduced restenosis rates to approximately 9%[1], but they might pose higher risk of late and very late stent thrombosis[1], with the common pathological finding of delayed neointimal healing and incomplete endothelialization[2,3]. In first generation DES the mechanism for incomplete neointimal coverage seems to go beyond the antiproliferative potency of the drug and involve also an inflammatory reaction[3-6]. The presence of intense eosinophilic infiltrates in the vessel wall[3] and in the thrombus harvested from patients suffering very late stent thrombosis[4] suggests inflammation might be mediated by delayed type IVb hypersensitivity. Hypersensitivity is likely triggered by the polymer rather than by other components of the device[6], given the timing of onset (later than 90 days, when the drug is no longer detectable in the vessel wall) and the presence of polymer fragments surrounded by giant cells[3,5]. An interesting approach to minimize polymer-induced inflammation consists of coating the metallic backbone of the stent with a biodegradable polymer that is fully resorbed after elution of the drug[7]. The risk of delayed hypersensitivity disappears together with the potential allergens, and complete neointimal healing is no longer in jeopardy.

The LEADERS trial was the first published randomized study to use optical coherehce tomography (OCT) for the evaluation of tissue coverage in two different types of DES[8,9]. It compared a new-generation biolimus-eluting stent (BES) with biodegradable polymer in abluminal coating vs. a 1st generation sirolimus-eluting stent (SES) with durable polymer in conformal coating. At 9-month BES showed lower proportion of uncovered struts than SES (weighted estimate 0.6 vs. 2.1%, p=0.04)[9]. The aim of this study is assessing whether this difference persists after complete resorption of the BES polymer.

METHODS

Study population and design

The design and main results from the LEADERS trial have been published elsewhere[8]. It was an international randomized multi-centre non-inferiority trial comparing the BES BioMatrix Flex™ stent (Biosensors International, Morges, CH) with the SES Cypher SELECT™ stent (Cordis, Miami Lakes, FL, USA), following an all-comers approach with minimal exclusion criteria: patients with symptomatic coronary heart disease or silent ischemia were eligible if they had at least one coronary lesion of ≥50% diameter stenosis in vessels with 2.25-3.50mm reference diameters, amenable for percutaneous treatment. The primary endpoint was a composite of cardiac death, myocardial infarction and clinically-indicated target vessel revascularization at 9 months follow-up.

Patients were randomly allocated on a 1:1 basis to receive either BES or SES using random computer-generated sequences, stratified according to centre. In a factorial design, they were additionally randomized on a 1:3 basis to angiographic and clinical follow-up at 9-month or clinical follow-up alone. Patients allocated to angiographic follow-up in two of the study sites (Royal Brompton Hospital, London, UK; and Erasmus MC, Rotterdam, NL) were also included in the OCT substudy. Serum creatinine ≥200mol/L and left ventricular ejection fraction <30% were exclusion criteria for the OCT substudy. The primary endpoint for the OCT substudy was the proportion of uncovered struts at 9 and 24 months. The study complied with the declaration of Helsinki, was approved by all institutional ethics committees and registered at clinicaltrials.gov (NCT00389220). All patients provided written informed consent for participation.

Intervention and study stents

Direct stenting was allowed and full lesion coverage was pursued by implanting one or several stents, as required. Only one type of DES was used per patient.

The BioMatrix Flex™ stent (Biosensors International, Morges, CH) consists of a stainless-steel platform (Juno TM, Biosensors International, Morges, CH), coated by an abluminal 11-µm layer of poly-lactide (PLA) polymer. The polymer contains Biolimus-A9 at a concentration of 15.6 µg/mm of stent length. PLA is linearly degraded by surface hydrolysis to lactide along a period of 6-12 months, resulting in simultaneous release of the drug[7]. The Cypher™ SELECT stent (Cordis, Miami Lakes, FL, USA) consists of a stainless steel platform, coated by a durable blend of poly(ethylene-vynil-acetate) and poly(butyl-methacrylate) containing sirolimus at a concentration of 8.3-10.4µg/mm, depending on the stent nominal diameter. The drug elution period is estimated in 90 days. After the intervention patients received at least 75mg of acetylsalicylic acid indefinitely and dual anti-platelet therapy with 75mg of clopidogrel for 12 months.

OCT study and analysis

OCT pullbacks were obtained at 9 and 24 months follow-up with M3 or C7 systems (Lightlab Imaging, Westford, Massachusetts, USA), depending on availability, using non-occlusive technique[10] (Table 1).

OCT pullbacks were analysed offline in a core-laboratory (Cardialysis BV, Rotterdam, NL) by independent staff blinded to allocation and to clinical or procedural characteristics of the patients, using proprietary software (Lightlab Imaging, Westford, Massachusetts, USA). Cross-sections at 1mm intervals within the stented segment were analyzed. Lumen and stent areas were drawn in each cross-section, and incomplete stent apposition (ISA) or neointimal hyperplasia (NIH) areas were calculated, as appropriate[11]. Apposition was assessed per strut

Table 1: Characteristics of the different OCT systems* in the study.

		M3	C7
Domain		Time	Fourier
Catheter*		ImageWire	Dragonfly
Rotation speed (Hz)		20	100
Pullback speed (mm/s)		3	20
Patients with SES	9m	11	0
	24m	3	8
Patients with BES	9m	10	0
	24m	3	7

* All systems and catheters from Lightlab Imaging, Westford, Massachusetts, USA.

by placing a marker at the adluminal leading edge, in the mid-point of the strut long-axis, and measuring the distance between this marker and the lumen contour following a straight line directed to the centre of gravity of the vessel[12]. Struts were considered malapposed if the distance was ≥170μm (for SES) or ≥140μm (for BES), the thresholds resulting from rounding up the sum of the strut-polymer thickness of each stent (SES 153μm, BES 120μm) plus the axial resolution of OCT (14μm). Struts located at the ostium of side branches, with no vessel wall behind, were labelled as non-apposed side-branch struts and excluded from the analysis of apposition[13,14].

Struts were classified as uncovered if any part of the strut was visibly exposed to the lumen, or as covered if a layer of tissue was visible over all the reflecting surfaces. In covered struts, thickness of coverage was measured from the strut marker to the adluminal edge of the tissue, following a straight line connecting the strut marker with the centre of gravity of the vessel[11,13-15].

The clustering and spatial distribution of uncovered struts was summarized in "spread-out vessel graphics" [13] (Figure 1).

Statistical analysis

Pre-specified primary outcome was the difference in percentage of uncovered struts at 24 months. Assuming an average number of 1.5 lesions per patient, 180 struts per lesion, an intracluster correlation coefficient of 0.04 for binary coverage of struts within lesions and a design factor of 1.3, we estimated that the inclusion of 22 patients (with 33 lesions and 5940 struts) per group would yield greater than 90% power to detect a difference in uncovered struts of 4% at 9 months between BESs and SESs at a two-sided type I error of 0.05. Secondary outcomes comprised other variables assessing coverage, incomplete stent apposition (ISA), and the geometric mean thickness of coverage. To estimate differences between BES and SES, we used a Bayesian hierarchical random-effects model based on Markov chain Monte

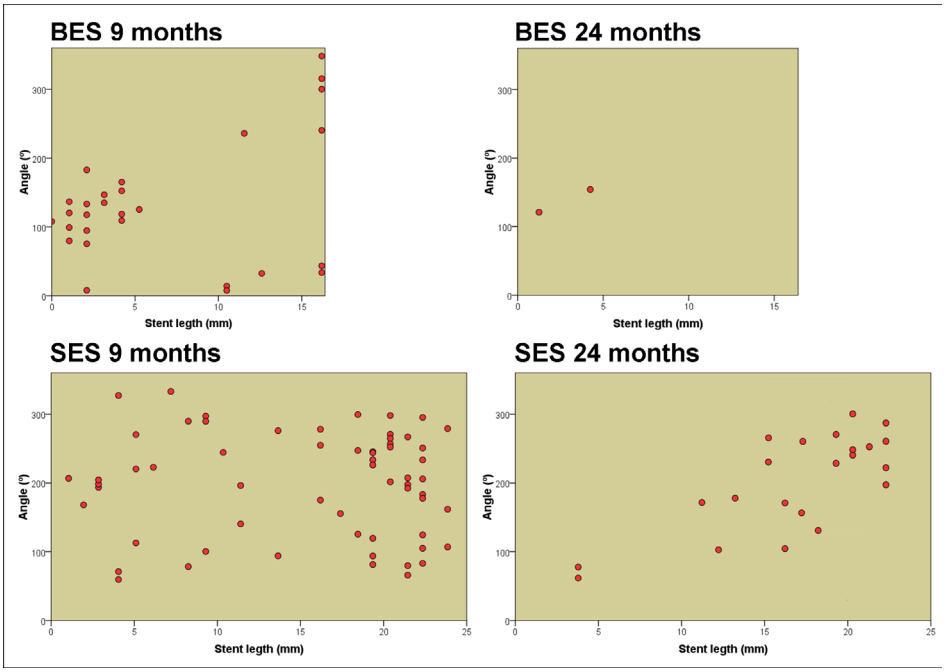

Figure 1: Examples of spatial distributions of uncovered struts in "spread-out-vessel" graphs.
Examples of one biolimus-eluting stent (upper panel) and one sirolimus-eluting stent (lower panel) studied with OCT at 9 and 24 months. X-axis represents the distance from the distal edge of the stent to the strut; the Y-axis represents the angle where the strut is located in the circular cross-section with respect to the centre of gravity of the vessel. The result is a graph representing the spatial distribution of the non-covered struts (red spots) along the stent, as if it had been cut along the reference angle (0º) and spread out on a flat surface.

Carlo simulations with minimally informative priors[9]. The model included random-effects at the level of lesions and patients, fully accounting for the correlation of lesion characteristics within patients and their variation between patients. We used Wilcoxon test for continuous variables and Pearson's chi-square or Fisher's exact test as appropriate for dichotomous variables to compare baseline characteristics as well as areas and volumetric parameters per stent. Statistical analyses were performed using WinBUGS version 1.4.3 (Imperial College and MRC, United Kingdom) and Stata, release 11 (StataCorp, College Station, TX).

Funding and authorship

The LEADERS trial (NCT00389220) and this OCT substudy have been sponsored by Biosensors International, Morges, CH. The authors are solely responsible for the design and conduct of this study, all study analyses, the drafting and editing of the paper and its final contents.

RESULTS

88 patients (43 BES, 45 SES) were allocated to angiographic follow-up in the OCT study centres. OCT studies from 46 patients were finally analysed at 9 months (figure 2). All 46 patients were contacted at 24 months, but 25 refused a second invasive follow-up (20 BES, 26 SES). Sequential OCT follow-up was analysed in 10 patients, 11 lesions, 12 stents in the BES group (2455 struts at 9 months, 2131 struts at 24 months) and in 10 patients, 11 lesions, 18 stents in the SES group (3421 struts at 9 months, 4170 struts at 24 months). All 9-month studies were performed with a time-domain M3 system, whilst 15 studies at 24 months (71%) were done with a Fourier-domain C7 system (table 1).

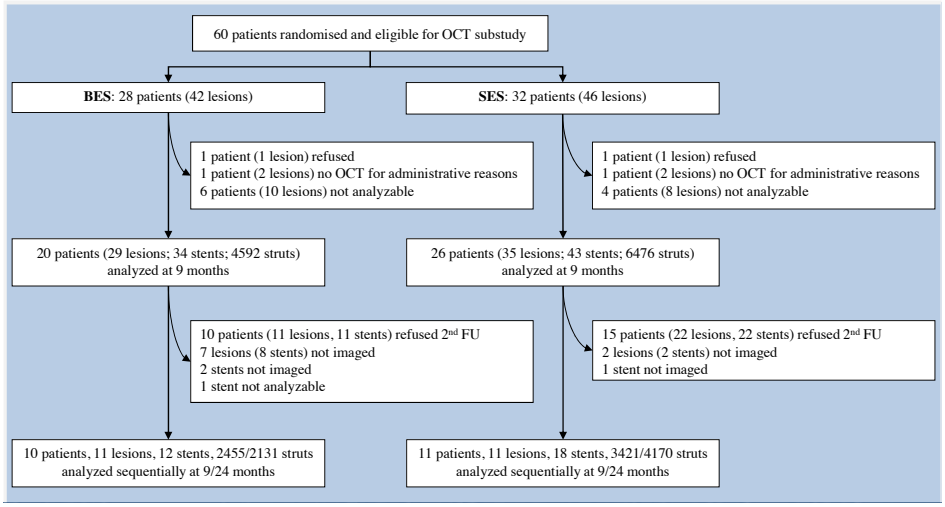

Figure 2: Flow chart of the OCT study and sequential follow-up.

Baseline characteristics of patients and lesions were comparable between both groups (tables 2 and 3). Table 4 shows mean areas and volumes per stent. At 9 months corrected ISA volume was higher in SES than in BES ($p \leq 0.047$), decreasing in both groups at 24 months and making the difference no longer significant ($p \leq 0.171$).

Figure 3 shows the evolution of coverage between 9 and 24 months in representative cross-sections, matched using fiduciary landmarks. A total of 121 out of 2455, and 69 out of 2131 struts were uncovered in the BES group at 9 and 24 months respectively; 286/3421 and 109/4170 struts were uncovered in the SES group at 9 and 24 months respectively. At 9 months the overall proportion of uncovered struts tended to be higher in SES than in BES, although it did not reach conventional levels of statistical significance (table 5). At 24 months, the proportion of uncovered struts decreased in both groups to similar levels (weighted percentage 2%), (table 5, figure 4). The spread-out-vessel charts present results for individual

Table 2: Patients' characteristics.

	BES (n=10)	SES (n=11)	p-value
Age (years)*	61.3 (6.6)	60.3 (10.8)	0.78
Males	7 (70%)	7 (64%)	1.00
Diabetes mellitus	2 (20%)	2 (18%)	1.00
Hypertension	3 (30%)	6 (55%)	0.39
Hypercholesterolemia	5 (50%)	9 (82%)	0.18
Smoking	3 (30%)	7 (64%)	0.20
Previous MI	4 (40%)	5 (45%)	1.00
Previous PCI	2 (20%)	3 (27%)	1.00
Previous CABG	1 (10%)	1 (9%)	1.00
Clinical presentation			
Stable angina	6 (60%)	6 (55%)	1.00
Acute coronary syndrome	4 (40%)	5 (45%)	1.00
Unstable angina	0 (0%)	2 (18%)	
NSTEMI	1 (10%)	2 (18%)	
STEMI	3 (30%)	1 (9%)	
Angiographic characteristics			
Number of lesions per patient*	1.8 (0.9)	1.2 (0.4)	0.09
Multi-vessel disease	4 (40%)	0 (0%)	0.035
Long lesions (>20mm)	3 (30%)	6 (55%)	0.39
Small-vessel disease (RVD < 2.75mm)	6 (60%)	8 (73%)	0.66

Results expressed as n(%) or *mean (SD).

CABG: Coronary Artery By-pass Graft; MI: Myocardial Infarction; PCI: Percutaneous Coronary Intervention; STEMI: ST elevation myocardial infarction.

patients, showing the spatial distribution and temporal evolution of uncovered struts in the 30 stents (figure 5). There was little evidence for differences in thickness of coverage or in the variables estimating apposition between the treatment groups at 9 or 24 months (table 5, figure 6).

DISCUSSION

In this sequential OCT study nested in a randomised comparison of two different DES, we found that the advantage of a BES with biodegradable polymer in abluminal coating over a SES with durable polymer in terms of strut coverage at 9 months[9] was followed by improvement of the SES coverage between 9-24 months, resulting in similar coverage in BES and SES at 24 months. Both types of stent converged at a maximum plateau around 98% strut coverage. Taken together, our results suggest that BES indeed is associated with faster healing than

Table 3: Angiographic and procedural characteristics of the lesions.

	BES (n=11)	SES (n=11)	p-value
Coronary artery of the target lesion			0.51
LAD	6 (55%)	3 (27%)	
LCX	1 (9%)	1 (9%)	
RCA	4 (36%)	7 (64%)	
De novo lesions	10 (91%)	11 (100%)	
Bifurcation	2 (18%)	2 (18%)	1.00
Total occlusion	5 (45%)	4 (36%)	1.00
Severe calcification	1 (9%)	2 (18%)	1.00
QCA (in-stent)			
Lesion length (mm)	18.4 (14.6)	30.0 (29.0)	0.53
RVD (mm)			
Pre	2.8 (0.5)	2.7 (0.6)	0.81
Post	2.5 (0.5)	2.7 (0.6)	0.45
9m	2.5 (0.4)	2.8 (0.6)	0.19
MLD (mm)			
Pre	0.7 (0.8)	0.7 (0.6)	0.94
Post	2.3 (0.4)	2.3 (0.5)	0.87
9m	2.1 (0.8)	2.1 (0.6)	0.68
Late lumen loss (mm)	1.4 (0.8)	1.3 (0.4)	0.65
Procedural characteristics			
Nr of study stents per lesion	1.5 (0.7)	2.0 (1.2)	0.33
Maximal stent diameter per lesion	3.1 (0.3)	3.1 (0.5)	0.87
Total stent length per lesion	28.6 (21.2)	45.5 (34.7)	0.18
Direct stenting	5 (45%)	4 (36%)	1.00

Results expressed as n(%) or mean(SD).
LAD: Left anterior descending; LCX: Left Circumflex; LM: Left Main Stem; QCA: Quantitative coronary angiography; MLD: Minimal lumen diameter; RVD: Reference vessel diameter; RCA: Right coronary artery.

SES, achieving a percentage of coverage close to the maximum plateau (97%) at 9 months, while SES is catching up subsequently.

To our knowledge, this is the first clinical in-vivo study using sequential OCT to compare the coverage of two different types of DES. Previous sequential studies had reported SES coverage at 6-12 months[16] and at 24-48 months[17] using OCT, or at 4-11-21 months using angioscopy[18], the latter compared with a control bare metal stent.

Table 4: Areas and volumetric analysis per stent (excluding overlap segments) at 24 months follow-up.

21 patients 22 lesions 30 stents	9 months			24 months		
	BES 10 patients 11 lesions 12 stents	**SES** 11 patients 11 lesions 18 stents	**p-value**	**BES** 10 patients 11 lesions 12 stents	**SES** 11 patients 11 lesions 18 stents	**p-value**
Stented length (mm)	23.43 (13.87)	35.84 (24.78)	0.193	23.05 (13.13)	35.82 (26.20)	0.401
MLA (mm^2)	4.86 (2.40)	4.58 (2.46)	0.748	4.89 (1.73)	4.96 (2.30)	0.898
Lumen volume (mm^3)	144.69 (69.37)	252.92 (189.96)	0.438	145.91 (77.34)	260.44 (176.21)	0.300
Min stent area (mm^2)	5.38 (2.11)	5.03 (2.18)	0.606	5.87 (1.52)	5.68 (2.42)	0.949
Stent volume (mm^3)	158.79 (73.43)	263.02 (197.75)	0.562	170.13 (87.40)	287.54 (196.02)	0.365
ISA volume (mm^3)	0.24 (0.45)	4.28 (10.09)	**0.040**	0.13 (0.44)	1.48 (2.11)	0.151
Corrected by stent volume (%)	0.15 (0.24)	1.76 (3.52)	**0.047**	0.11 (0.35)	0.78 (1.34)	0.171
NIH volume (mm^3)	14.33 (18.57)	14.50 (18.17)	1.000	24.35 (18.86)	28.58 (29.12)	0.949
Percent NIH vol obstruction (%)	9.02 (10.02)	5.76 (5.03)	0.606	14.53 (9.57)	9.43 (5.37)	0.171

ISA: Incomplete stent apposition; MLA: Minimal lumen area; NIH : Neointimal hyperplasia.

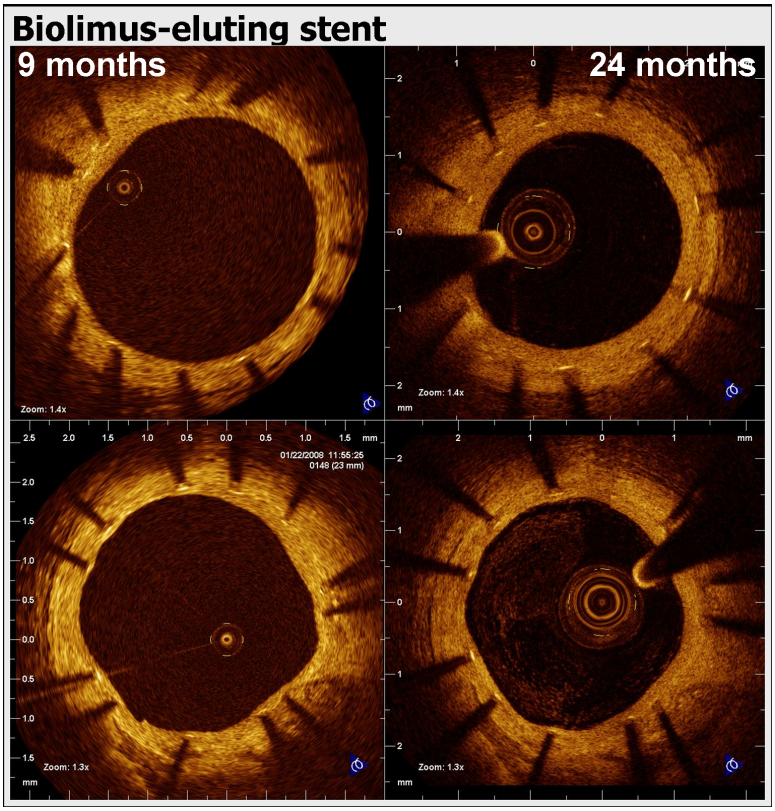

Figure 3 (panel A): Representative examples of matched cross-sections at 9 and 24 months in biolimus-eluting stents, showing the pattern of coverage.

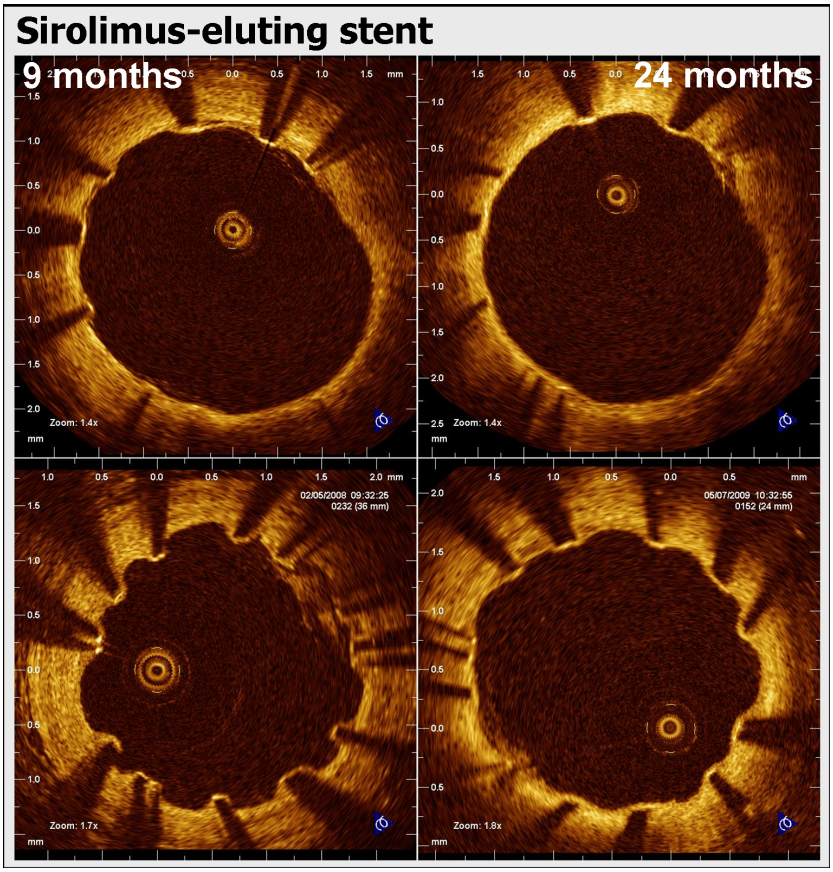

Figure 3 (panel B): Representative examples of matched cross-sections at 9 and 24 months in sirolimus-eluting stents, showing the pattern of coverage.

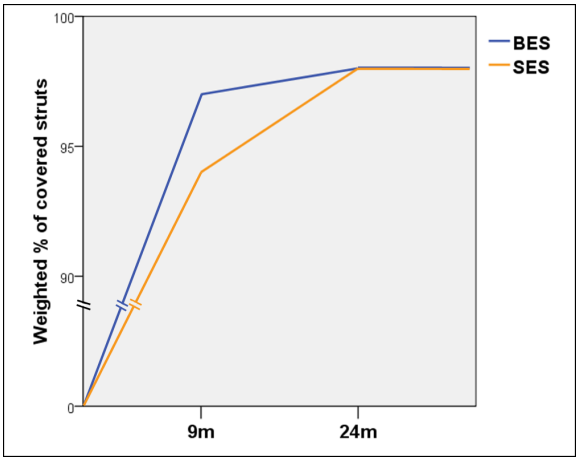

Figure 4: Trend graphic showing the weighted percentage of covered struts at 9 and 24 months for the both types of stent.

Table 5: Analysis of apposition and coverage per strut at 9 months and 24 months.

			21 patients 22 lesions 30 stents	BES 10 patients 11 lesions 12 stents	SES 11 patients 11 lesions 18 stents	Comparison	
				Weighted % (95% CrI)	Weighted % (95% CrI)	Difference (95% CrI)	P value
9 months	Struts		6226	2640	3586		
	Coverage	Uncovered struts*		2.8 (0.9 to 7.3)	5.7 (2.0 to 14.3)	-2.9 (-11.6 to 2.9)	0.31
		Lesions with					
		≥ 10% uncovered struts		18.6 (2.2 to 60.3)	29.8 (5.2 to 71.7)	-9.6 (-57.2 to 37.8)	0.66
		≥ 5% uncovered struts		42.9 (9.8 to 82.9)	58.0 (17.7 to 90.6)	-14.0 (-65.3 to 43.2)	0.63
		any uncovered struts		91.6 (59.5 to 99.4)	100.0 (92.6 to 100.0)	-7.9 (-40.0 to 0.2)	0.054
		Thickness of coverage (µm)†		56.7 (32.5 to 101.9)	41.6 (23.4 to 70.2)	14 (-21 to 64)	0.41
	Apposition	ISA struts		0.5 (0.2 to 1.5)	1.4 (0.5 to 3.5)	-0.8 (-3.0 to 0.4)	0.18
		Lesions with					
		≥ 10% ISA struts		0.0 (0.0 to 1.3)	3.2 (0.1 to 27.2)	-3.1 (-27.2 to -0.0)	0.035
		≥ 5% ISA struts		0.0 (0.0 to 1.3)	3.2 (0.1 to 27.2)	-3.1 (-27.2 to -0.0)	0.035
		Any ISA struts		73.2 (29.9 to 96.1)	91.6 (56.2 to 99.3)	-16.2 (-61.8 to 22.5)	0.34
24 months	Struts		6490	2337	4153		
	Coverage	Uncovered struts*		1.5 (0.5 to 4.2)	1.8 (0.6 to 4.5)	-0.2 (-3.2 to 2.6)	0.84
		Lesions with					
		≥ 10% uncovered struts		2.9 (0.1 to 25.4)	0.0 (0.0 to -)¶	2.9 (0.0 to 25.4)	0.012
		≥ 5% uncovered struts		31.2 (5.5 to 74.3)	8.2 (0.6 to 41.4)	20.2 (-18.1 to 66.7)	0.27
		any uncovered struts		73.1 (30.1 to 96.0)	97.2 (74.7 to 100.0)	-21.9 (-65.7 to 6.0)	0.12
		Thickness of coverage (µm)†		86.4 (60.2 to 121.4)	62.2 (44.5 to 87.7)	24 (-15 to 62)	0.17
	Apposition	ISA struts		0.1 (0.0 to -) ¶	0.4 (0.1 to 1.4)	-0.3 (-1.3 to 0.1)	0.15
		Lesions with					
		≥ 10% ISA struts		0.0 (0.0 to 0.7)	0.0 (0.0 to 0.7)	-0.0 (-0.7 to 0.6)	0.49
		≥ 5% ISA struts		0.0 (0.0 to 1.1)	2.7 (0.0 to 25.0)	-2.6 (-24.9 to -0.0)	0.042
		any ISA struts		18.6 (2.3 to 60.3)	71.3 (27.0 to 95.1)	-48.7 (-85.1 to 5.2)	0.08

CrI: Credibility Interval

ISA: Incomplete stent apposition.

Weighted percentages and differences are derived from medians, 2.5th and 97.5th percentiles of the corresponding posterior distributions in WinBugs

*Pre-specified primary outcome of OCT substudy.

¶ Note that the upper limit of the 95% CrI could not be estimated.

†Averages are geometric means and differences in geometric means derived from posterior distributions in WinBugs.

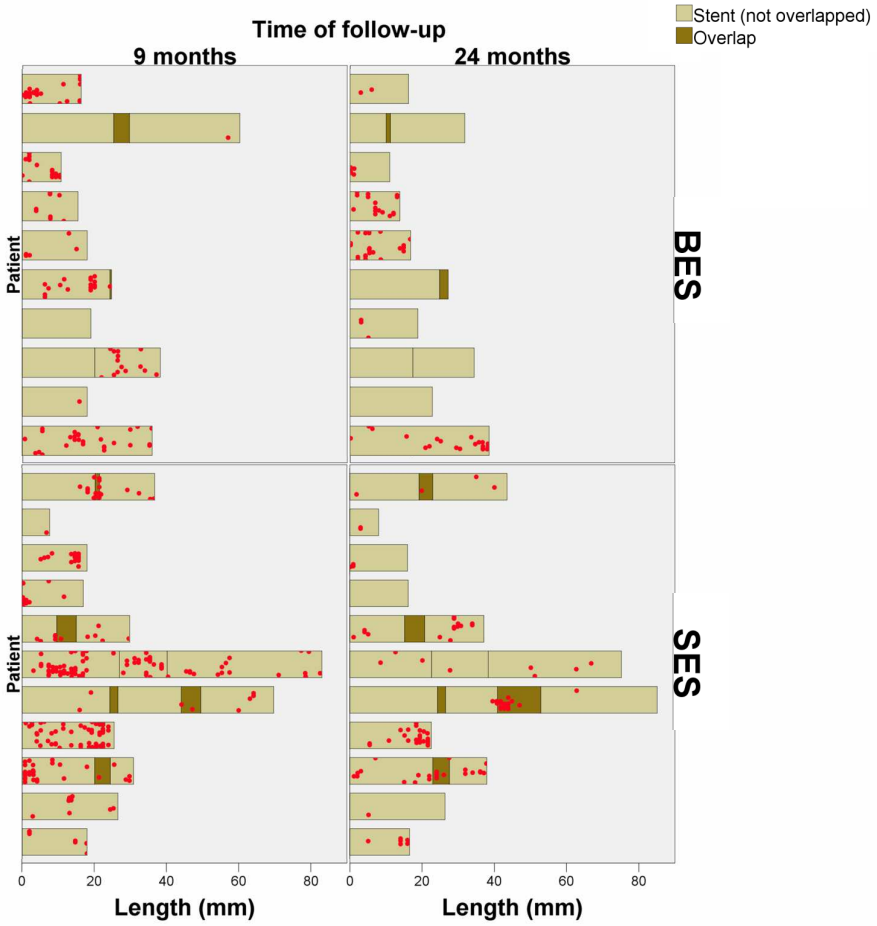

Figure 5: Spread-out-vessel charts showing the spatial distribution of uncovered struts at 9 and 24 months in the matched stents.

"Very late healing" phenomenon

The improvement in coverage observed in SES between 9-24 months challenges the currently accepted evidence about the healing process after stenting and compels us to reconsider the initial interpretation of the 9-month results[9]. Experimental studies suggested that the re-endothelialization process ensuing a vessel injury, e.g. stenting, was limited in time[19-21]. Endothelial denudation of carotid arteries is followed by re-endothelialization that stops after 2 weeks (in the rabbit) or after 6 weeks (in the rat), even though the endothelial continuity has not been restored[22,23]. This experimental evidence seemed consistent with the results of sequential angioscopic studies in SES, showing no improvement in the minimum coverage between 6 and 24 months, with increase in the maximum[24], and only slight improvement in the predominant score between 4-11-21 months[18], eventually suggesting an arrested heal-

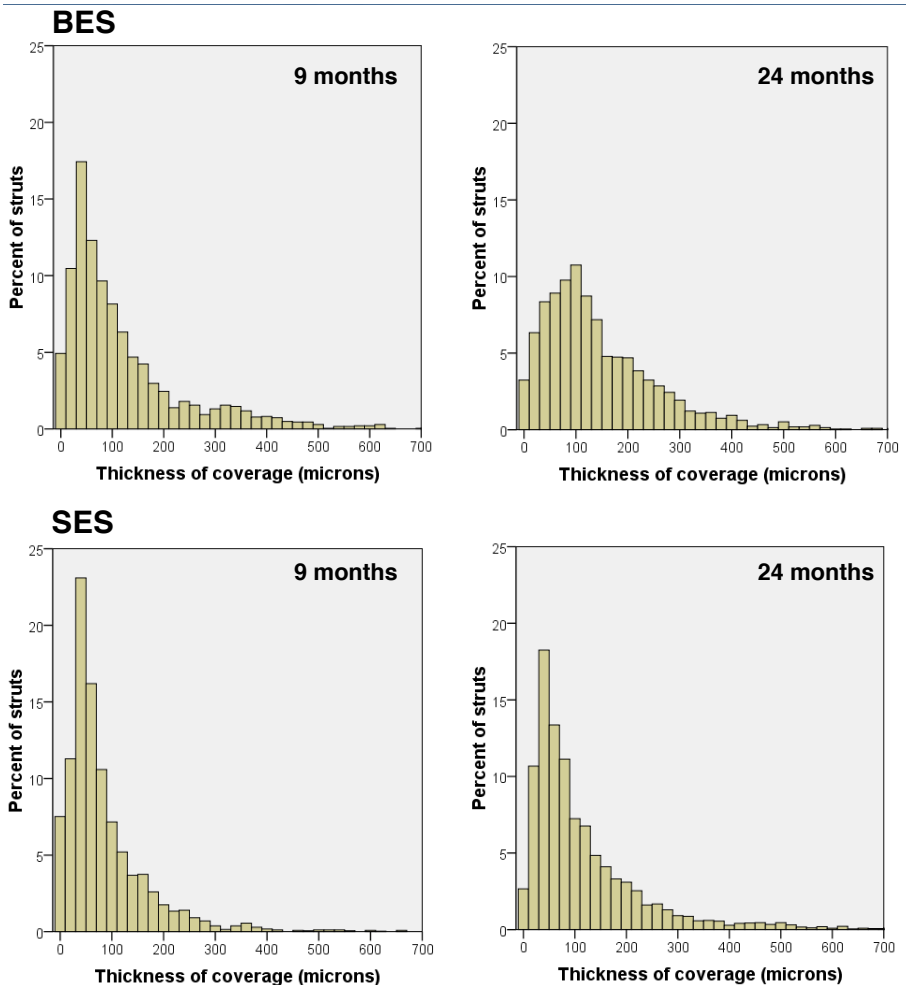

Figure 6: Histograms showing the distribution of the thickness of coverage at 9 and 24 months in the two types of stent.

ing process undergoing phenomena of intima maturation or plaque progression. Our results question this static time-limited model of neointimal healing, suggesting a more dynamic process, still evolving between 9 and 24 months. Previous non-comparative studies using OCT suggested also this possibility: improvement of SES coverage has been reported between 3-24-48[17,25,26] months or between 6-12 months[16]. Owed to its high resolution (10-20µm) and ability for detailed analysis, OCT could detect subtle changes in neointimal coverage, unnoticed for angioscopy or other imaging techniques. The evolution of neointimal volumes, increasing similarly in both stent groups between 9 and 24 months (table 4) might indicate an actively repairing neointima, but also be the consequence of intima maturation or plaque progression. The ISA reduction between 9 and 24 months is more specific as indicator of "very late healing". Higher incidence of ISA in the SES group had been reported at 9-month[9] and

interpreted in terms of late-acquired ISA. This interpretation becomes now unlikely, because the most pronounced reduction in ISA between 9 and 24 months is observed in SES. This is at variance with previous sequential studies reporting increase in ISA areas and ISA struts between 24 and 48 months in SES[17]. This discrepancy will deserve further clarification in the future.

Different healing rates in different types of stent

The design of our study does not permit to elucidate the mechanism for the different healing rates observed between the devices. Although inflammation was the driving hypothesis for this study and was advocated to explain the differences reported at 9-month[9], it cannot satisfactorily explain the "very late healing". Why does not the initial advantage in coverage persist after the pro-inflammatory polymer has completely disappeared in one of the devices? The role played by polymer-induced inflammation[6] in the neointimal healing after stenting should be revisited: its deleterious effect might be not as sustained in time as currently assumed, with the exception of infrequent delayed hypersensitivity reactions[3,4]. The kinetics of release are also at variance with the coverage rates observed: the elution periods for SES and BES are 90 days and 6-9 months respectively. The different inhibitory potency, lipophilicity, concentration or pleiotropic effects of biolimus and sirolimus can have played a role: the effective neointimal inhibition could be more intense in SES than in BES. Likewise, the design and geometry of the stent platforms could have promoted faster healing in the BES, especially the strut thickness. Both platforms are made of stainless steel, hence requiring thick struts (>100μm) to provide enough radial strength for vessel scaffolding, but BES struts are slightly thinner (120μm) than SES struts (140μm, 154μm if we add the polymer thickness), what is associated with faster healing[27]. The selective abluminal coating of the BES appears as more plausible explanation: the abluminal release of the drug might modulate the proliferation of smooth muscle cells in the media, interfering minimally with the re-endothelialization of the adluminal side, thus promoting a faster reendothelialization.

Clinical implications

Very late healing could be the key to understand why clinical studies have failed to demonstrate higher rates of stent thrombosis in SES[28], even though angioscopy[18,24] or OCT[16,17,25,26] have reported suboptimal coverage between 3-48 months. As suggested by our results and also by other studies[18,26] longer follow-up intervals would be required to assess the final neointimal coverage achieved.

To our knowledge, this is the first sequential OCT study suggesting that different types of stent can promote different healing rates. This may be relevant for tailoring the duration of dual antiplatelet therapy after stenting.

Limitations

The refusal of some patients to undergo the 24 month OCT follow-up is the main limitation of this study. It might have induced some selection bias, since the patients with more favourable outcome might have been more prone to refuse a second invasive follow-up. The lack of statistical significance at 9 months in this second analysis is also explained by the substantial loss of statistical precision resulting from the restricted sample size, and not contradictory with the previously published results[9]. The high percentage of refusals turned this study underpowered to detect a difference of the same magnitude.

CONCLUSION

Better strut coverage of a biolimus-eluting stent with a biodegradable polymer and abluminal coating as compared with a first-generation sirolimus-eluting stent with durable polymer at 9 months was followed by improvement in coverage of the latter stent and similar long-term OCT outcomes in both stent types at 24 months.

FUNDING

Biosensors International, Morges, CH.

Conflict of interest: This trial has been sponsored by Biosensors International, Morges, CH. The participating centres (Royal Brompton, Erasmus MC and Bern University Hospitals) and the core lab (Cardialysis BV) have received grants from Biosensors to run the LEADERS trial and this substudy. Windecker, Serruys and di Mario have received speaker's fees from the sponsor. Susanne Meis is a full-time employee in Biosensors International.

REFERENCES

1. Garg S, Serruys PW. Coronary Stents: Current Status. *J Am Coll Cardiol* 2010;56:S1-S42.
2. Finn AV, Joner M, Nakazawa G, Kolodgie F, Newell J, John MC, Gold HK, Virmani R. Pathological Correlates of Late Drug-Eluting Stent Thrombosis: Strut Coverage as a Marker of Endothelialization. *Circulation* 2007;115:2435-2441.
3. Virmani R, Guagliumi G, Farb A, Musumeci G, Grieco N, Motta T, Mihalcsik L, Tespili M, Valsecchi O, Kolodgie FD. Localized Hypersensitivity and Late Coronary Thrombosis Secondary to a Sirolimus-Eluting Stent: Should We Be Cautious? *Circulation* 2004;109:701-705.
4. Cook S, Ladich E, Nakazawa G, Eshtehardi P, Neidhart M, Vogel R, Togni M, Wenaweser P, Billinger M, Seiler C, Gay S, Meier B, Pichler WJ, Juni P, Virmani R, Windecker S. Correlation of Intravascular Ultrasound Findings With Histopathological Analysis of Thrombus Aspirates in Patients With Very Late Drug-Eluting Stent Thrombosis. *Circulation* 2009;120:391-399.
5. Wilson GJ, Nakazawa G, Schwartz RS, Huibregtse B, Poff B, Herbst TJ, Baim DS, Virmani R. Comparison of Inflammatory Response After Implantation of Sirolimus- and Paclitaxel-Eluting Stents in Porcine Coronary Arteries. *Circulation* 2009;120:141-149.
6. van der Giessen WJ, Lincoff AM, Schwartz RS, van Beusekom HM, Serruys PW, Holmes DR, Jr., Ellis SG, Topol EJ. Marked inflammatory sequelae to implantation of biodegradable and nonbiodegradable polymers in porcine coronary arteries. *Circulation* 1996;94:1690-1697.
7. Grube E, Buellesfeld L. BioMatrix-« Biolimus A9-«-eluting coronary stent: a next-generation drug-eluting stent for coronary artery disease. *Expert Review of Medical Devices* 2006;3:731-741.
8. Windecker S, Serruys PW, Wandel S, Buszman P, Trznadel S, Linke A, Lenk K, Ischinger T, Klauss V, Eberli F, Corti R, Wijns W, Morice MC, di Mario C, Davies S, van Geuns RJ, Eerdmans P, Van Es GA, Meier B, Juni P. Biolimus-eluting stent with biodegradable polymer versus sirolimus-eluting stent with durable polymer for coronary revascularisation (LEADERS): a randomised non-inferiority trial. *Lancet* 2008;372:1163-1173.
9. Barlis P, Regar E, Serruys PW, Dimopoulos K, van der Giessen WJ, van Geuns RJ, Ferrante G, Wandel S, Windecker S, Van Es GA, Eerdmans P, Juni P, di Mario C. An optical coherence tomography study of a biodegradable vs. durable polymer-coated limus-eluting stent: a LEADERS trial sub-study. *Eur Heart J* 2010;31:165-176.
10. Gonzalo N, Tearney GJ, Serruys PW, van Soest G, Okamura T, Garcia-Garcia HM, van Geuns RJ, van der Ent M, Ligthart JM, Bouma BE, Regar E. Second-generation optical coherence tomography in clinical practice. High-speed data acquisition is highly reproducible in patients undergoing percutaneous coronary intervention. *Rev Esp Cardiol* 2010;63:893-903.
11. Gonzalo N, Garcia-Garcia HM, Serruys PW, Commissaris KH, Bezerra H, Gobbens P, Costa M, Regar E. Reproducibility of quantitative optical coherence tomography for stent analysis. *EuroIntervention* 2009;5:224-232.
12. Tanigawa J, Barlis P, di Mario C. Intravascular optical coherence tomography: optimisation of image acquisition and quantitative assessment of stent strut apposition. *EuroIntervention* 2007;3:128-136.
13. Gutierrez-Chico JL, van Geuns RJ, Regar E, van der Giessen WJ, Kelbaek H, Saunamaki K, Escaned J, Gonzalo N, Di MC, Borgia F, Nuesch E, Garcia-Garcia HM, Silber S, Windecker S, Serruys PW. Tissue coverage of a hydrophilic polymer-coated zotarolimus-eluting stent vs. a fluoropolymer-coated everolimus-eluting stent at 13-month follow-up: an optical coherence tomography substudy from the RESOLUTE All Comers trial. *Eur Heart J* 2011;(e-pub ahead of print).

14. Gutiérrez-Chico JL, Regar E, Nüesch E, Okamura T, Wykrzykowska JJ, di Mario C, Windecker S, van Es GA, Gobbens P, Jüni P, Serruys PW. Delayed coverage in malapposed and side-branch struts with respect to well-apposed struts in drug-eluting stents: in vivo-assessment with optical coherence tomography. *Circulation* 2011;(E-pub ahead of print).
15. Templin C, Meyer M, Muller MF, Djonov V, Hlushchuk R, Dimova I, Flueckiger S, Kronen P, Sidler M, Klein K, Nicholls F, Ghadri JR, Weber K, Paunovic D, Corti R, Hoerstrup SP, Luscher TF, Landmesser U. Coronary optical frequency domain imaging (OFDI) for in vivo evaluation of stent healing: comparison with light and electron microscopy. *Eur Heart J* 2010;31:1792-1801.
16. Katoh H, Shite J, Shinke T, Matsumoto D, Tanino Y, Ogasawara D, Sawada T, Miyoshi N, Kawamori H, Yoshino N, Hirata K. Delayed neointimalization on sirolimus-eluting stents: 6-month and 12-month follow up by optical coherence tomography. *Circ J* 2009;73:1033-1037.
17. Takano M, Yamamoto M, Mizuno M, Murakami D, Inami T, Kimata N, Murai K, Kobayashi N, Okamatsu K, Ohba T, Seino Y, Mizuno K. Late vascular responses from 2 to 4 years after implantation of sirolimus-eluting stents: serial observations by intracoronary optical coherence tomography. *Circ Cardiovasc Interv* 2010;3:476-483.
18. Awata M, Kotani Ji, Uematsu M, Morozumi T, Watanabe T, Onishi T, Iida O, Sera F, Nanto S, Hori M, Nagata S. Serial Angioscopic Evidence of Incomplete Neointimal Coverage After Sirolimus-Eluting Stent Implantation: Comparison With Bare-Metal Stents. *Circulation* 2007;116:910-916.
19. Haudenschild CC, Schwartz SM. Endothelial regeneration. II. Restitution of endothelial continuity. *Lab Invest* 1979;41:407-418.
20. Reidy MA, Schwartz SM. Endothelial regeneration. III. Time course of intimal changes after small defined injury to rat aortic endothelium. *Lab Invest* 1981;44:301-308.
21. Bjorkerud S, Bondjers G. Arterial repair and atherosclerosis after mechanical injury. 5. Tissue response after induction of a large superficial transverse injury. *Atherosclerosis* 1973;18:235-255.
22. Reidy MA, Standaert D, Schwartz SM. Inhibition of endothelial cell regrowth. Cessation of aortic endothelial cell replication after balloon catheter denudation. *Arteriosclerosis* 1982;2:216-220.
23. Reidy MA, Clowes AW, Schwartz SM. Endothelial regeneration. V. Inhibition of endothelial regrowth in arteries of rat and rabbit. *Lab Invest* 1983;49:569-575.
24. Takano M, Yamamoto M, Xie Y, Murakami D, Inami S, Okamatsu K, Seimiya K, Ohba T, Seino Y, Mizuno K. Serial long-term evaluation of neointimal stent coverage and thrombus after sirolimus-eluting stent implantation by use of coronary angioscopy. *Heart* 2007;93:1533-1536.
25. Takano M, Inami S, Jang IK, Yamamoto M, Murakami D, Seimiya K, Ohba T, Mizuno K. Evaluation by optical coherence tomography of neointimal coverage of sirolimus-eluting stent three months after implantation. *Am J Cardiol* 2007;99:1033-1038.
26. Takano M, Yamamoto M, Inami S, Murakami D, Seimiya K, Ohba T, Seino Y, Mizuno K. Long-Term Follow-Up Evaluation After Sirolimus-Eluting Stent Implantation by Optical Coherence Tomography: Do Uncovered Struts Persist? *Journal of the American College of Cardiology* 2008;51:968-969.
27. Simon C, Palmaz JC, Sprague EA. Influence of topography on endothelialization of stents: clues for new designs. *J Long Term Eff Med Implants* 2000;10:143-151.
28. Kastrati A, Mehilli J, Pache J, Kaiser C, Valgimigli M, Kelbaek H, Menichelli M, Sabaté M, Suttorp MJ, Baumgart D, Seyfarth M, Pfisterer ME, Schömig A. Analysis of 14 Trials Comparing Sirolimus-Eluting Stents with Bare-Metal Stents. *New England Journal of Medicine* 2007;356:1030-1039.

"Wissenschaft und Kunst gehören der Welt an, und vor ihnen verschwinden die Schranken der Nationalität".

(Science and art belong to the whole world, and before them vanish the barriers of nationality)

Conversation with a German historian

Johann Wolfgang von Goethe

PART 7

BIORESORBABLE SCAFFOLDS

CHAPTER 9

Structural defects affecting optical backscattering

Spatial distribution and temporal evolution of scattering centers by optical coherence tomography in the poly(L-lactide) backbone of a bioresorbable vascular scaffold.

Gutiérrez-Chico JL, Radu M, Diletti R, Sheehy A, Kossuth MB, Oberhauser JP, Glauser T, Harrington J, Rapoza R, Onuma Y, Serruys PW.

Circ J 2012;76:342-350.

STRUCTURED ABSTRACT

Background: Scattering centers (SC) are often observed with optical coherence tomography (OCT) in some struts of bioresorbable vascular scaffolds (BVS). These SC might be caused by crazes in the polymer during crimping-deployment (more frequent at inflection points) or by other processes, like physiological loading or hydrolysis (eventually increasing with time). The spatial distribution and temporal evolution of SC in BVS might help to understand their meaning.

Methods and results: Three patients were randomly selected out of the 12 imaged with Fourier-domain OCT at both baseline and 6 months in the ABSORB cohort B study (NCT00856856). Frame-by-frame analysis of the SC distribution was performed using spread-out vessel charts, and the results between baseline and 6 months were compared. A total of 4328 struts were analyzed. At baseline and follow-up all SC appeared at inflection points. No significant difference was observed between baseline and 6 months in the number of SC struts (14.9 vs. 14.5%, p=0.754) or in the distribution of scattering centers. The proportion and distribution of SC did not vary substantially between the patients analyzed.

Conclusion: The SC observed in OCT imaging of the BVS are located exclusively at inflection points and do not increase with time. These findings strongly suggest that SC are due to crazes in the polymer during crimping-deployment, ruling out any major role of hydrolysis or other time-dependant processes.

Clinical trial registration: NCT00856856; URL: http://clinicaltrials.gov

Key words: Coronary stenosis; poly(lactide); drug-eluting stents; tomography, optical coherence.

INTRODUCTION

The Abbott Vascular bioresorbable vascular scaffold (BVS) (Santa Clara, CA, USA) consists of a semicrystalline poly(L-lactide) (PLLA) backbone and conformal coating of amorphous poly(D,L-lactide) (PDLLA) and the antiproliferative agent, everolimus. The molecular weight of the BVS polymers is degraded primarily through hydrolysis of the ester bonds present in each monomer subunit. Crystalline residues with characteristic dimension less than 2 µm are phagocytosed by macrophages. Ultimately, PLLA and PDLLA degrade to lactate, which is metabolised via the Krebs' cycle and other metabolic pathways(1), similarly to other biodegradable polymers(2). Complete polymer resorption occurs approximately two years after implantation(3;4). BVS is laser-cut from a single piece of polymer tubing and then crimped onto a balloon. The structural design of the BVS consists of 19 W-shaped *rings* connected longitudinally by straight *links* (Figure 1). BVS has delivered acceptable and durable clinical and angiographic results up to 2 years post-procedure when the scaffold has been completely resorbed(5;6).

Unlike metallic stents(2;7-11), the translucency of the processed polylactide used in the Abbott Vascular BVS makes it particularly suitable for optical coherence tomography (OCT) imaging. The optical radiation can penetrate the translucent polymer with significant backscattering occurring only at the borders of struts where the refractive index of the medium changes. Alternatively, the strut core has been characterized as a "black box"(3;5;6), signifying the absence of refractive index changes within the material (Figure 2). However, some OCT images show a focal hyperintense signal in the strut core without apparent contact with either the axial or transversal strut edges (Figure 2). The cause of this backscattering signal remains to be elucidated: it might reflect a change in the polymer optical properties induced by

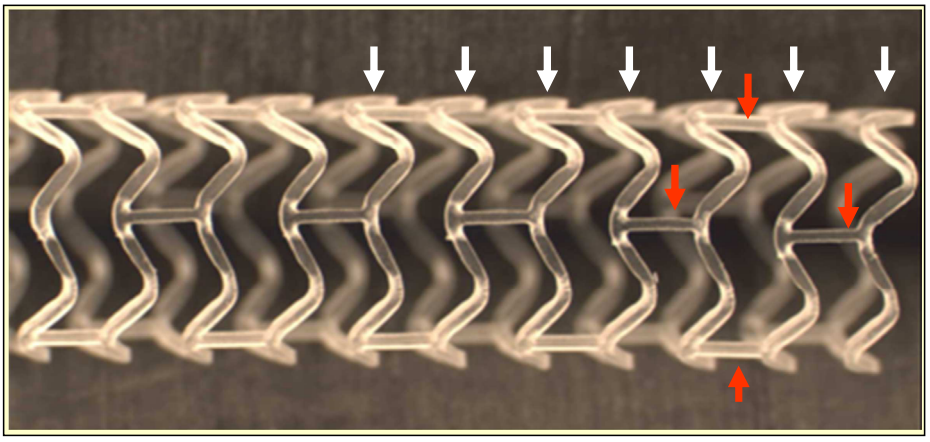

Figure 1: Structure of the Abbott Vascular bioresorbable vascular scaffold (BVS), revision 1.1.
An 18 mm length scaffold consists of 19 W-shaped rings (white arrows), connected with the adjacent rings by 3 straight longitudinal units (red arrows).

the hydrolysis process or they might correspond to deformation-induced crazes in backbone of the PLLA polymer, the latter preferentially located at hinge points of the BVS structure. The existence of regions with accelerated hydrolysis in humans or the presence of polymer crazes, eventually growing under continuous physiologic load, could both jeopardize the structural integrity of the BVS required to be functional.

This study explores the hypothesis that scattering centers (SC) observed in strut cores at baseline OCT imaging are derived from polymer crazing caused by the mechanical deformation of scaffold crimping and deployment, analyzing whether the spatial distribution of the SC at baseline is consistent with that hypothesis. The temporal evolution of these SC at 6

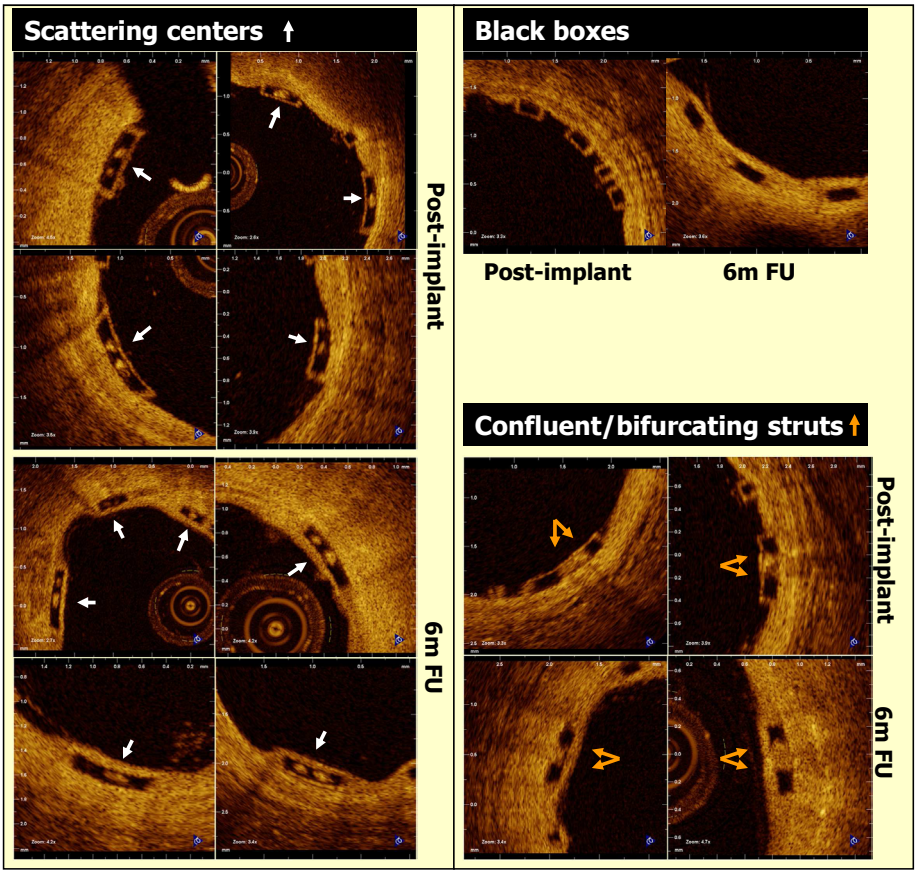

Figure 2: Definition of scattering centers (SC).
The struts classified as having SC present a focal hyperintense backscattering signal in the core of the strut that typically does not reach either the axial or the transversal strut edges, thus taking the appearance of a "dot" inside a box (left panel). Notice the difference with the typical "black box" appearance of the BVS struts (right panel, upper part). It is important to differentiate between SC from the optical appearance of confluent or bifurcating struts, where there is also a hyperintense signal in the core of the strut; however, in this case, it reaches its axial edges (right panel, lower part).

months permits to assess the eventual influence of physiological loading, polymer degradation, or tissue integration in the genesis of the SC.

METHODS

Study sample

The ABSORB Cohort B registry (NCT00856856) design has been published elsewhere.(3) The study enrolled patients older than 18 years, with diagnosis of stable or unstable angina pectoris or silent ischemia, and *de novo* lesions in native coronary arteries amenable for percutaneous treatment with the BVS (percent diameter stenosis ≥ 50% by visual estimation, reference vessel diameter of 2.5-3.5 mm). Exclusion criteria included: acute myocardial infarction, unstable arrhythmias, left ventricular ejection fraction ≤ 30%, restenotic lesions, lesions located in the left main coronary artery or in bifurcations involving a side branch > 2 mm, a second clinically or hemodynamically significant lesion in the target vessel, documentation of intracoronary thrombus, or initial TIMI 0 flow. For invasive follow-up purposes, the cohort was subdivided into two groups: cohort B1, undergoing multimodality invasive imaging (QCA, intravascular ultrasound, virtual histology, palpography, and OCT) at 6 and 24 months; and cohort B2, with identical imaging follow-up protocol scheduled at 12 and 36 months. All of the study lesions were treated with the BVS Revision 1.1 design 3.0 x 18 mm (Figure 1). The registry was approved by the ethics committee at each participating institution, and each patient gave written informed consent before inclusion.

For the present pilot study, a random sample of 3 patients in the cohort B1 was selected among those patients on whom OCT imaging had been performed with a Fourier-domain C7 system (Lightlab Imaging, Westford, Massachusetts, USA) at baseline and at the 6-month follow-up.

OCT study

OCT pullbacks were obtained at baseline and follow-up with a Fourier-domain C7 system using a Dragonfly catheter (Lightlab Imaging, Westford, Massachusetts, USA) at a rotation speed of 100 frames/second with non-occlusive technique(12). After infusion of intracoronary nitroglycerine, the imaging wire was withdrawn by a motorized pullback at a constant speed of 20 mm/second, while Iodixanol 320 contrast (Visipaque™, GE Health Care, Cork, Ireland) was infused through the guiding catheter at a continuous rate of 2-6 mL/min.

Two independent operators analyzed the selected OCT pullbacks offline using proprietary software (Lightlab Imaging, Westford, Massachusetts, USA). The region of interest was defined as that between the most distal and the most proximal frames in which struts could be detected by OCT. In this region of interest, a frame-by-frame analysis (0.2 mm longitudinal

intervals) was performed. In every cross-section the lumen contour was drawn and a marker set at the mid-point of the adluminal leading edge of each strut. The markers defined the circumferential position of the strut with respect to the gravitational center of the vessel as an angle, taking the position at 3 o'clock as the 0º reference.

Struts were labelled as containing SC if one or more focal hyperintense regions could be seen in the core of the strut, separated from the axial and transverse strut border interfaces. Struts with hyperintense central regions extending to the lumen border were considered to be related to the optical appearance of bifurcating/confluent struts but not classified as SC. In some of these cases, an indentation between the two bifurcating/confluent struts can be even identified (Figure 2). Two investigators classified the struts independently, and the discrepancies resolved by consensus.

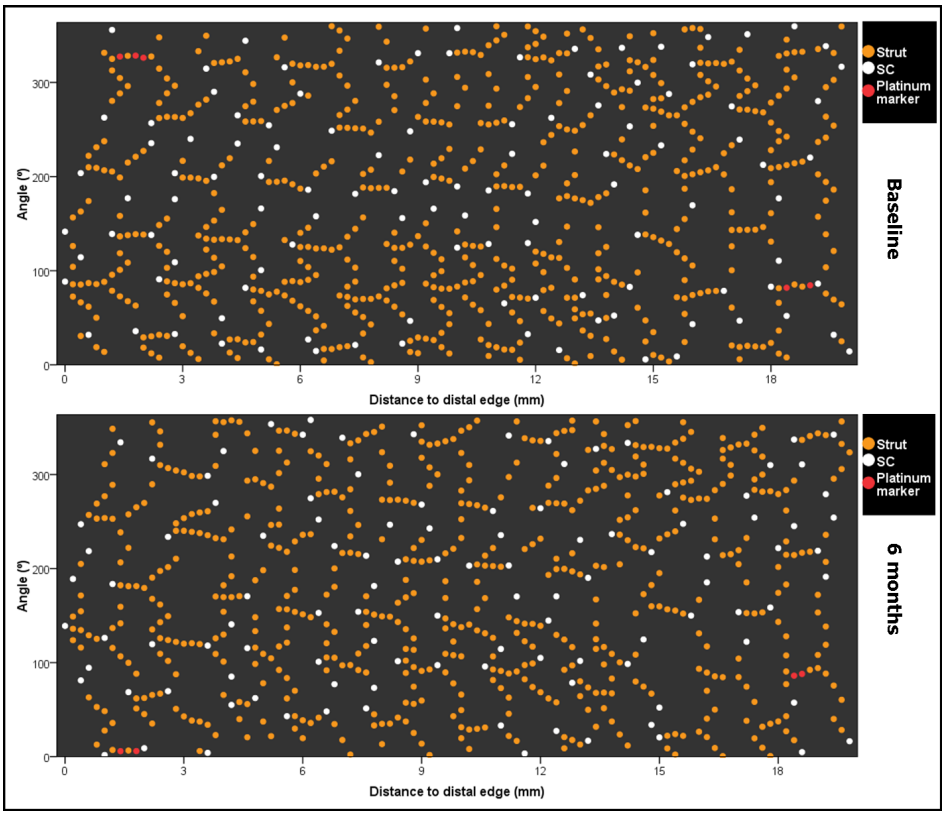

Figure 3: Spread-out vessel chart, patient 3.

Spread-out vessel graph showing the spatial distribution of the struts with scattering centers in the scaffolded vessel immediately post-implantation (baseline) and at the 6-month follow-up. The x-axis represents the distance from the distal edge of the stent to the strut; the y-axis represents the angle where the strut is located in the circular cross section respect to the centre of gravity of the vessel, taking as reference 0º the position at three o'clock. The result is a graphic representation of the spatial distribution of the struts along the scaffolded vessel as if it had been cut along the reference angle (0º) and spread out on a flat surface.

Spread-out vessel charts

The spatial distribution of the struts along the scaffolded vessel was analyzed through spread-out vessel charts. These graphics were obtained by correlating the longitudinal distance of each strut from the distal edge of the scaffold (abscises) with the angle defining its circumferential position with respect to the center of gravity of the vessel (ordinates) in each OCT pullback(13;14). The resulting charts represent the scaffolded vessel as if it had been cut longitudinally along the reference angle 0º and spread out on a flat surface (Figure 3).

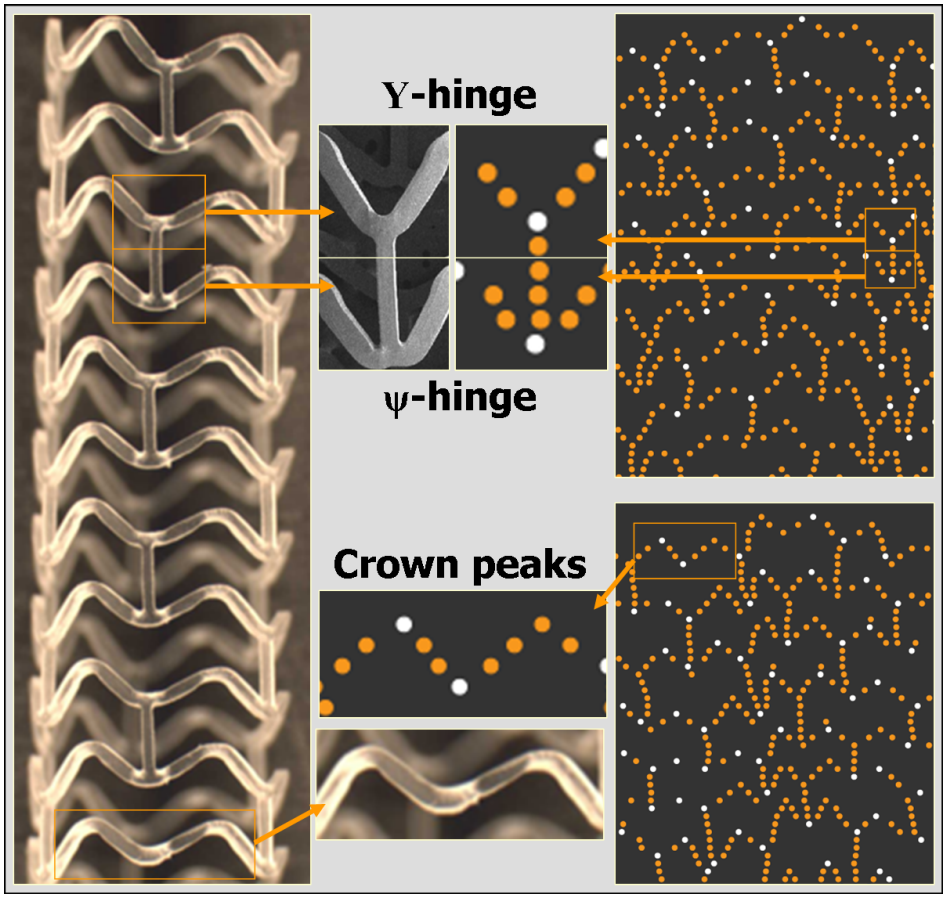

Figure 4: Schematic representation of the three different types of hinges in the scaffold structure and their locations in the spread-out vessel diagram.

The longitudinal connectors between the rings define inflection points that include ψ- and Y-hinges (see schematic). Angulations in the zig-zag ring at a point where there is no longitudinal connector are denominated "crown peaks". The scaffold has 19 rings; each ring contains three ψ-hinges, three Y-hinges and six crown peaks, except the most distal ring (three ψ-hinges and nine crown peaks) and the most proximal ring (three Y-hinges and nine crown peaks).

Inflection points (hinges) analysis

The results displayed on the spread-out vessel charts permit the visual identification of the different inflection points(15) in the scaffold structure. The inflection points were classified into three types (Figure 4): 1) ψ-hinges (psi-hinges) at the distal part of a longitudinal connector, where the angle between the connector and the W-shaped ring is acute; 2) Υ-hinges (ipsilon-hinges) at the proximal part of a longitudinal connector, where the angle between the connector and the W-shaped ring is obtuse; 3) crown peaks, hinges in the W-shaped rings at inflection points with no longitudinal connector. A 3.0 x 18 mm BVS consists of 19 W-shaped rings, 54 longitudinal connectors and 120 crown peaks. In each BVS ring three ψ-hinges, three Υ-hinges, and six crown peaks can be identified, except in the most distal (three ψ-hinges and nine crown peaks) and the most proximal (three Υ-hinges and nine crown peaks).

At least four points are required to define the shape of ψ or Υ, while three points are sufficient to define the shape of a crown peak. A hinge was considered associated with scattering centers if a SC appeared in any of the struts minimally required to define the hinge shape around the inflection point.

Individual tracking of the temporal evolution of each hinge was performed by matching the hinges in the spread-out vessel charts at baseline and 6-month follow-up.

Bench Analysis

Devices from the same design as BVS cohort B were utilized for bench evaluation. Scaffolds were analyzed under light microscopy for the presence of enhanced opacity due to scattering. Three uncrimped and three deployed devices were examined with optical microscopy (Keyence VHX-600) with incident light to maximize scattering within the bulk of the polymer and minimize surface reflection. Scattering centers were defined as areas of whitening greater than 20μm in diameter (figure 5). The spatial distribution of scattering centers along the scaffolded vessel was recorded through spread-out vessel charts.

Statistical analysis

The fraction of struts and hinge points with scattering centers was calculated and the results compared with Pearson's chi-square test. The ability of OCT to track SC hinges between baseline and follow-up pullbacks of the same patient was tested with a weighted kappa coefficient for the number count of white dotted hinges per ring. Interobserver variability for the count of struts and of struts containing SC was calculated per cross section by Kendall's tau b and Spearman correlations. All the analyses and graphics were performed with the PASW 17.0.2 statistical package (SPSS Inc., Chicago, IL, USA).

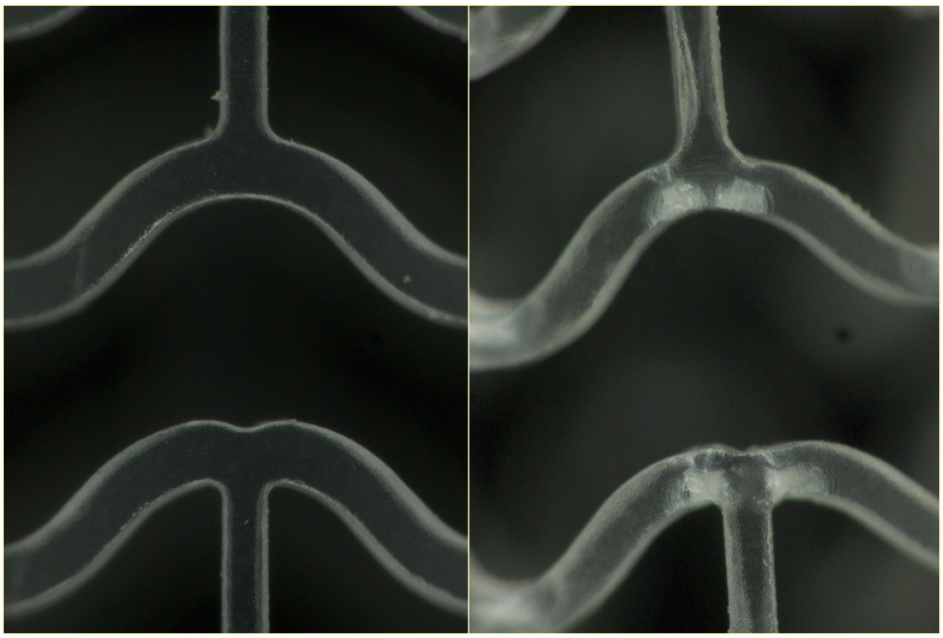

Figure 5: Representative images from bench analysis of pre-crimp (upper panel) and post-deployment (lower panel), showing the stress whitening at hinge points.
Before crimp/deployment, scaffolds appeared transparent under optical microscopy. After deployment, scattering evidenced by increased opacity was observed at all hinge regions of the device.

RESULTS

24 patients in the ABSORB cohort B1 received OCT at baseline and the 6-month follow-up; in 12 of these cases, the images were acquired with a Fourier-domain C7 system. No case was excluded from the analysis due to image quality issues. From these 12 cases, three were randomly selected for the spatial and temporal analysis of the SC. In all cases but one (patient 1, baseline OCT), the operator removed the guidewire before starting the OCT pullback to improve the image quality.

A total or 4328 struts were analyzed, 1502 in patient 1 (718 at baseline, 784 at 6 months), 1403 in patient 2 (700 at baseline, 703 at 6 months) and 1423 in patient 3 (728 at baseline, 695 at 6 months). The interobserver agreement was excellent for the count of struts per cross-section (Kendall's tau-b= 0.872, Spearman rho=0.932 at baseline, $p<0.001$; Kendall's tau-b= 0.851, Spearman rho=0.912 at follow-up, $p<0.001$), and for the count of struts containing SC (Kendall's tau-b= 0.936, Spearman rho=0.959 at baseline, $p<0.001$; Kendall's tau-b= 0.954, Spearman rho=0.971 at follow-up, $p<0.001$). Analyst 1 tended to count on average 0.18 struts more per cross-section than analyst 2 at baseline ($p=0.014$), and 0.22 struts more at follow-up ($p=0.04$). No significant interobserver bias was detected in the count of struts with SC.

Analysis of the proportion of SC with respect to the total number of struts showed no significant difference between baseline and follow-up in any of the patients (table 1). No significant difference in the proportion of SC was found between patients at any time point.

Figure 4 and suppl. figures 1-2 present the spread-out vessel charts at baseline and 6-month follow-up of the three patients. All of the SC were located around hinges; no SC was detected in straight segments. Some hinges were sliced in different cross-sections, due to the coincidence with systolic cardiac motion; in those cases it can be seen that the SC are located in the inner curvature of the bending (acute angle), without corresponding SC in the outer curvature (obtuse angle) (figure 6).

Table 1: Proportion of struts with scattering centers immediately post-implantation and at the 6-month follow-up.

		Post-implant	6 months	p-value
Patient 1	**Nr struts**	718	784	0.919
	SC	91 (12.7%)	98 (12.5%)	
Patient 2	**Nr struts**	700	703	0.586
	SC	116 (16.6%)	109 (15.5%)	
Patient 3	**Nr struts**	728	695	0.818
	SC	112 (15.4%)	110 (15.8%)	
TOTAL	**Nr struts**	2146	2182	0. 754
	SC	319 (14.9%)	317 (14.5%)	
Patient 1 vs. Patient 2 (p-value)		0.106	0.130	

SC: Scattering Centers
Cells are n (%)

A comparison of the proportion of SC hinges did not show any significant difference between baseline and follow-up or between patients (table 2).

Visual analysis of figures 4-6 highlights the difficulty of tracking specific SC between baseline and the 6-month follow-up. The spatial distribution of SC does not match exactly, suggesting that different features are revealed with any given pullback. To assess the ability to match the SC location at the two time points, the agreement in the number count of white-dotted hinges per ring between baseline and follow-up was tested with a weighted kappa., that showed very poor agreement between the different hinges: best agreement for ψ-hinges (weighted kappa range 0.23 – 0.62), for the rest of hinges, weighted kappa <0.34 (suppl table 1).

In the bench study a total of 684 hinge regions in each group of uncrimped and deployed devices were evaluated by optical microscopy. Analysis revealed the complete absence of SC in uncrimped devices at all regions. In contrast, after deployment, there were SC at all hinge regions (Figure 3).

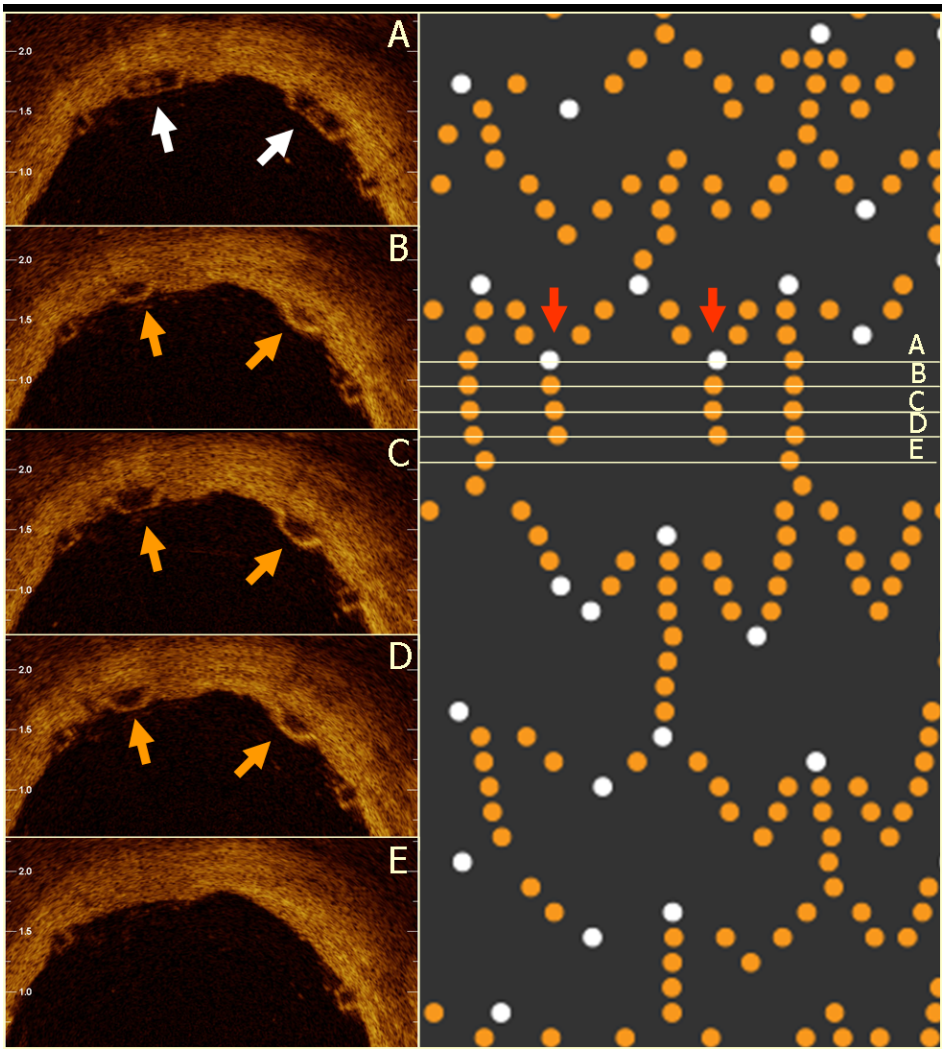

Figure 6: Hinges sliced in different cross section due to the coincidence with systolic cardiac motion (vessel and catheter moving in the same direction).
The image shows two crown peaks with scattering centers and illustrates how the scattering is located in the inner curvature of the hinge (right part, red arrows; panel A), with no scattering in the slices corresponding to the outer curvature (B to E).

DISCUSSION

In this study we use a novel methodology for analyzing morphological changes in the polymeric scaffold of a BVS using OCT. The spread-out vessel charts have been previously described in trials comparing the performance of intracoronary devices using OCT per strut analysis(13;14;16). They are simple and intuitive graphic representations of the spatial distribution and clustering of the studied phenomenon, in this case of the SC along the BVS, pro-

Table 2: Number and percentage of struts characterized by the presence of scattering centers immediately post-implantation and at the 6-month follow-up.

		Post-implant	6 months	p-value
Patient 1*	ψ-hinges n=54	27 (54.0%)	33 (61.1%)	0.463
	Y-hinges n=54	25 (49.0%)	27 (50.0%)	0.920
	Crown peaks n=120	36 (31.6%)	37 (30.8%)	0.902
	All inflection points n=228	88 (40.9%)	97 (42.5%)	0.731
Patient 2	ψ-hinges n=54	34 (63.0%)	36 (66.7%)	0.687
	Y-hinges n=54	25 (46.3%)	25 (46.3%)	1.000
	Crown peaks n=120	53 (44.2%)	45 (37.5%)	0.293
	All hinges n=228	112 (49.1%)	106 (46.5%)	0.574
Patient 3	ψ-hinges n=54	38 (70.4%)	41 (75.9%)	0.515
	Y-hinges n=54	21 (38.9%)	27 (50.0%)	0.245
	Crown peaks n=120	53 (43.3%)	42 (35.0%)	0.186
	All hinges n=228	111 (48.7%)	110 (48.2%)	0.925
Between patients (p-value)	ψ-hinges	0.226	0.250	
	Y-hinges	0.555	0.906	
	Crown peaks	0.091	0.547	
	All hinges	0.154	0.457	

Cells are n (%)

* In patient 1 only 50 ψ-hinges, 51 Y-hinges and 114 crown peaks were analyzable at baseline, due to the presence of a guidewire in the pullback. (Table presents corrected %).

viding insight into how the scaffold material may be changing over time post-implantation. This study is the first to use spread-out vessel charts as primary tool for detailed spatial analysis, and the results presented here prove its potential and motivate future development of the technique. This methodology may complement 3D-rendering technologies, which are appealing imaging tools but limited in analytical capability.

The spread-out vessel charts here presented also illustrate another unanticipated phenomenon, namely the effect of cardiac motion on the images obtained during the OCT pullback. One can see the elongation of the segments imaged in systole (when the vessel moves in the

same direction as the pullback catheter) and the compression of the segments imaged in diastole (when vessel and pullback move in opposite directions).

The visual analysis of the struts displayed in the spread-out vessel charts show that all of the SC are located at hinge points. OCT relies upon changes in refractive index on a length scale greater than that of the wavelength of light used in the instrument to create signal intensity(17;18). Thus, the presence of SC within the strut core is suggestive of the creation of new interfaces in the polymeric material, leading to microscopic changes in the refractive index. *In vivo*, mechanical deformation, polymer molecular weight degradation, and tissue integration are all potential causes of refractive index changes. The exclusive location of the SC at hinge points, strongly suggests that they represent micro-crazes in the polymer. Deformation-induced crazing has long been demonstrated in both amorphous and semicrystalline polymers(19). In semicrystalline polymers, crazes are typically microvoids traversed by fibrils in the direction of the applied stress, a combination that preserves the strength of the material while creating a discontinuity in the index of refraction(19-21). BVS undergoes varying magnitudes of mechanical deformation during crimping and deployment depending upon the location on the scaffold, but the highest strain (and stress) is experienced at the *hinge points*, the points about which the scaffold collapses and expands during crimping and deployment, respectively. Optically, this deformation manifests in the deployed device as *stress whitening* at the hinge points (Figure 3), which is also evidence of crazing. The spatial distribution of the SC in OCT parallels that of the crazing observed in optical microscopy, clustering around the hinge points and leaving the scaffold areas that experience little or no mechanical deformation as unblemished "black boxes".

Though hydrolysis is a natural part of PLLA degradation the presence of SC immediately post-implantation in a proportion comparable to that at the 6-month follow-up, likely rules out the involvement of hydrolysis in the genesis of these images during the first 6 months. Likewise, the similar proportion of SC at baseline and at the 6-months follow-up suggests that other processes, like physiological loading induce minimal crazing of the polymer after deployment. Therefore the structural integrity of the scaffold is not jeopardized by hydrolysis or crazing up to 6 month. The preservation of structural integrity, especially in the first 3 months after implantation (the so called "revascularization phase"), is of capital importance to counteract vessel recoil and adverse remodeling, hence to mantain the initial luminal gain(1). Our finding is consistent with the excellent clinical outcomes reported for the BVS to date(3;5;6).

Previous studies from our group attempted to track the individual SC between baseline and follow-up without success using 3D-rendering technologies (unpublished data). The current approach offers a clearer and more visual representation of the spatial location of the scattering centers, but still fails to track them individually between both time points. Furthermore, the poor agreement between baseline and follow-up regarding the SC count per ring discourages any further attempt of matching. At a rotation speed of 100 Hz and a pullback speed of 20 mm/s, any feature smaller than 200 μm will be difficult to capture in

multiple pullbacks, and the OCT study should be rather considered a random sampling of the study phenomenon. This might explain the failure to match individual SC, and also why OCT detected SC in only 43-49% of the hinges, even though light microscopy had shown stress-whitening in 100%. Consistent with this, OCT had the highest sensitivity for SC detection in the largest hinges (ψ-hinges: 61-76%) and the lowest sensitivity in the smallest hinges (crown peaks: 31-44%).

Limitations

The OCT longitudinal image co-registration is limited in this study due to the pullback and rotation speeds used in the acquisition, which are the standard for clinical applications with a Fourier-domain C7 system. This study is a retrospective analysis from patients included in a clinical study, aimed at interpreting intriguing imaging observations; therefore, the pullback speed could not be altered to examine the factors that may govern longitudinal co-registration. For *in vitro*, preclinical, or prospective designs, a slower pullback speed (e.g., 10 mm/s) would improve the ability to reproducibly observe features smaller than 200 μm and improve co-registration accuracy.

The presence of a guidewire in one of the pullbacks might affect the comparability of the OCT studies, since the projected shadow hides a random sector of the cross-section. We have minimised this problem by analyzing the proportion of SC with respect to the number of visible struts/hinges in the pullback.

The similarity between anomalous SC and the images generated by confluent or bifurcating struts might have affected the results. Although the defined analysis methodology attempted to differentiate between these essentially different images and showed excellent reproducibility, classification imprecision cannot be totally excluded.

The compression of the images during diastole made the reconstruction of the BVS structure difficult in some segments. Although the reconstruction was possible in all cases, following the pattern of the device, the accuracy of the analysis is hampered in those segments.

CONCLUSIONS

The scattering centers observed in the Abbott Vascular BVS are located exclusively at hinge points and present at baseline and 6-month follow-up in similar proportions, suggesting that these images may represent polymer crazing caused by the mechanical deformation of the crimping and deployment processes, likely ruling out any role of hydrolysis in their genesis. Consistent number and location of scattering centers between baseline and the 6-month follow-up suggests that physiological loading is not inducing further crazing on length scales greater than spatial resolution capability of OCT.

REFERENCE LIST

1. Oberhauser JP, Hossainy S, Rapoza RJ. Design principles and performance of bioresorbable polymeric vascular scaffolds. EuroIntervention Supplement 2009 Dec;5(Supplement F):F15-F22.
2. Kozuki A, Shite J, Shinke T, Miyoshi N, Sawada T, Hellig F, et al. STELLIUM 1: First-In-Man Follow-up Evaluation of Bioabsorbable Polymer-Coated Paclitaxel-Eluting Stent. Circ J 2010 Sep 24;74(10):2089-96.
3. Serruys PW, Onuma Y, Ormiston JA, De Bruyne B, Regar E, Dudek D, et al. Evaluation of the second generation of a bioresorbable everolimus drug-eluting vascular scaffold for treatment of de novo coronary artery stenosis: 6-month clinical and imaging outcomes. Circulation 2010 Nov 30;122(22):2301-12.
4. Onuma Y, Serruys PW, Perkins LE, Okamura T, Gonzalo N, Garcia-Garcia HM, et al. Intracoronary Optical Coherence Tomography and Histology at 1 Month and 2, 3, and 4 Years After Implantation of Everolimus-Eluting Bioresorbable Vascular Scaffolds in a Porcine Coronary Artery Model. An Attempt to Decipher the Human Optical Coherence Tomography Images in the ABSORB Trial. Circulation 2010 Nov 30;122(22):2288-300.
5. Ormiston JA, Serruys PW, Regar E, Dudek D, Thuesen L, Webster MW, et al. A bioabsorbable everolimus-eluting coronary stent system for patients with single de-novo coronary artery lesions (ABSORB): a prospective open-label trial. Lancet 2008 Mar 15;371(9616):899-907.
6. Serruys PW, Ormiston JA, Onuma Y, Regar E, Gonzalo N, Garcia-Garcia HM, et al. A bioabsorbable everolimus-eluting coronary stent system (ABSORB): 2-year outcomes and results from multiple imaging methods. Lancet 2009 Mar 14;373(9667):897-910.
7. Teramoto T, Ikeno F, Otake H, Lyons JK, van Beusekom HM, Fearon WF, et al. Intriguing peri-strut low-intensity area detected by optical coherence tomography after coronary stent deployment. Circ J 2010 May 25;74(6):1257-9.
8. Kim JS, Kim JS, Kim TH, Fan C, Lee JM, Kim W, et al. Comparison of neointimal coverage of sirolimus-eluting stents and paclitaxel-eluting stents using optical coherence tomography at 9 months after implantation. Circ J 2010 Feb;74(2):320-6.
9. Miyoshi N, Shite J, Shinke T, Otake H, Tanino Y, Ogasawara D, et al. Comparison by optical coherence tomography of paclitaxel-eluting stents with sirolimus-eluting stents implanted in one coronary artery in one procedure. - 6-month follow-up -. Circ J 2010 May;74(5):903-8.
10. Liu Y, Imanishi T, Kubo T, Tanaka A, Kitabata H, Tanimoto T, et al. Assessment by optical coherence tomography of stent struts across side branch. -Comparison of bare-metal stents and drug-elution stents.-. Circ J 2010 Dec 24;75(1):106-12.
11. Goto I, Itoh T, Kimura T, Fusazaki T, Matsui H, Sugawara S, et al. Morphological and quantitative analysis of vascular wall and neointimal hyperplasia after coronary stenting. - Comparison of bare-metal and sirolimus-eluting stents using optical coherence tomography-. Circ J 2011 Jun 24;75(7):1633-40.
12. Prati F, Cera M, Ramazzotti V, Imola F, Giudice R, Giudice M, et al. From bench to bedside: a novel technique of acquiring OCT images. Circ J 2008 May;72(5):839-43.
13. Gutierrez-Chico JL, van Geuns RJ, Regar E, van der Giessen WJ, Kelbaek H, Saunamaki K, et al. Tissue coverage of a hydrophilic polymer-coated zotarolimus-eluting stent vs. a fluoropolymer-coated everolimus-eluting stent at 13-month follow-up: an optical coherence tomography substudy from the RESOLUTE All Comers trial. Eur Heart J 2011 Jun 9;(e-pub ahead of print).
14. Gutiérrez-Chico J, van Geuns RJ, Koch K, Koolen J, Duckers HJ, Regar E, et al. Paclitaxel-coated balloon in combination with bare metal stent for treatment of de novo coronary lesions: an optical

coherence tomography first-in-human randomized trial balloon-first vs. stent first. EuroIntervention 2011;(e-pub ahead of print).
15. Sangiorgi G, Melzi G, Agostoni P, Cola C, Clementi F, Romitelli P, et al. Engineering aspects of stents design and their translation into clinical practice. Ann Ist Super Sanita 2007;43(1):89-100.
16. Gutiérrez-Chico J, Jüni P, García-García HM, Regar E, Nüesch E, Borgia F, et al. Long term tissue coverage of a biodegradable polylactide polymer-coated biolimus-eluting stent: comparative sequential assessment with optical coherence tomography until complete resorption of the polymer. Am Heart J 2011;(in press).
17. Schmitt JM. Optical Coherence Tomography (OCT): A Review. IEEE J Sel Top Quantum Electron 1999;5(4):1205-15.
18. Fujimoto J, Drexler W. Introduction to Optical coherence Tomography. Greenbaum E, editor. Biological and Medical Physics, Biomedical Engineering. [1], 1-45. 2008. Springer.
Ref Type: Serial (Book,Monograph)
19. Olf HG, Peterlin A. Crazing and fracture in crystalline, isotactic polypropylene and the effect of morphology, gaseous environments, and temperature. J Polym Sci Polym Phys Ed 1974;12(11):2209-51.
20. Kojima M. Stress whitening in crystalline propylene-ethylene block copolymers. Journal of Macromolecular Science, Part B: Physics 1981;19(3):523-41.
21. Liu Y, Kennard CHL, Truss RW, Calos NJ. Characterization of stress-whitening of tensile yielded isotactic polypropylene. Polymer 1997 May;38(11):2797-805.

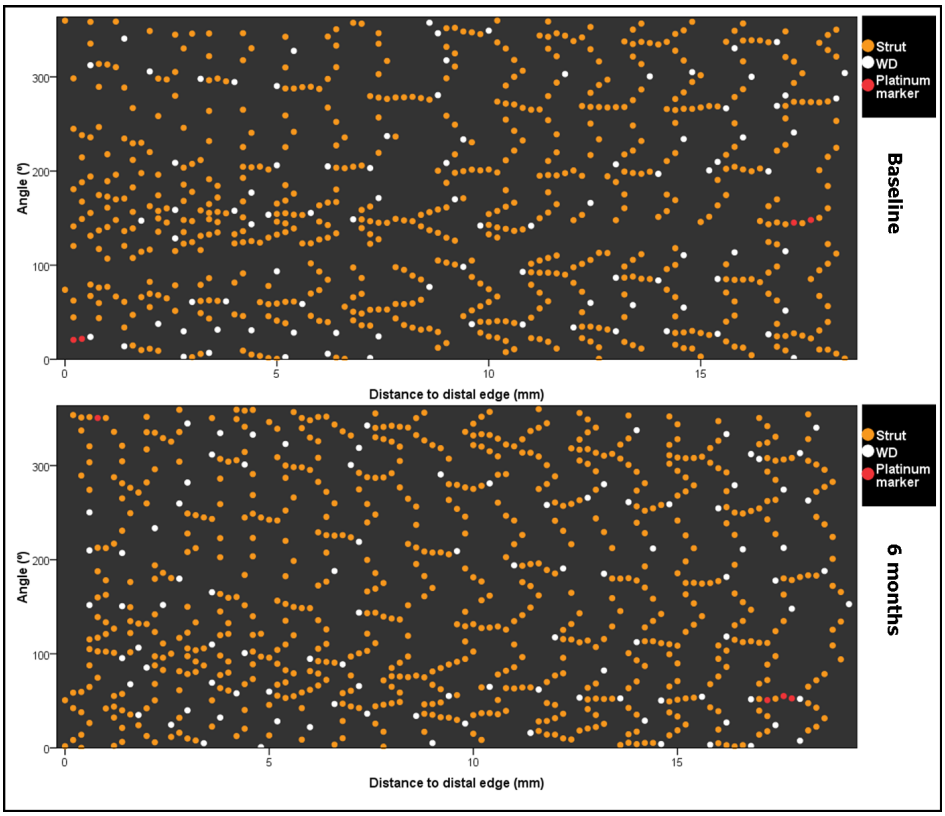

Suppl. figure 1: Spread-out vessel chart, patient 1.

Spread-out vessel graph showing the spatial distribution of the struts with scattering centers in the scaffolded vessel immediately post-implantation (baseline) and at the 6-month follow-up. The x-axis represents the distance from the distal edge of the stent to the strut; the y-axis represents the angle where the strut is located in the circular cross section respect to centre of gravity of the vessel, taking as reference 0º the position at three o'clock. The result is a graphic representation of the spatial distribution of the struts along the scaffolded vessel as if it had been cut along the reference angle (0º) and spread out on a flat surface. Notice the shadow corresponding to the presence of a guidewire in the baseline pullback.

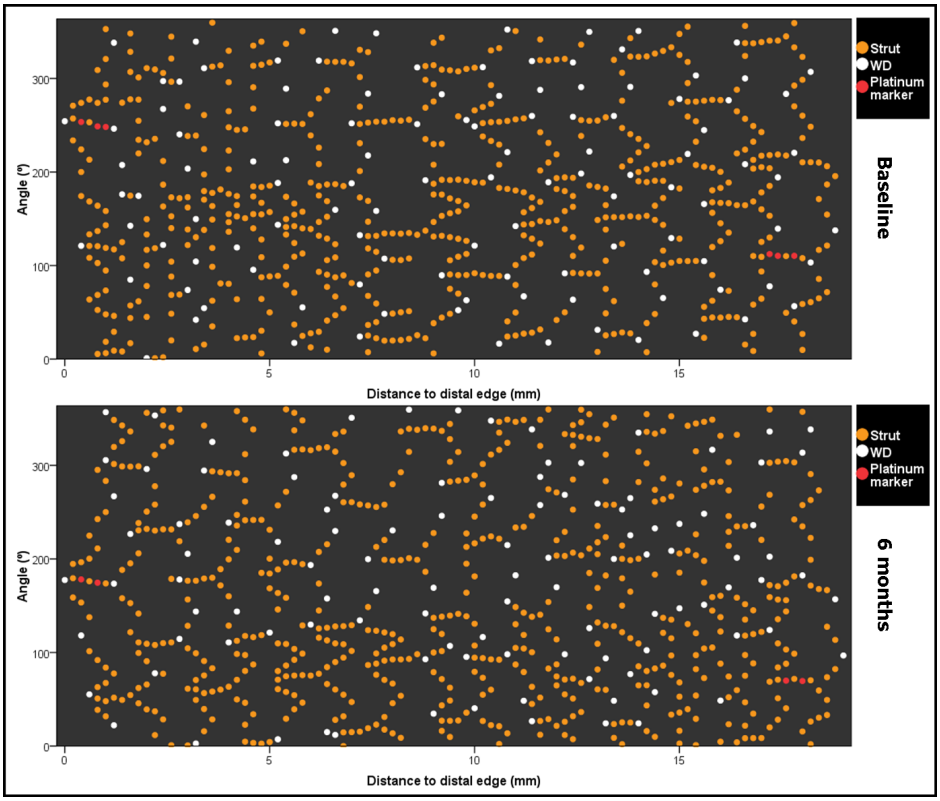

Suppl. figure 2: Spread-out vessel chart, patient 2.

Spread-out vessel graph showing the spatial distribution of the struts with scattering centers in the scaffolded vessel immediately post-implantation (baseline) and at the 6-month follow-up. The x-axis represents the distance from the distal edge of the stent to the strut; the y-axis represents the angle where the strut is located in the circular cross section respect to the centre of gravity of the vessel, taking as reference 0º the position at three o'clock. The result is a graphic representation of the spatial distribution of the struts along the scaffolded vessel as if it had been cut along the reference angle (0º) and spread out on a flat surface.

Suppl. table 1: Agreement on the number count of white-dotted hinge points per scaffold ring between baseline and the 6-month follow-up (n=19 scaffold rings): weighted kappa coefficient.

Agreement baseline vs. 6 months: Weighted kappa (n=19 scaffold rings)		Estimate	95% CI	
			Lower	Upper
Patient 2	**ψ-hinges**	0.23	-0.20	0.67
	Y-hinges	0.07	-0.38	0.52
	Crown peaks	-0.25	-0.58	0.07
	All hinges	-0.51	-0.86	-0.15
Patient 3	**ψ-hinges**	0.62	0.27	0.97
	Y-hinges	0.34	-0.01	0.69
	Crown peaks	0.05	-0.20	0.31
	All hinges	-0.12	-0.34	0.16

CHAPTER 10

Volumetric peculiarities of the BVS

Quantitative multi-modality imaging analysis of a fully bioresorbable stent: a head-to-head comparison between QCA, IVUS and OCT.

Gutiérrez-Chico JL, Serruys PW, Girasis C, Garg S, Onuma Y, Brugaletta S, Garcia-Garcia H, Van Es GA, Regar E.

Int J Cardiovasc Imaging 2012; 28: 467-478.

STRUCTURED ABSTRACT

Background: The bioresorbable vascular stent (BVS) is totally translucent and radiolucent, leading to challenges when using conventional invasive imaging modalities. Agreement between quantitative coronary angiography (QCA), intravascular ultrasound (IVUS) and optical coherence tomography (OCT) in the BVS is unknown.

Methods and results: 45 patients enrolled in the ABSORB cohort B1 study underwent coronary angiography, IVUS and OCT immediately post BVS implantation, and at 6 months. OCT estimated stent length accurately compared to nominal length (95% CI of the difference: -0.19; 0.37 and -0.15; 0.47mm^2 for baseline and 6 months, respectively), whereas QCA incurred consistent underestimation of the same magnitude at both time points (Pearson correlation = 0.806). IVUS yielded low accuracy (95% CI of the difference: 0.77; 3.74 and -1.15; 3.27mm^2 for baseline and 6 months, respectively), with several outliers and random variability test-retest. Minimal lumen area (MLA) decreased substantially between baseline and 6 months on QCA and OCT and only minimally on IVUS (95% CI: 0.11; 0.42). Agreement between the different imaging modalities is poor: worst agreement Videodensitometry-IVUS post-implantation (ICCa 0.289); best agreement IVUS-OCT at baseline (ICCa 0.767). All pairs deviated significantly from linearity ($p<0.01$). Passing-Bablok non-parametric orthogonal regression showed constant and proportional bias between IVUS and OCT.

Conclusion: OCT is the most accurate technique for measuring stent length, whilst QCA incurs systematic underestimation (foreshortening) and solid state IVUS incurs random error. Volumetric calculations using solid state IVUS are therefore not reliable. There is poor agreement for MLA estimation between all the imaging modalities studied, including IVUS-OCT, hence their values are not interchangeable.

Clinical trial registration: NCT00856856; URL: http://clinicaltrials.gov/ct2/results?term=NCT00856856

Key words: Coronary angiography; poly(lactide); quantitative coronary angiography; intravascular ultrasound; Tomography, optical coherence.

INTRODUCTION

The Bioresorbable Vascular Stent (BVS) (Abbott Vascular, Santa Clara, CA, USA) consists of a semi-crystalline poly-L-lactide (PLLA) backbone, coated by a thin amorphous layer of poly-D,L-lactide (PDLLA) containing the antiproliferative agent everolimus. The device has enough radial strength to counteract vascular recoil after angioplasty, while the sustained elution of everolimus inhibits neointimal hyperplasia. BVS struts are progressively degraded by hydrolysis and fully resorbed 2 years after implantation[1]. Two small platinum markers at the proximal and distal edges ease fluoroscopic visualization during deployment and angiographic follow-up.

In contrast to metallic stents, the BVS is translucent to optical radiation and totally radiolucent to gamma radiation, with the only exception the radiopaque platinum markers at the edges. Therefore, imaging the BVS with optical coherence tomography (OCT) or quantitative coronary angiography (QCA) requires a specific approach. In the case of QCA, videodensitometry (VD) is particularly interesting because the radiodensity of metallic stents leads to overestimation of minimal lumen area (MLA)[2], which the BVS can theoretically circumvent.

The BVS has been clinically tested in multi-national studies involving highly specialized centres[1,3,4] with multiple imaging techniques, including intravascular ultrasound (IVUS)[1,3-5], three-dimensional QCA[5], multi-slice computed tomography (MSCT)[5] and OCT[1,3,4]. Nevertheless, in anticipation of the forthcoming widespread availability of the BVS, comprehensive comparative studies are needed for the correct interpretation of these results. Recent studies have compared QCA with MSCT immediately after stent deployment[5], however they included neither IVUS or OCT, or the comparison between VD and edge detection (ED). Furthermore they also failed to provide any data on the eventual influence of shrinkage or resorption on the imaging parameters.

The present study compares different imaging modalities in the BVS immediately after implantation and at 6 months. This time point represents the transition between the restoration phase (loss of structural integrity, restoration of vascular reactivity) and the resorption phase (loss of mass) of the device[6]. Stent length and MLA were the parameters chosen for the head-to-head comparison: the former for being stable with time and known a priori, the latter for being the most clinically relevant[7-9].

METHODS

Study sample

The design of the ABSORB Cohort B study (NCT00856856) has been previously described[4]. It enrolled patients with stable/unstable angina pectoris or silent ischemia, due to *de novo*

coronary lesions amenable for percutaneous treatment with the BVS: diameter stenosis ≥50% and reference vessel diameter 2.5-3.5mm. Major exclusion criteria were: acute myocardial infarction, unstable arrhythmias, left ventricular ejection fraction ≤ 30%, restenotic lesions, lesions located in the left main or in bifurcations involving a side branch >2 mm, a second clinically or hemodynamically significant lesion in the target vessel, intracoronary thrombus, or initial TIMI flow 0. The cohort was subdivided in two groups: cohort B1 underwent multi-modality invasive imaging (QCA, IVUS, virtual histology, palpography and OCT) at 6 and 24 months; whereas cohort B2 underwent an identical imaging follow-up protocol scheduled at 12 and 24 months. The availability of the different imaging modalities varied depending on the sites. All the study lesions were treated with the BVS revision 1.1 (3.0 x 18 mm). The registry was approved by the ethics committee at each participating institution and each patient gave written informed consent before inclusion.

The present study compares the multi-imaging results of cohort B1 (figure 1), post-implantation and at 6 months, analyzed in a core-lab setting (Cardialysis BV, Rotterdam, The Netherlands).

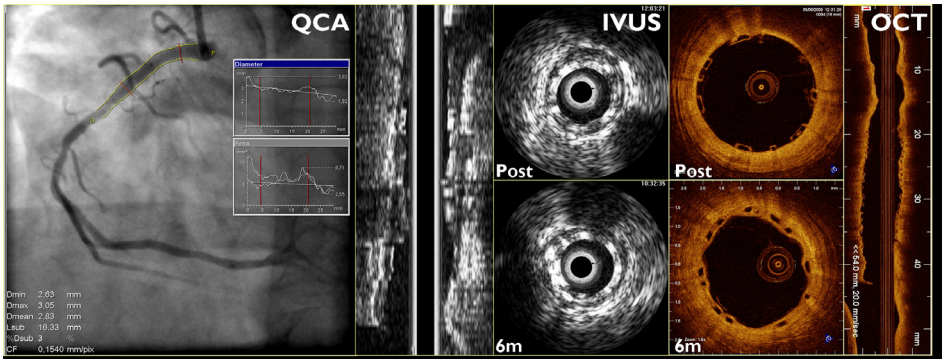

Figure 1: Case example illustrating the three imaging modalities compared in this study: quantitative coronary angiography (QCA), phased array solid state intravascular ultrasound (IVUS) and optical coherence tomography (OCT).

Angiography and QCA analysis

Coronary arteriography was performed according to standard procedures[10], using consecutive single-plane orthogonal projections of the target lesion. QCA was performed with the CAAS II system[11] (Pie Medical BV, Maastricht, The Netherlands). The small radiopaque markers at the ends of the stent helped with the localisation of the radiolucent device for definition of the in-stent segment. In-stent MLA by VD was automatically calculated by the software through densitometric analysis. In-stent MLA by ED was calculated from the in-stent minimal lumen diameter (MLD), which was provided by the software, using the formula: MLA = 3.14 * $(MLD/2)^2$.

IVUS study

The stented segments were examined with phased array solid state IVUS catheters (EagleEye; Volcano Corporation, Rancho Cordova, CA, USA) with an automated pullback at 0.5 mm/s. A region of interest beginning 5 mm distal and extending 5 mm proximal to the stented segment was defined for off-line analysis. Areas were measured with a validated computer-based contour detection programme (CURAD BV, Wijk bij Duurstede, The Netherlands) that allows for semi-automatic detection of lumen, stent and vessel boundaries in longitudinally reconstructed views of the region of interest[12,13].

OCT study

OCT pullbacks were obtained with M2, M3 or C7 systems (Lightlab Imaging, Westford, Massachusetts, USA), depending on the site, using the occlusive[14] or non-occlusive technique[15], as appropriate. Supplement table 1 provides detailed technical specifications for each system. OCT cross-sections were analysed offline at 1mm longitudinal intervals within the stented segment and 5mm proximal and distal to the stent edges, using proprietary software (Lightlab Imaging, Westford, Massachusetts, USA). Lumen contour was automatically detected and manually edited if needed. OCT in-stent MLA was defined as the minimal lumen area in the segment between the distal and proximal tips of the stent.

Statistical analysis

Descriptive statistics and Saphiro-Wilks test for normality of the distribution were reported for each variable. Means were compared with t-test for paired samples.

For MLA, agreement between methods was tested by intraclass correlation coefficients (for absolute agreement and consistency). Passing-Bablok non-parametric orthogonal regression analysis was performed in order to detect constant or proportional biases between imaging modalities, using OCT values in the y axis, since it has been validated in vitro and in vivo for measurement of lumen area[16,17] and showed the best reproducibility of all the methods hitherto[18-20]. Systematic constant or proportional biases were defined as a constant or a slope significantly different than 0 or 1 in the orthogonal regression equation, respectively. CUSUM test for deviation from linearity respect to the orthogonal regression equation was performed, and absolute agreement tested with Lin's coefficient.

For stent length no proper analysis of agreement between methods could be performed because all the cases in the sample had the same objective measurement (18mm). Test-retest variability was assessed graphically with a "target chart", correlating MLA measurements post-implantation with those at 6 months follow-up, and drawing the corresponding refer-

ence lines at 18mm. The intersection of both reference lines defines the centre of a target corresponding to the methods measuring exactly 18mm of length at both time points.

All the analyses and graphics were performed with the PASW 17.0.2 statistical package (SPSS Inc., Chicago, IL, USA).

RESULTS

Immediately post-stenting, QCA analysis was available in 45 patients, IVUS in 40, OCT in 29 and all the imaging techniques together in 26 patients. At 6 months follow-up, QCA was available in 42, IVUS in 40, OCT in 28 and the three techniques in 27 patients.

Table 1 shows the descriptive statistics of the stent length measured by the different imaging modalities. Figures 1 and 2 show the box-plot distribution and the individual measurements, with a reference line at 18mm (nominal length of the stent). QCA underestimates length, whilst OCT remains very close to the nominal value, with very low variability. Solid state IVUS shows the lowest accuracy for length measurements, with wide dispersion and several outliers.

Table 1: Stent length measured by the different imaging modalities immediately post-stenting and at 6 months follow-up.

Stent length (mm)		n	Mean	Median	SD	P25	P75	Min	Max	Saphiro-Wilk
QCA	Post	26	14.62	14.49	1.40	14.09	15.43	11.64	17.63	0.285
	6m FU	27	15.01	14.69	1.60	13.86	16.18	12.67	17.81	0.153
IVUS	Post	26	20.26	19.89	3.67	17.69	21.90	13.02	29.35	0.127
	6m FU	27	19.06	19.14	5.59	17.29	20.82	7.99	34.20	0.060
OCT	Post	26	18.10	18.15	0.65	17.82	18.37	16.05	19.36	0.107
	6m FU	27	18.16	18.00	0.79	17.40	18.60	16.80	20.00	0.551

IVUS: Intravascular ultrasound; OCT: Optical Coherence Tomography; QCA: Quantitative Coronary Angiography; 6m FU: 6 months follow-up.

Table 2 shows the paired comparison of the means for length measurement, as a chess table. QCA significantly underestimates length compared to IVUS, OCT and to the nominal length, post implant (white squares) and at 6 months (orange squares). On the contrary, IVUS overestimates length with respect to OCT and the nominal value, only significantly at baseline.

Figure 3 shows the "target chart", depicting the test-retest variability between post-implant and 6 months follow-up for stent length measurements. QCA shows a typical systematic bias: variable underestimation of length in the different cases, but consistent underestimation of the same magnitude at both time points (Pearson correlation = 0.806; ICCa = 0.808; ICCc = 0.803), eventually due to the effect of foreshortening on length measurements. OCT proves

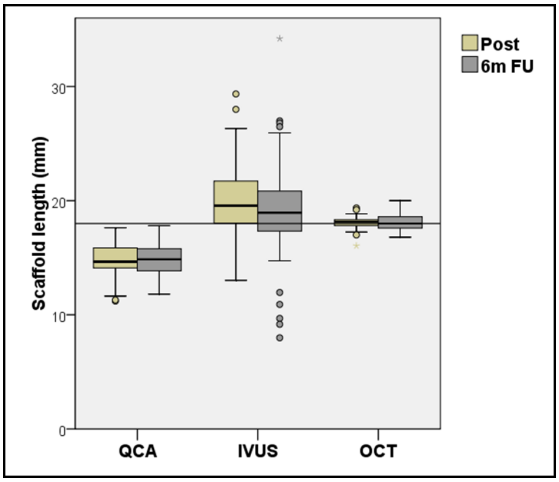

Figure 2: Box plot showing the length of the stent measured by the different imaging modalities immediately post-implantation and at 6 months follow-up. The reference line represents the nominal length of the device (18mm).
IVUS: Intravascular ultrasound; OCT: Optical Coherence Tomography; QCA: Quantitative Coronary Angiography; 6m FU: 6 months follow-up.

Table 2: Stent length measured by the different imaging modalities immediately post-stenting and at 6 months follow-up. "Chess table" showing the paired comparison of the means: white cells for post-post; yellow cells for post-6m; orange cells for 6m-6m comparisons.

Stent length (mm)				B					
				QCA	IVUS		OCT		Nominal length (18mm)
				6m	Post	6m	Post	6m	
A	QCA	Post	Mean diff (A-B)	-0.04	-5.63	-4.35	-3.47	-3.49	-3.38
			95% CI	-0.46; 0.39	-7.25; -4.01	-6.26; -2.44	-4.03; -2.91	-4.10; -2.89	-3.94; -2.81
			p-value	0.867	**<0.001**	**<0.001**	**<0.001**	**<0.001**	**<0.001**
		6m	Mean diff (A-B)		-4.90	-4.05	-3.21	-3.15	-2.99
			95% CI		-6.26; -3.53	-6.35; -1.75	-3.81; -2.61	-3.88; -2.43	-3.62; -2.35
			p-value		**<0.001**	**0.001**	**<0.001**	**<0.001**	**<0.001**
	IVUS	Post	Mean diff (A-B)			0.95	2.17	1.29	2.26
			95% CI			-0.88; 2.79	0.79; 3.54	-0.08; 2.65	0.77; 3.74
			p-value			0.294	**0.003**	0.063	**0.004**
		6m	Mean diff (A-B)				1.29	0.90	1.06
			95% CI				-1.22; 3.79	-1.37; 3.17	-1.15; 3.27
			p-value				0.299	0.424	0.333
	OCT	Post	Mean diff (A-B)					-0.30	0.09
			95% CI					-0.70; 0.10	-0.19; 0.37
			p-value					0.131	0.508
		6m	Mean diff (A-B)						0.16
			95% CI						-0.15; 0.47
			p-value						0.289

CI: Confidence Interval; IVUS: Intravascular ultrasound; OCT: Optical Coherence Tomography; QCA: Quantitative Coronary Angiography; 6m: 6 months follow-up.

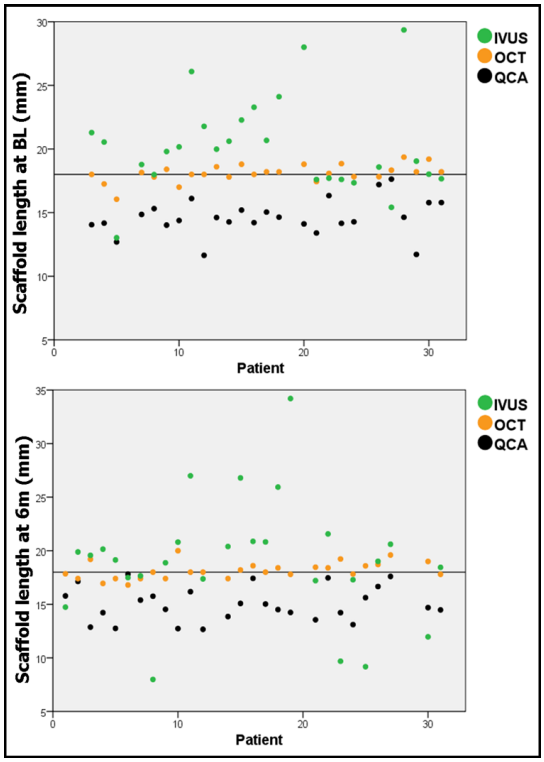

Figure 3: Individual measurements of the stent length by the different imaging modalities immediately post-implantation and at 6 months follow-up. The reference line represents the nominal length of the device (18mm).
BL: Baseline (immediately post-implantation); IVUS: Intravascular ultrasound; OCT: Optical Coherence Tomography; QCA: Quantitative Coronary Angiography.

reproducible accuracy, being close to the nominal length at both time points, whilst IVUS shows random variability, with an unpredictable pattern.

Table 3 shows the descriptive statistics of the in-stent MLA measured by the different imaging modalities. Figure 5 shows the MLA box-plots. Both QCA methods (ED and VD) have similar distribution, and OCT provides the largest MLA at baseline. At 6 months MLA decreases on ED, VD and OCT. In contrast, IVUS MLA decreases to a lesser extent and by 6-months becomes larger than OCT MLA. Individual measurements of in-stent MLA (figure 6) show very wide variability between different imaging modalities within the same patient, with no clear ranking as for the magnitude.

Table 4 shows the paired comparison of the means for MLA, as a chess table. Both QCA methods (ED and VD) significantly underestimate MLA compared to IVUS and OCT at baseline (white cells) and at 6 months (orange cells). IVUS significantly underestimates MLA compared to OCT at baseline, but not at 6 months. The reason for this is that the reduction in MLA between baseline and 6 months (yellow squares) detected by IVUS (mean 0.26mm^2) is much

Table 3: In-stent minimal lumen area measured by the different imaging modalities immediately post-stenting and at 6 months follow-up.

MLA (mm^2)		n	Mean	Median	SD	P25	P75	Min	Max	Saphiro-Wilk
QCA-ED	**Post**	26	4.08	4.06	0.97	3.15	4.98	2.34	5.70	0.370
	6m FU	27	3.61	3.68	1.02	2.65	4.68	1.76	5.07	0.107
QCA-VD	**Post**	26	4.12	3.93	1.26	3.14	5.09	2.31	6.54	0.179
	6m FU	27	3.73	3.73	1.23	2.71	4.48	1.76	6.63	0.669
IVUS	**Post**	26	5.39	5.51	1.01	4.58	6.08	3.17	7.64	0.965
	6m FU	27	5.11	5.29	0.94	4.21	5.71	3.06	6.66	0.236
OCT	**Post**	26	5.97	6.01	1.21	4.97	7.05	3.10	7.78	0.366
	6m FU	27	4.92	4.92	1.45	3.63	6.19	2.05	6.97	**0.040**

IVUS: Intravascular ultrasound; ED: Edge detection; MLA: Minimal lumen area; OCT: Optical Coherence Tomography; QCA: Quantitative Coronary Angiography; VD: Videodensitometry; 6m FU: 6 months follow-up.

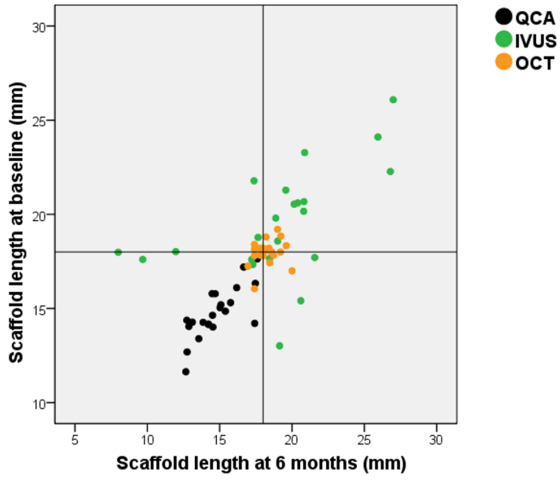

Figure 4: "Target graphic" depicting the variability test-retest of the different imaging modalities for the measurement of stent length. Reference lines represent the nominal length of the device (18mm).
IVUS: Intravascular ultrasound; OCT: Optical Coherence Tomography; QCA: Quantitative Coronary Angiography.

less than in any other imaging modality: ½ of that detected by QCA (mean 0.66mm^2 for ED, 0.63 for VD) or 1/5 of that detected by OCT (mean 1.24mm^2), (figure 6).

Table 5 shows the agreement between the different imaging modalities for MLA. ED and VD have moderate agreement at baseline (ICCa=0.687) and follow-up (ICCa=0.568). Both QCA methods have very poor agreement with either IVUS or OCT. IVUS has good agreement with OCT at baseline (ICCa=0.767) but only moderate at 6 months (ICCa=0.684).

The low level of agreement between QCA and OCT for in-stent MLA measurement prevents the reliable detection of any type of bias in Passing-Bablok non-parametric orthogonal regression (table 6, figure 7). Significant constant and proportional bias is detected between ED and OCT at 6 months, due to a somewhat better agreement between both methods

Table 4: In-stent minimal lumen area measured by the different imaging modalities immediately post-stenting and at 6 months follow-up. "Chess table" showing the paired comparison of the means: white cells for post-post; yellow cells for post-6m; orange cells for 6m-6m comparisons.

				B						
In-stent MLA (mm2)				QCA-ED	QCA-VD		IVUS		OCT	
				6m	Post	6m	Post	6m	Post	6m
A	QCA-ED	Post	Mean diff (A-B)	0.66	-0.04	0.53	-1.31	-1.02	-1.88	-0.64
			95% CI	0.39; 0.93	-0.40; 0.33	0.06; 0.99	-1.61; -1.02	-1.28; -0.76	-2.19; -1.58	-1.05; -0.24
			p-value	**<0.001**	0.835	**0.027**	**<0.001**	**<0.001**	**<0.001**	**0.003**
		6m	Mean diff (A-B)		-0.81	-1.13	-1.98	-1.50	-2.50	-1.31
			95% CI		-1.22; -0.40	-0.54; 0.29	-2.31; -1.65	-1.83; -1.18	-2.87; -2.13	-1.59; -1.04
			p-value		**<0.001**	0.544	**<0.001**	**<0.001**	**<0.001**	**<0.001**
	QCA-VD	Post	Mean diff (A-B)			0.63	-1.28	-0.92	-1.85	-0.50
			95% CI			0.32; 0.94	-1.71; -0.84	-1.32; -0.51	-2.26; -1.44	-1.06; -0.06
			p-value			**<0.001**	**<0.001**	**<0.001**	**<0.001**	0.079
		6m	Mean diff (A-B)				-1.83	-1.38	-2.38	-1.19
			95% CI				-2.29; -1.36	-1.80; -0.95	-2.89; -1.88	-1.74; -0.63
			p-value				**<0.001**	**<0.001**	**<0.001**	**<0.001**
	IVUS	Post	Mean diff (A-B)					0.26	-0.57	0.68
			95% CI					0.11; 0.42	-0.81; -0.34	0.27; 1.08
			p-value					**0.002**	**<0.001**	**0.002**
		6m	Mean diff (A-B)						-0.89	0.19
			95% CI						-1.23; -0.61	-0.19; 0.57
			p-value						**<0.001**	0.320
	OCT	Post	Mean diff (A-B)							1.24
			95% CI							0.88; 1.61
			p-value							**<0.001**

CI: Confidence Interval; ED: Edge detection; IVUS: Intravascular ultrasound; MLA: Minimal lumen area; OCT: Optical Coherence Tomography; QCA: Quantitative Coronary Angiography; VD: Videodensitometry; 6m FU: 6 months follow-up.

(Lin's coefficient=0.550). IVUS incurs a significant constant and proportional bias respect to OCT (at baseline only the constant is significant, but the slope is close to reaching statistical significance: 95% CI 0.97; 1.49).

DISCUSSION

Coronary stenting is one of those exceptional scenarios in biological sciences, in which a structure of fixed and known size can be repeatedly measured with different diagnostic tools and along different time points. Stent length is known a priori and does not change with time. This applies also to the BVS device, with an additional peculiarity: all the analyzed stents have exactly the same nominal length (18mm). This rare situation precludes the application

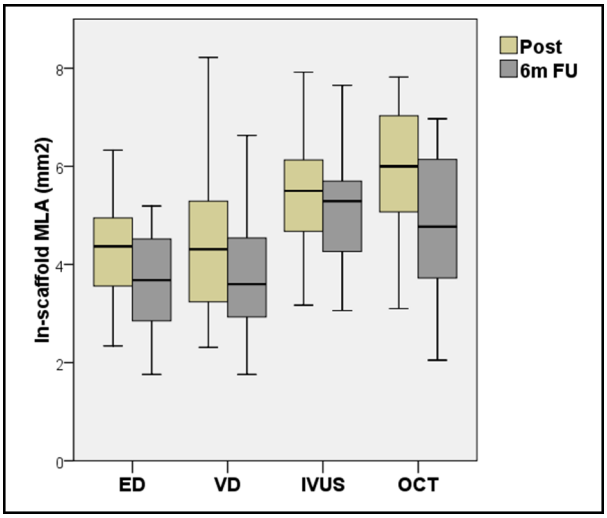

Figure 5: Box plot showing the minimal lumen area (MLA) of the stent measured by the different imaging modalities immediately post-implantation and at 6 months follow-up.
ED: Edge detection; IVUS: Intravascular ultrasound; MLA: Minimal lumen area; OCT: Optical Coherence Tomography; QCA: Quantitative Coronary Angiography; VD: Videodensitometry; 6m FU: 6 months follow-up.

Table 5: Concordance between different imaging modalities for in-stent minimal lumen area.

MLA (mm^2)			VD	IVUS	OCT
Post-implant (n=26)	ED	ICCa	0.687 (0.411, 0.847)	0.391 (-0.097, 0.748)	0.310 (-0.064, 0.694)
		ICCc	0.679 (0.402, 0.842)	0.731 (0.485, 0.870)	0.765 (0.542, 0.887)
	VD	ICCa		0.343 (-0.097; 0.672)	0.315 (-0.096, 0.681)
		ICCc		0.551 (0.215, 0.770)	0.665 (0.380, 0.834)
	IVUS	ICCa			0.767 (0.184, 0.919)
		ICCc			0.864 (0.719, 0.936)
6 months (n=27)	ED	ICCa	0.568 (0.245, 0.777)	0.300 (-0.095, 0.664)	0.549 (-0.088, 0.850)
		ICCc	0.562 (0.238, 0.773)	0.648 (0.361, 0.822)	0.848 (0.694, 0.928)
	VD	ICCa		0.289 (-0.103, 0.623)	0.329 (-0.050, 0.629)
		ICCc		0.512 (0.171, 0.744)	0.450 (0.091, 0.705)
	IVUS	ICCa			0.684 (0.421, 0.842)
		ICCc			0.684 (0.417, 0.843)

All values are significant at a level of $p<0.01$
CI: Confidence Interval; ED: Edge detection; ICCa: Intraclass correlation coefficient for absolute agreement; ICCc: Intraclass correlation coefficient for consistency; IVUS: Intravascular ultrasound; MLA: Minimal lumen area; OCT: Optical Coherence Tomography; QCA: Quantitative Coronary Angiography; VD: Videodensitometry.

of conventional statistical tests for the analysis of agreement, which are initially conceived to test a linear relationship between two different methods along a range of different values. Nevertheless, it is an opportunity to extract unique information through a different approach.

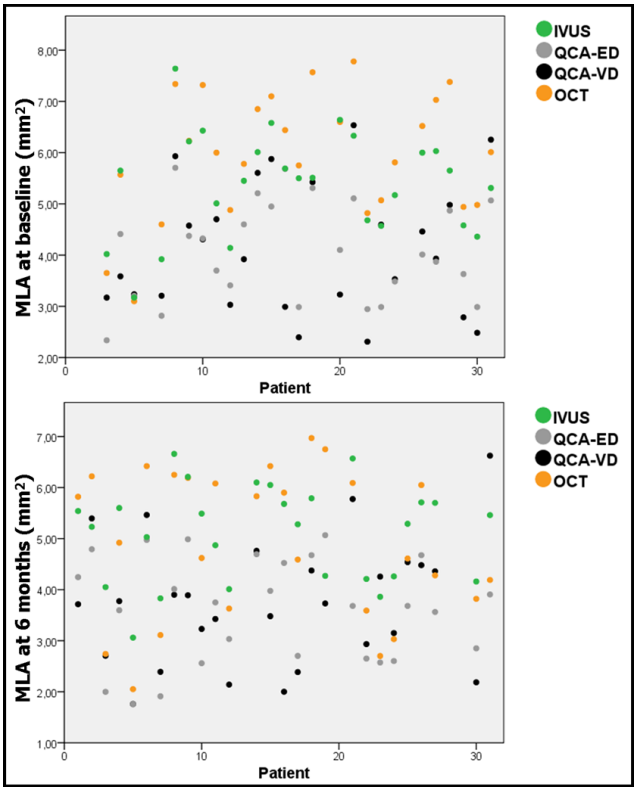

Figure 6: Individual measurements of the minimal lumen area (MLA) by the different imaging modalities immediately post-implantation and at 6 months follow-up.
ED: Edge detection; IVUS: Intravascular ultrasound; MLA: Minimal lumen area; OCT: Optical Coherence Tomography; QCA: Quantitative Coronary Angiography; VD: Videodensitometry.

Table 6: Concordance between different imaging modalities for in-stent minimal lumen area immediately post-implantation and at 6 months follow-up: results of Passing-Bablok non-parametric orthogonal regression. CUSUM test for deviation of normality <0.01 in all cases.

MLA (mm²)			Y = OCT							
			Constant	95% CI		Slope	95% CI		Discordance	Lin's coefficient (absolute agreement)
				Lower	Upper		Lower	Upper		
Post	X=	QCA-ED	0.31	-1.19	1.70	1.28	0.89	1.69	NS	0.325
		QCA VD	2.33	0.74	3.08	0.94	0.67	1.51	Constant	0.306
		IVUS	-1.19	-2.34	-0.23	1.20	0.97	1.49	Constant	0.764
6m	X=	QCA-ED	-1.16	-2.07	-0.32	1.37	1.15	1.60	Const & prop	0.550
		QCA VD	0.92	-1.75	2.92	1.32	0.78	2.04	NS	0.330
		IVUS	-2.53	-6.26	-0.82	1.51	1.20	2.18	Const & prop	0.676

X= CI: Confidence Interval; ED: Edge detection; IVUS: Intravascular ultrasound; MLA: Minimal lumen area; OCT: Optical Coherence Tomography; QCA: Quantitative Coronary Angiography; VD: Videodensitometry; 6m: 6 months follow-up; NS: Non-significant; Const & prop: Constant and proportional.

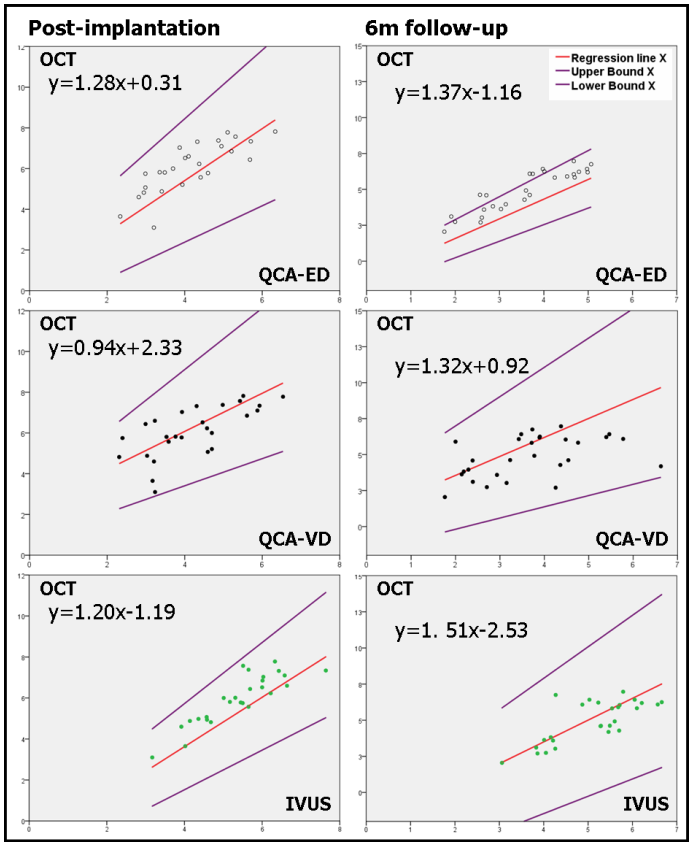

Figure 7: Passing-Bablok non-parametric orthogonal regression of minimal lumen area (MLA) measured by the different imaging modalities (x axis) and that measured by optical coherence tomography (y axis). Data immediately post-implantation and at 6 months follow-up.
ED: Edge detection; IVUS: Intravascular ultrasound; MLA: Minimal lumen area; OCT: Optical Coherence Tomography; QCA: Quantitative Coronary Angiography; VD: Videodensitometry.

Thus, the so called "target chart" (figure 3) depicts the effect of foreshortening on QCA length measurements, in a clear and illustrative way, hereby described for the first time.

Likewise, we can understand graphically the unpredictable random error of IVUS for length measurement, although most of the time, stent length is overestimated. Taking into account that a solid state IVUS was employed in this study, the overestimation is most likely due to an irregular pullback speed. The inaccuracy of solid state IVUS for length measurements is a relevant finding, since it questions the validity of any volumetric analysis performed by this technique, as performed in several trials[21-23], and is an additional argument to favour other estimative parameters of neointimal hyperplasia[24,25].

OCT appears as a more accurate and reliable tool for length measurements. Several reasons might explain this extra accuracy compared to IVUS. First, OCT is a rotational mechanical scanning system, with the optical catheter pulled back within a sheath; therefore there is less

irregularity in the pullback speed. Secondly, OCT systems have fast pullbacks (up to 20 mm/s in the Fourier-domain systems) that minimize the potential error due to cardiac structure motion around the catheter. Finally, the metallic markers at the stent edges, with a typical appearance in the optical image, act as clear landmarks, improving the reproducibility of longitudinal measurements.

The findings regarding in-stent MLA are more problematic to interpret. The first conclusion would be that MLAs measured by the different methods are neither equivalent, nor can they be reliably estimated by any of the others. Even between QCA modalities (ED vs. VD) or between intraluminal imaging techniques (IVUS vs. OCT), no linear relation could be defined. Although this conclusion might sound disheartening, it is the expected result when methods of very different accuracy are compared head-to-head. Therefore, we can conclude that the different imaging modalities in this study have substantial differences in their accuracy to estimate in-stent MLA in the BVS, and thus their values are not interchangeable. The chart in figure 6 illustrates at first glance these discrepancies, with no need of any statistical testing. The question which arises, is therefore which technique is the most accurate? Although OCT has been validated in-vitro and in-vivo for lumen measurements[16,17], with proven high reproducibility[18-20]. IVUS has also undergone a similar extensive validation process[26-28]. Unfortunately the current study design does not help in answering this question.

In this study in-stent MLA immediately post-stenting was larger when measured by OCT compared with IVUS. This is at variance with other comparative publications in non-stented vessels where IVUS areas were systematically larger than those measured by OCT, using occlusive or non-occlusive techniques[16,17,20]. At 6 months follow-up, however, IVUS MLA, was slightly but non-significantly larger than OCT MLA, which is more consistent with the published literature. This might be specific to the BVS, due to its particular design and optical properties that enable OCT to accurately measure the lumen area in the inter-struts spaces, enlarging substantially the OCT lumen areas after implant. Conversely, IVUS signals are very sensitive to artefact induced by the stent, and hence the lumen contour usually follows the adluminal side of the struts, neglecting the inter-struts spaces, and thus underestimating lumen areas with respect to OCT at baseline. At 6 months follow-up the inter-strut spaces have been integrated in the neointimal layer and both OCT and IVUS draw the lumen contour inside the adluminal side of the stent struts. This might explain why the reduction in MLA is maximal in OCT whilst minimal in IVUS.

ED and VD yield similar MLA values in scenarios where the circular shape of the vessel is preserved or restored, like immediately after stenting[29], and more dissimilar values in scenarios where the lumen symmetry is altered, like after atherectomy[30] or after plain balloon angioplasty[29,31]. In this study, no significant difference between ED and VD MLA was detected either at baseline or at 6 months, suggesting that the circular shape of the vessel is preserved at both time points, in contrast to the findings on BVS revision 1.0[1]. The device tested in this

study is the BVS revision 1.1., which has improved mechanical properties which have been achieved by altering the crystallization process of the polymer, and through some changes to the device design that reduce the maximal circular unsupported stent area[32]. Improved mechanical radial support could result in less shrinkage, with better preservation of luminal symmetry, and thus explain the lack of significant differences between ED and VD MLA. In prior studies VD correlated better and yielded closer values to IVUS than ED[33,34]. This is not observed in the present study, suggesting that additional factors other than the preservation of regular luminal geometry might also be playing a role.

Limitations

The reduced sample size is a limiting factor in this study. A larger sample size might have permitted a more accurate description of some of the bias detected between techniques.

All the implanted devices in this cohort had the same nominal length (18mm) and diameter (3mm). Additional comparative studies including different stent lengths will be required to better understand the accuracy of the imaging modalities for length measurement, since the present analysis is limited in this respect.

Likewise, the linear relations between different diagnostic tests regarding MLA can become unstable when all the measurements are in a narrow range, as it is the case. Further studies including different stent diameters might eventually result in better agreement between the same imaging modalities with respect to MLA.

The poor results found with IVUS might be partially explained by the use of a solid state system. The agreement between IVUS and OCT for length measurement is likely to improve using a mechanical sheath-based scanning system with a more regular pullback speed.

31% of the OCT studies at baseline and 18% at 6 months were acquired using the occlusive technique. This is a limitation of the study, since the occlusive technique provides lower areas and volumes than the non-occlusive one[17]. Nevertheless, in the charts comparing individual measurements this fact did not seem to significantly influence the MLA results.

CONCLUSIONS

OCT is the most accurate method to measure BVS length immediately post-implantation and at 6 months follow-up, whilst QCA incurs systematic underestimation and solid state IVUS incurs random error. There is very poor agreement between QCA, IVUS and OCT for the estimation of in-stent MLA, and no linear relation between any of the methods could be demonstrated.

DISCLOSURES

This study analyzes data from a registry sponsored by ABBOTT Vascular, Santa Clara, CA, USA. The core-lab and CRO responsible for the analysis (Cardialysis BV, Rotterdam) and the participating centres have received grants from the sponsor to run the trial, but the content of this manuscript is an investigator-driven post-hoc analysis. Serruys PW has received speakers' fees from the sponsor.

REFERENCES

1. Serruys PW, Ormiston JA, Onuma Y, Regar E, Gonzalo N, Garcia-Garcia HM, Nieman K, Bruining N, Dorange C, Miquel-Hebert K, Veldhof S, Webster M, Thuesen L, Dudek D. A bioabsorbable everolimus-eluting coronary stent system (ABSORB): 2-year outcomes and results from multiple imaging methods. *Lancet* 2009;373:897-910.
2. Strauss BH, Rensing BJ, den BA, van der Giessen WJ, Reiber JH, Serruys PW. Do stents interfere with the densitometric assessment of a coronary artery lesion? *Cathet Cardiovasc Diagn* 1991;24:259-264.
3. Ormiston JA, Serruys PW, Regar E, Dudek D, Thuesen L, Webster MW, Onuma Y, Garcia-Garcia HM, McGreevy R, Veldhof S. A bioabsorbable everolimus-eluting coronary stent system for patients with single de-novo coronary artery lesions (ABSORB): a prospective open-label trial. *Lancet* 2008;371:899-907.
4. Serruys PW, Onuma Y, Ormiston JA, De Bruyne B, Regar E, Dudek D, Thuesen L, Smits PC, Chevalier B, McClean D, Koolen J, Windecker S, Whitbourn R, Meredith I, Dorange C, Veldhof S, Hebert KM, Rapoza RJ, Garcia-Garcia HM. Evaluation of the second generation of a bioresorbable everolimus drug-eluting vascular scaffold for treatment of de novo coronary artery stenosis: 6-month clinical and imaging outcomes. *Circulation* 2010;122:2301-2312.
5. Bruining N, Tanimoto S, Otsuka M, Weustink A, Ligthart J, de WS, van MC, Nieman K, de Feyter PJ, van Domburg RT, Serruys PW. Quantitative multi-modality imaging analysis of a bioabsorbable poly-L-lactic acid stent design in the acute phase: a comparison between 2- and 3D-QCA, QCU and QMSCT-CA. *EuroIntervention* 2008;4:285-291.
6. Oberhauser JP, Hossainy S, Rapoza RJ. Design principles and performance of bioresorbable polymeric vascular scaffolds. *EuroIntervention Supplement* 2009;5:F15-F22.
7. Zijlstra F, van Ommeren J, Reiber JH, Serruys PW. Does the quantitative assessment of coronary artery dimensions predict the physiologic significance of a coronary stenosis? *Circulation* 1987;75:1154-1161.
8. Harrison DG, White CW, Hiratzka LF, Doty DB, Barnes DH, Eastham CL, Marcus ML. The value of lesion cross-sectional area determined by quantitative coronary angiography in assessing the physiologic significance of proximal left anterior descending coronary arterial stenoses. *Circulation* 1984;69:1111-1119.
9. Nishioka T, Amanullah AM, Luo H, Berglund H, Kim CJ, Nagai T, Hakamata N, Katsushika S, Uehata A, Takase B, Isojima K, Berman DS, Siegel RJ. Clinical validation of intravascular ultrasound imaging for assessment of coronary stenosis severity: comparison with stress myocardial perfusion imaging. *J Am Coll Cardiol* 1999;33:1870-1878.
10. Judkins MP. Selective coronary arteriography. I. A percutaneous transfemoral technic. *Radiology* 1967;89:815-824.
11. Gronenschild E, Janssen J, Tijdens F. CAAS. II: A second generation system for off-line and on-line quantitative coronary angiography. *Cathet Cardiovasc Diagn* 1994;33:61-75.
12. Bruining N, von BC, de Feyter PJ, Ligthart J, Li W, Serruys PW, Roelandt JR. ECG-gated versus nongated three-dimensional intracoronary ultrasound analysis: implications for volumetric measurements. *Cathet Cardiovasc Diagn* 1998;43:254-260.
13. von Birgelen C, de Vrey EA, Mintz GS, Nicosia A, Bruining N, Li W, Slager CJ, Roelandt JR, Serruys PW, de Feyter PJ. ECG-gated three-dimensional intravascular ultrasound: feasibility and reproducibility of the automated analysis of coronary lumen and atherosclerotic plaque dimensions in humans. *Circulation* 1997;96:2944-2952.

14. Guagliumi G, Sirbu V. Optical coherence tomography: high resolution intravascular imaging to evaluate vascular healing after coronary stenting. *Catheter Cardiovasc Interv* 2008;72:237-247.
15. Prati F, Cera M, Ramazzotti V, Imola F, Giudice R, Giudice M, Propris SD, Albertucci M. From bench to bedside: a novel technique of acquiring OCT images. *Circ J* 2008;72:839-843.
16. Kawase Y, Hoshino K, Yoneyama R, McGregor J, Hajjar RJ, Jang IK, Hayase M. In vivo volumetric analysis of coronary stent using optical coherence tomography with a novel balloon occlusion-flushing catheter: a comparison with intravascular ultrasound. *Ultrasound Med Biol* 2005;31:1343-1349.
17. Gonzalo N, Serruys PW, Garcia-Garcia HM, van Soest G, Okamura T, Ligthart J, Knaapen M, Verheye S, Bruining N, Regar E. Quantitative ex vivo and in vivo comparison of lumen dimensions measured by optical coherence tomography and intravascular ultrasound in human coronary arteries. *Rev Esp Cardiol* 2009;62:615-624.
18. Gonzalo N, Garcia-Garcia HM, Serruys PW, Commissaris KH, Bezerra H, Gobbens P, Costa M, Regar E. Reproducibility of quantitative optical coherence tomography for stent analysis. *EuroIntervention* 2009;5:224-232.
19. Gonzalo N, Tearney GJ, Serruys PW, van Soest G, Okamura T, Garcia-Garcia HM, van Geuns RJ, van der Ent M, Ligthart JM, Bouma BE, Regar E. Second-generation optical coherence tomography in clinical practice. High-speed data acquisition is highly reproducible in patients undergoing percutaneous coronary intervention. *Rev Esp Cardiol* 2010;63:893-903.
20. Okamura T, Gonzalo N, Gutierrez-Chico JL, Serruys PW, Bruining N, de WS, Dijkstra J, Commossaris KH, van Geuns RJ, van SG, Ligthart J, Regar E. Reproducibility of coronary Fourier domain optical coherence tomography: quantitative analysis of in vivo stented coronary arteries using three different software packages. *EuroIntervention* 2010;6:371-379.
21. Tsuchida K, Colombo A, Lefevre T, Oldroyd KG, Guetta V, Guagliumi G, von SW, Ruzyllo W, Hamm CW, Bressers M, Stoll HP, Wittebols K, Donohoe DJ, Serruys PW. The clinical outcome of percutaneous treatment of bifurcation lesions in multivessel coronary artery disease with the sirolimus-eluting stent: insights from the Arterial Revascularization Therapies Study part II (ARTS II). *Eur Heart J* 2007;28:433-442.
22. Tsuchida K, Garcia-Garcia HM, Ong AT, Valgimigli M, Aoki J, Rademaker TA, Morel MA, Van Es GA, Bruining N, Serruys PW. Revisiting late loss and neointimal volumetric measurements in a drug-eluting stent trial: analysis from the SPIRIT FIRST trial. *Catheter Cardiovasc Interv* 2006;67:188-197.
23. Aoki J, Abizaid AC, Serruys PW, Ong ATL, Boersma E, Sousa JE, Bruining N. Evaluation of Four-Year Coronary Artery Response After Sirolimus-Eluting Stent Implantation Using Serial Quantitative Intravascular Ultrasound and Computer-Assisted Grayscale Value Analysis for Plaque Composition in Event-Free Patients. *Journal of the American College of Cardiology* 2005;46:1670-1676.
24. Tanabe K, Serruys PW, Degertekin M, Guagliumi G, Grube E, Chan C, Munzel T, Belardi J, Ruzyllo W, Bilodeau L, Kelbaek H, Ormiston J, Dawkins K, Roy L, Strauss BH, Disco C, Koglin J, Russell ME, Colombo A. Chronic arterial responses to polymer-controlled paclitaxel-eluting stents: comparison with bare metal stents by serial intravascular ultrasound analyses: data from the randomized TAXUS-II trial. *Circulation* 2004;109:196-200.
25. Aoki J, Colombo A, Dudek D, Banning AP, Drzewiecki J, Zmudka K, Schiele F, Russell ME, Koglin J, Serruys PW. Peristent remodeling and neointimal suppression 2 years after polymer-based, paclitaxel-eluting stent implantation: insights from serial intravascular ultrasound analysis in the TAXUS II study. *Circulation* 2005;112:3876-3883.

26. Nishimura RA, Edwards WD, Warnes CA, Reeder GS, Holmes J, Tajik AJ, Yock PG. Intravascular ultrasound imaging: In vitro validation and pathologic correlation. *Journal of the American College of Cardiology* 1990;16:145-154.
27. Nissen SE, Grines CL, Gurley JC, Sublett K, Haynie D, Diaz C, Booth DC, DeMaria AN. Application of a new phased-array ultrasound imaging catheter in the assessment of vascular dimensions. In vivo comparison to cineangiography. *Circulation* 1990;81:660-666.
28. Nissen SE, Gurley JC, Grines CL, Booth DC, McClure R, Berk M, Fischer C, DeMaria AN. Intravascular ultrasound assessment of lumen size and wall morphology in normal subjects and patients with coronary artery disease. *Circulation* 1991;84:1087-1099.
29. Strauss BH, Juilliere Y, Rensing BJ, Reiber JHC, Serruys PW. Edge detection versus densitometry for assessing coronary stenting quantitatively. *The American Journal of Cardiology* 1991;67:484-490.
30. Umans VA, Strauss BH, de Feyter PJ, Serruys PW. Edge detection versus videodensitometry for quantitative angiographic assessment of directional coronary atherectomy. *Am J Cardiol* 1991;68:534-539.
31. Serruys PW, Reiber JH, Wijns W, van den BM, Kooijman CJ, ten Katen HJ, Hugenholtz PG. Assessment of percutaneous transluminal coronary angioplasty by quantitative coronary angiography: diameter versus densitometric area measurements. *Am J Cardiol* 1984;54:482-488.
32. Okamura T, Garg S, Gutierrez-Chico JL, Shin ES, Onuma Y, Garcia-Garcia HM, Rapoza RJ, Sudhir K, Regar E, Serruys PW. In vivo evaluation of stent strut distribution patterns in the bioabsorbable everolimus-eluting device: an OCT ad hoc analysis of the revision 1.0 and revision 1.1 stent design in the ABSORB clinical trial. *EuroIntervention* 2010;5:932-938.
33. Ozaki Y, Violaris AG, Kobayashi T, Keane D, Camenzind E, di Mario C, de Feyter P, Roelandt JRTC, Serruys PW. Comparison of Coronary Luminal Quantification Obtained From Intracoronary Ultrasound and Both Geometric and Videodensitometric Quantitative Angiography Before and After Balloon Angioplasty and Directional Atherectomy. *Circulation* 1997;96:491-499.
34. Tanimoto S, Serruys PW, Thuesen L, Dudek D, de BB, Chevalier B, Ormiston JA. Comparison of in vivo acute stent recoil between the bioabsorbable everolimus-eluting coronary stent and the everolimus-eluting cobalt chromium coronary stent: insights from the ABSORB and SPIRIT trials. *Catheter Cardiovasc Interv* 2007;70:515-523.

Supplementary table 1: Characteristics of the different OCT systems* in the study, with the corresponding number of patients imaged by each of them.

	M2	M3	C7
Technique	Occlusive	Non-occlusive	Non-occlusive
Domain	Time	Time	Fourier
Catheter*	ImageWire	ImageWire	Dragonfly
Rotation speed (frames/s)	15.6	20	100
Pullback speed (mm/s)	2	3	20
Nr of patients at baseline	9	5	15
Nr of patients at 6 months	5	5	18

* All systems and catheters from Lightlab Imaging, Westford, Massachusetts, USA.

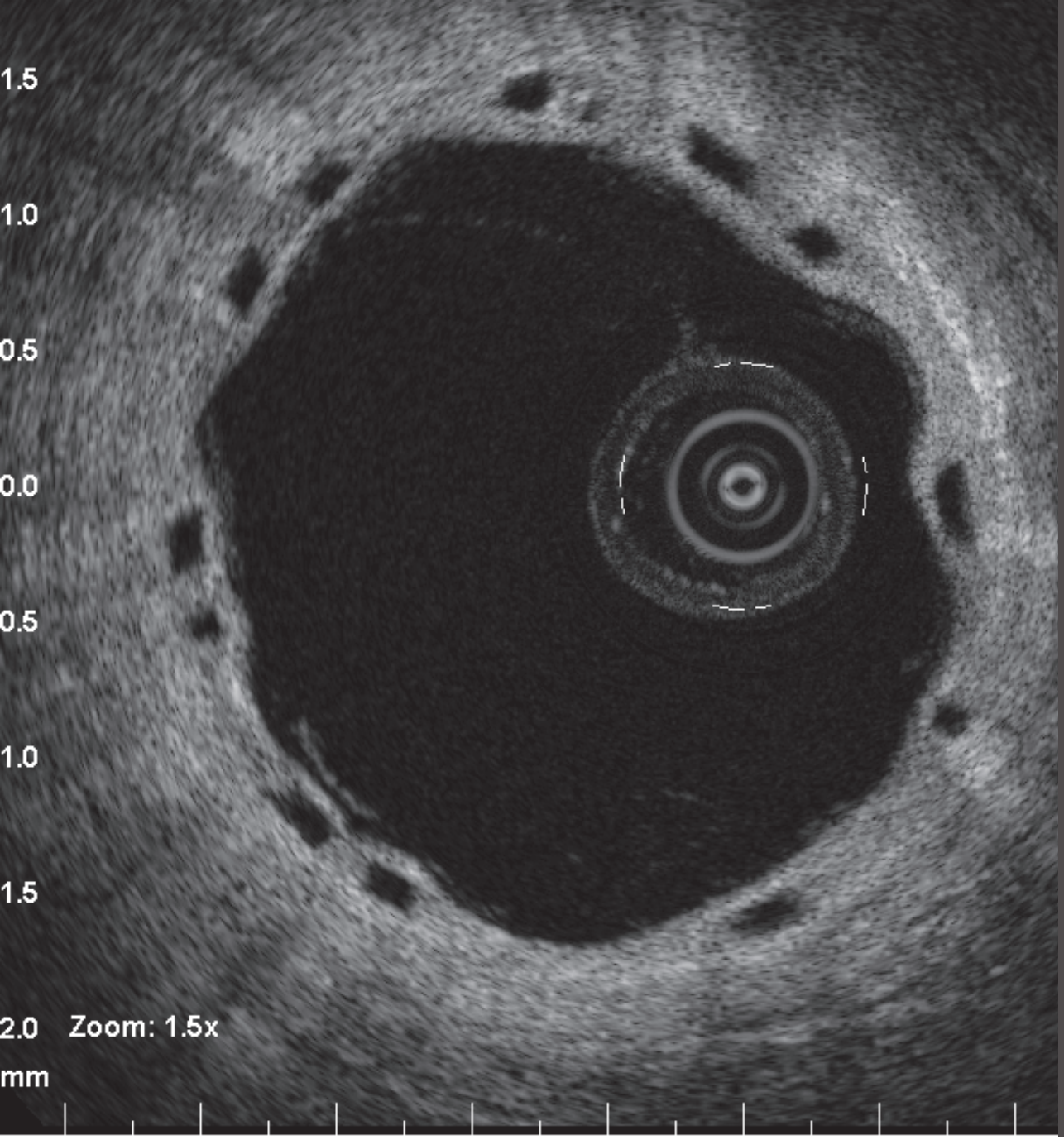
1.5
1.0
0.5
0.0
0.5
1.0
1.5
2.0
Zoom: 1.5x
mm

CHAPTER 11

Assessment of coverage in the BVS

In-vivo characterization of the strut borders in a bioresorbable vascular scaffold at baseline and after neointimal coverage using analysis of the optical coherence tomography intensity spread function.

Sheehy A, Gutiérrez-Chico J (equally contributed), Oberhauser JP, Glauser T, Harrington J, Kossuth MB, Rapoza R, Onuma Y, Serruys PW.

EuroIntervention 2012;7:1227-1235.

CONDENSED ABSTRACT

Optical coherence tomography (OCT) of bioresorbable scaffolds (BVS) produces a signal outlining struts that interferes with the measurement of strut thickness and coverage. In 48 BVS struts from 12 patients and 4 Yucatan minipigs, raw OCT signal intensities were fit to Gaussian linear spread functions (LSFs), from which full-width-at-half-max (FWHM) were calculated. Neointimal coverage resulted in significantly different LSFs and higher FWHM than baseline uncovered struts. Using half-max location, the average strut thickness was not significantly different from nominal.

STRUCTURED ABSTRACT

Aims: Optical coherence tomography (OCT) of a bioresorbable vascular scaffold (BVS) produces a highly reflective signal outlining struts. This signal interferes with the measurement of strut thickness, as the boundaries cannot be accurately identified, and with the assessment of coverage, because the neointimal backscattering convolutes that of the polymer, frequently making them indistinguishable from one another. We hypothesize that Gaussian line spread functions (LSFs) can facilitate identification of strut boundaries, improving the accuracy of strut thickness measurements and coverage assessment.

Methods and results: 48 randomly selected BVS struts from 12 patients in the ABSORB Cohort B clinical study and 4 Yucatan minipigs were analyzed at baseline and follow-up (6 months in humans, 28 days in pigs). Signal intensities from the raw OCT backscattering were fit to Gaussian LSFs for each interface, from which peak intensity and full-width-at-half-maximum (FWHM) were calculated. Neointimal coverage resulted in significantly different LSFs and higher FWHM values relative to uncovered struts at baseline ($p<0.0001$). Abluminal polymer-tissue interfaces were also significantly different between baseline and follow-up ($p=0.0004$ in humans, $p<0.0001$ in pigs). Using the location of the half-max of the LSF as the polymer-tissue boundary, the average strut thickness was 158 ± 11 μm at baseline and 152 ± 20 μm at 6 months (p=0.886), not significantly different from nominal strut thickness.

Conclusion: Fitting the raw OCT backscattering signal to a Gaussian LSF facilitates identification of the interfaces between BVS polymer and lumen or tissue. Such analysis enables more precise measurement of the strut thickness and an objective assessment of coverage.

Clinical trial registration: NCT00856856; URL: http://clinicaltrials.gov/ct2/results?term=NCT00856856

Key words: Coronary stenosis; polylactide; drug-eluting stents; tomography, optical coherence; bioresorbable vascular scaffold.

INTRODUCTION

The ABSORB™ bioresorbable vascular scaffold (BVS) (Abbott Vascular, Santa Clara, CA, USA) consists of a semicrystalline poly(L-lactide) (PLLA) backbone and conformal coating of amorphous poly(D,L-lactide) (PDLLA) and the antiproliferative agent everolimus. The ABSORB BVS struts are fully resorbed approximately two years after implantation,[1,2] following a process in which the long chains of PLLA and PDLLA are progressively shortened as the ester bonds present in each lactic acid repeat unit are hydrolyzed. Ultimately, PLLA and PDLLA degrade to lactic acid, which is metabolised via the Krebs' cycle.[3] ABSORB has exhibited excellent clinical and angiographic results up to two years follow-up.[1,4]

A BVS is particularly suitable for optical coherence tomography (OCT) imaging, given the translucency of the polymers from which it is manufactured. The transmitted light can readily penetrate the material, and any backscattering stems from changes in refractive index on a length scale greater than or equal to the wavelength of the light. Immediately post-implantation, backscattering associated with the BVS is only significant at the borders of the strut, and changes in backscattering at later time points suggest an evolution in polymer microstructure on the length scale described above. Struts imaged with OCT post-implantation typically appear as a box-shaped highly reflective frame that marks the refractive index change at the lumen-polymer and polymer-tissue interfaces.[1,4] However, measuring the strut thickness from leading-edge to leading-edge of the adluminal and abluminal boundaries of this frame results in values greater than the nominal 158 μm value characteristic of the backbone and coating of the ABSORB BVS strut. This discrepancy highlights a lack of precision in the measurement and the need to develop a methodology by which OCT signals may be used to accurately discern the true edges of BVS struts. Even histological assessment may not provide accurate strut measurements at all time points due to processing artifacts,[2] reinforcing the importance of improving the accuracy of OCT measurements.

OCT is an experimental tool for the evaluation of neointimal coverage after implantation of metallic stents[5-10] and translucent polymeric scaffolds.[2] Coverage assessed by OCT in vivo correlates well with neointimal coverage assessed by histology in experimental animal models.[2,5-10] Unlike metallic stents, the assessment of coverage in the ABSORB BVS is more challenging, because the backscattering from thin neointimal layers mixes with that from the polymer interface and can be difficult to discern in a conventional analysis of the log-transformed OCT signal.

The basic principles of light and its interaction with matter provide the means by which these challenges may be addressed. A point spread function (PSF) describes the response of an imaging system to a point source or point object. Similarly, the spreading of light along a perfect line or slit has been called the line spread function (LSF).[11] Because OCT is a measurement of backscattering intensity, the edge of a BVS strut forms a relatively uniform line from which a LSF can be measured. However, when tissue or other backscattering media are

present, the uniformity of the optical response at the edge may vary. By smoothing the edge response variance due to backscattering tissue, the LSF may facilitate the definition of BVS strut edges and provide an objective criterion for the measurement of strut thickness and tissue coverage.

METHODS

Clinical Study

The ABSORB Cohort B study (NCT00856856) design has been published elsewhere.[12] It enrolled patients older than 18 years with diagnosis of stable or unstable angina pectoris or silent ischemia and *de novo* lesions in native coronary arteries amenable to percutaneous treatment with the ABSORB BVS. Target lesions were required to be characterized by percent diameter stenosis greater than or equal to 50% by visual estimation and reference vessel diameter of 2.5 – 3.5 mm. Major exclusion criteria were: acute myocardial infarction, unstable arrhythmias, left ventricular ejection fraction less than or equal to 30%, restenotic lesions, lesions located in the left main coronary artery or in bifurcations involving a side branch greater than 2 mm, a second clinically or hemodynamically significant lesion in the target vessel, documentation of intracoronary thrombus, or initial TIMI 0 flow. All the study lesions were treated with the ABSORB BVS revision 1.1 (3.0 x 18 mm). Fifty percent of the cohort underwent scheduled invasive follow-up 6 months after the implantation, including OCT study whenever available at the participating site. The registry was approved by the ethics committee at each participating site, and each patient gave written informed consent before inclusion in the study.

Preclinical (Porcine) Study

All experimentation conformed with the Animal Welfare Act, the Guide for Care and Use of Laboratory Animals (NIH Publication 85-23, 1996), and the Canadian Council on Animal Care regulations. All procedures were performed at AccelLab, Inc (Montreal, Quebec, Canada), accredited by the Association for Assessment and Accreditation of Laboratory Animal Care (AAALAC) and in accordance with the protocol approved by the institutions animal care and use committee (IACUC).

Four Yucatan mini-swine implanted with BVS were used in this analysis. Animals were administered oral acetylsalicylic acid (325 mg initial dose, 81 mg daily subsequently) and clopidogrel (300 mg initial dose and 75 mg daily subsequently) beginning three days prior to BVS implantation. Animals were tranquilized with ketamine (0.04 mg/kg), azaperone (4.0 mg/kg), and atropine (25 mg/kg) intramuscularly. Anesthesia was achieved with propofol,

(1.66 mg/kg IV), and maintained with inhaled isofluorane (1-3%) throughout the procedure. A vascular access sheath was placed in the femoral artery percutaneously. Before catheterization, heparin (5,000 to 10,000 U) was injected to maintain an activated clotting time greater than 250 s. For each BVS deployment, an arterial segment was chosen so as to achieve a balloon-to-artery ratio of 1.1:1, ensuring full apposition based on angiographic assessment. Each animal received a single BVS revision 1.1 in one of the three main coronary arteries. Although a 3.0 x 12 mm BVS was used in the animal studies, the design was the same as that used in the clinical study. Animals recovered from anesthesia under veterinary care for future time point analysis following the procedure. All the devices were imaged by OCT immediately after implantation and at 28-day follow-up.

OCT Image Acquisition and Analysis

In both animal and human procedures, OCT pullbacks were obtained at baseline and follow-up with a Fourier-domain C7 system using a Dragonfly™ catheter (St. Jude Medical Inc., Saint Paul, MN, USA; 10-15 µm axial and 20-40 µm lateral resolution[13]) at a rotation speed of 100 frames/s with non-occlusive technique.[14] After infusion of intracoronary nitroglycerine, the imaging wire was withdrawn by a motorized pullback at a constant speed of 20 mm/s, while Iodixanol 320 contrast (Visipaque™, GE Health Care, Cork, Ireland) was infused through the guiding catheter at a continuous rate of 2 – 4 mL/min.

A random sampling of 12 struts at each time point from both the animal and the human studies was selected using the following criteria: (1) OCT images were obtained with a Fourier-domain C7 system at both baseline and follow-up; (2) the luminal edge of the strut was perpendicular to the light source in order to minimize the effect of wire eccentricity and vessel-catheter misalignment; and (3) the strut was well-apposed.

Light intensity analysis was performed in the region surrounding the selected struts using ImageJ 1.43u software (Wayne Rasband, National Institutes of Health, USA). The raw polar image was used to ensure that interpolation, dynamic range compression, or other image processing did not alter the signal and bias the analysis. Because the strut boundaries are expected to be found within the reflective frame, an intensity profile was created by averaging consecutive pixels aligned parallel to the frame boundary and spanning the whole reflective frame orthogonally through the frame boundaries beginning on the adluminal side. Since the C7 system displays 500 A-lines per frame, 976 pixels per line, and a depth of field 5mm, the axial dimension of a single pixel in raw polar coordinates is ca. 5.12 µm for in vivo coronary imaging with this OCT catheter. Using the catheter dimensions as a standard (0.89mm), we measured the pixel/µm conversion factor at 5.05 µm and used this for the measurements herein. The result is a two-dimensional profile plot of intensity versus distance through the center of the strut. The following interfaces were analyzed (figure 1): Lumen-polymer, defined as the optical signal generated by the adluminal border of the strut at baseline (LP-bl);

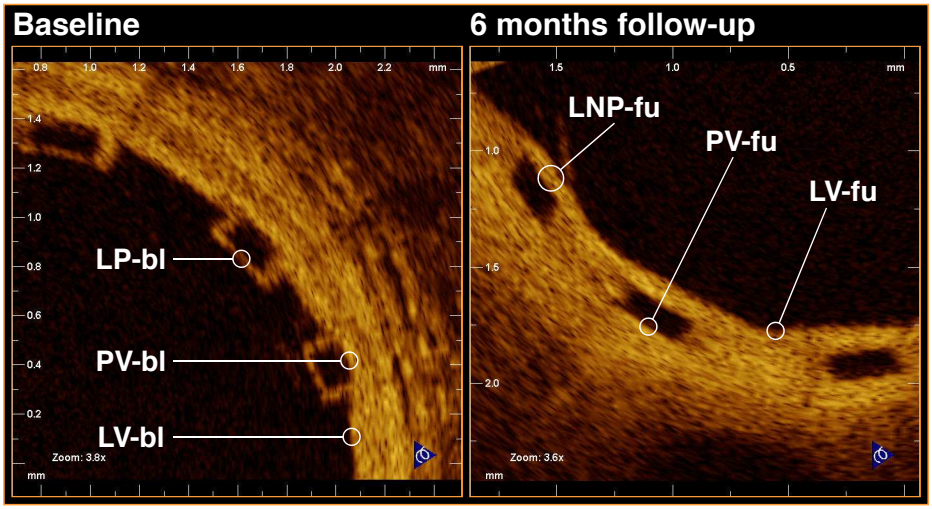

Figure 1: Denomination of the different optical interfaces analyzed.
LNP-fu: Lumen-neointima-polymer at follow-up; LP-bl: Lumen-polymer at baseline; LV-bl: Lumen-vessel at baseline; LV-fu: Lumen-vessel at follow-up; PV-bl: Polymer-vessel at baseline; PV-fu: Polymer-vessel at follow-up.

lumen-neointima-polymer, defined as the optical signal generated by the adluminal border of the strut at follow-up (LNP-fu); polymer-vessel wall, defined as the optical signal generated by the abluminal border of the well-apposed strut at baseline or follow-up (PV-bl; PV-fu); lumen-vessel wall, defined as the optical signal generated by the vessel wall of a strut-free sector at baseline or follow-up (LV-bl; LV-fu).

The data corresponding to each interface were individually summarized in plots of optical intensity versus distance, where the origin of the plot was located at the point corresponding to the strut center and zero optical intensity (figure 2). The center of the strut was determined as the point equidistant from the points at which the intensity signal exceeded a consistent threshold value at the strut interior side of the adluminal and abluminal interfaces.

The curves for each type of interface were fit to a Gaussian form given by:

$$f(x) = a\exp^{(-x-b^2)/2c^2}$$

where a is the maximum intensity of the curve, b is the midpoint of the Gaussian curve, and c is a function of the full-width-at-half-maximum (FWHM), namely $c = \text{FWHM} / 2\sqrt{2\ln(2)}$. Coefficients for the Gaussian curve fits were determined using an iterative least squares minimization process (figure 3). Gaussian curves were chosen to remain consistent with the practice commonly used for PSFs. Because the LSF differs from the PSF and includes scattering components, other functions commonly used to describe optical profiles, Lorentzian and exponential functions[15-17], were also evaluated and found inferior to the Gaussian fits (data not shown). Where tissue was present, the LSF was derived through symmetry of a one-tailed Gaussian fit with the first peak defining the peak of the Gaussian function. Though the transition between polymer and tissue appears to be sigmoidal or step-like, mirroring

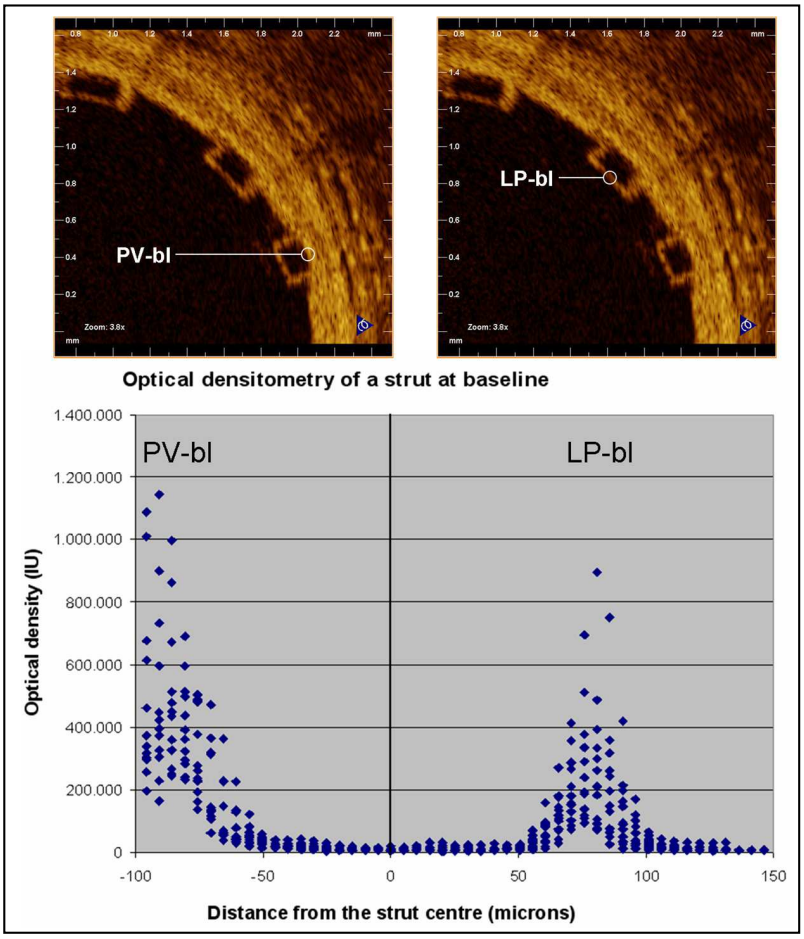

Figure 2: Graphic representation of the 12 struts analyzed at baseline.
The coordinate system origin is located at the calculated center of the strut (x-axis) and zero optical intensity (y-axis). The strut center is defined as the point equidistant to the rises of the adluminal (LP-bl interface) and abluminal (PV-bl interface) strut borders.
LP-bl: Lumen-polymer interface at baseline; PV-bl: Polymer-vessel interface at baseline.

a one-sided Gaussian function enabled comparison with the Gaussian fit of the uncovered strut. Additionally, the convolution of two Gaussian functions is a Gaussian function, and thus this best represented the optics of the system.

Two approaches were used to determine the location of strut interfaces. For struts without tissue coverage (e.g., LP-bl), the strut interface was assigned to the location of the peak of the signal intensity. The justification is that the high signal contrast of the LP interface represents an ideal LSF example, and the peak of the LSF defines the line. Alternatively, for interfaces adjacent to tissue (e.g., LNP-fu, PV-bl, PV-fu, LV-bl, LV-fu), the location of the half-max was assigned to the interface to represent the spatial location of intensity halfway between the low polymer intensity and high tissue intensity[18]. Because there was no normalization of the

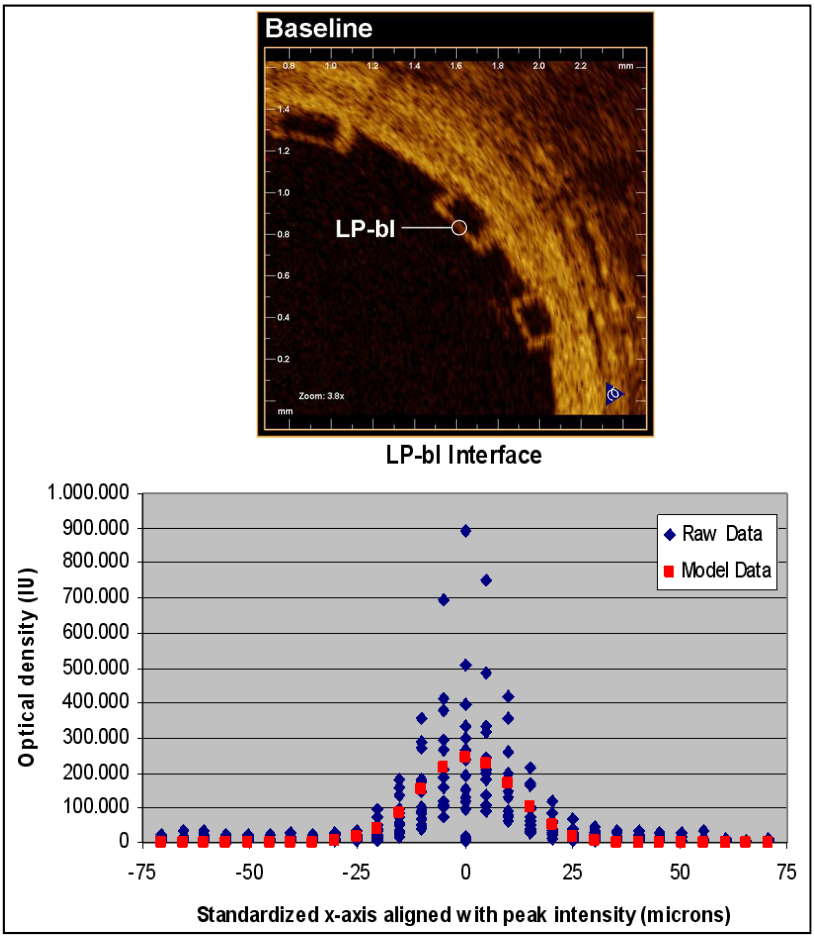

Figure 3: Lumen-polymer interface curve fit.
LP-bl: Lumen-polymer interface at baseline.

intensity signal, the half-max was chosen to enable objective threshold based filtering. All strut width measurements were performed according to these definitions.

Statistical analysis

Non-linear least squares curve fits were compared with a Snedecor F-test using sum of squares for two separate curves and sum of squares of a single curve generated from combined data. Strut width measurements were compared using a two tailed Fisher's student t-test. All the analysis was performed with Microsoft Excel 2003, SP3 with solver toolkit.

Table 1: Parameters characterizing the curve fit for each type of interface.

Interface	Swine		Human	
	Max Intensity	FWHM (μm)	Max Intensity	FWHM (μm)
LP-bl	303.33	22.24	244.78	25.86
PV-bl	1118.22	50.69	544.32	45.32
LV-bl	801.67	49.42	338.71	52.00
LNP-fu	635.54	60.71	475.06	38.89
PV-fu	542.40	54.37	490.91	42.97
LV-fu	681.54	54.00	739.27	56.91

RESULTS

Results in human

24 patients in the ABSORB Cohort B study received OCT at baseline and 6-month follow-up. In only 12 of these cases were the images acquired with a Fourier-domain C7 system. One strut

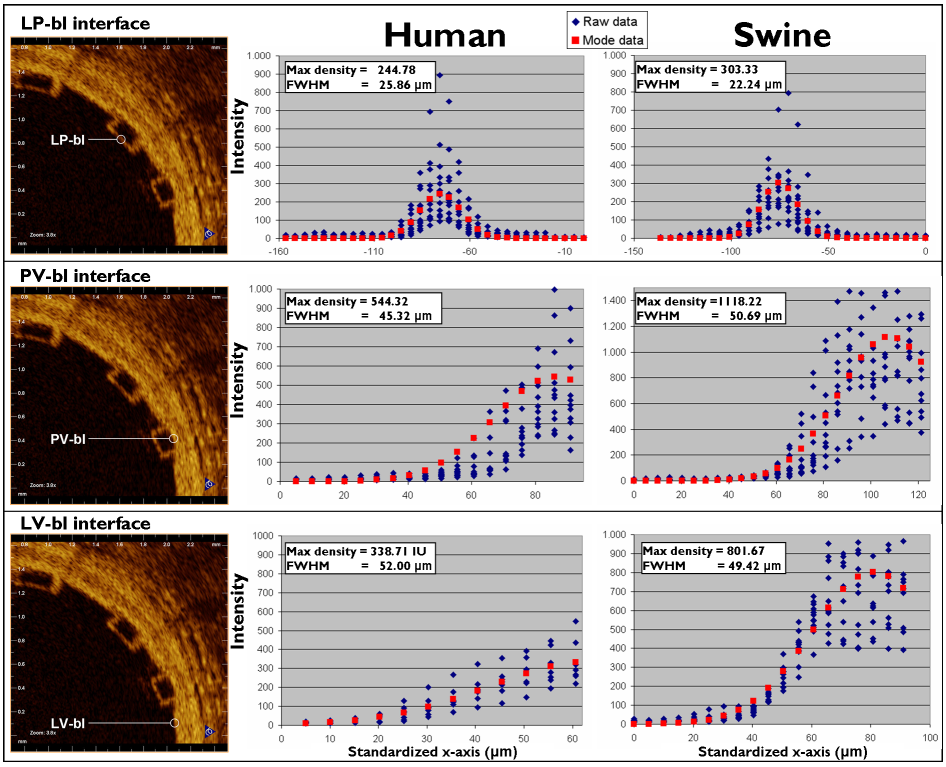

Figure 4: Fitting curves characterizing the different interfaces at baseline in human and swine studies.
FWHM: Full width at half max; LP-bl: Lumen-polymer at baseline; LV-bl: Lumen-vessel at baseline; PV-bl: Polymer-vessel at baseline.

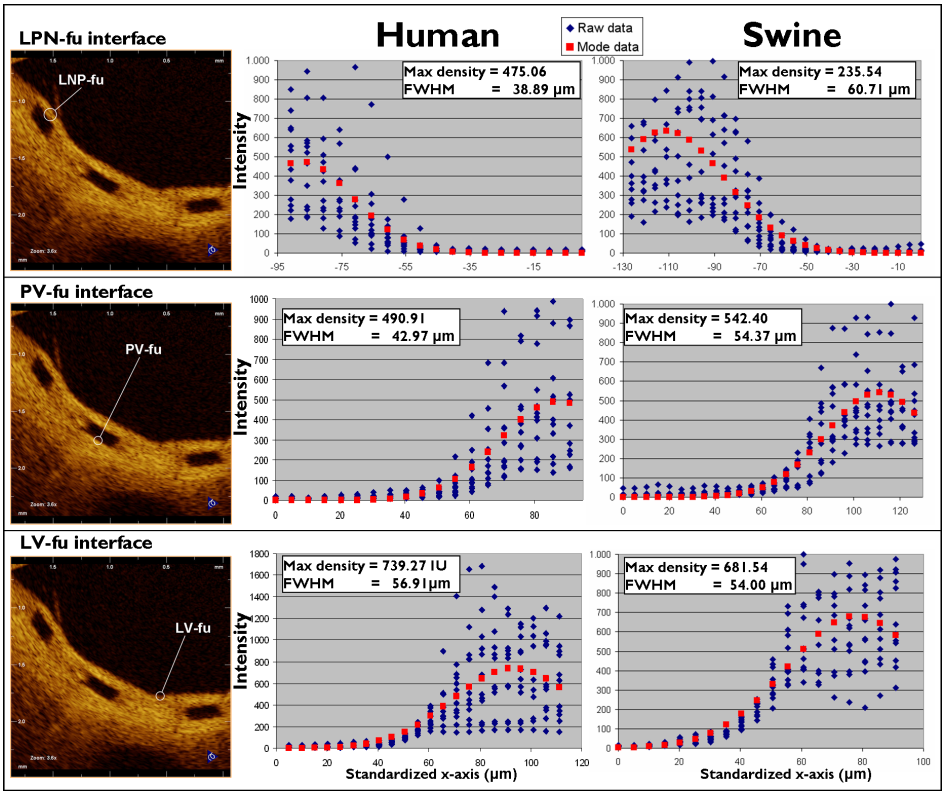

Figure 5: Fitting curves characterizing the different interfaces at follow-up in human (6 months) and swine (28 days) studies.
FWHM: Full width at half max; LNP-fu: Lumen-neointima-polymer at follow-up; LV-fu: Lumen-vessel at follow-up; PV-fu: Polymer-vessel at follow-up.

Table 2: Statistical comparison of curve fit: p-values from Snedecor F-tests.

Swine interface	LP-bl	PV-bl	LV-bl	LNP-fu	PV-fu	LV-fu
LP-bl	—	<0.0001	<0.0001	<0.0001	<0.0001	<0.0001
PV-bl		—	<0.0001	<0.0001	<0.0001	<0.0001
LV-bl			—	<0.0001	<0.0001	0.005
LNP-fu				—	0.99	<0.0001
PV-fu					—	<0.0001
LV-fu						—
Human interface	LP-bl	PV-bl	LV-bl	LNP-fu	PV-fu	LV-fu
LP-bl	—	<0.0001	<0.0001	<0.0001	<0.0001	<0.0001
PV-bl		—	<0.0001	<0.0001	0.0004	<0.0001
LV-bl			—	<0.0001	<0.0001	0.073
LNP-fu				—	0.347	<0.0001
PV-fu					—	<0.0001
LV-fu						—

meeting the selection criteria of the study was randomly selected for each OCT pullback (12 at baseline, 12 at follow-up).

Across all types of interface, the FWHM of the signal was greatest for LV-fu (56.91 µm) and least for LP-bl at baseline (25.86 µm). Table 1 summarizes the curve fit parameters for each interface type (figures 4 and 5). Neointimal coverage of struts resulted in an increase of the FWHM, and the curves corresponding to LP-bl and LNP-fu interfaces differed significantly ($p<0.0001$, Table 2). There was no significant difference between LNP-fu and PV-fu interfaces (LNP-fu vs. PV-fu, $p=0.347$). However, the PV-bl interface differed significantly from the PV-fu interface (PV-bl vs. PV-fu, $p=0.0004$) as well as the LV-bl, LV-fu, and LPN-fu interfaces (PV-bl vs. LV-bl, $p<0.0001$; PV-bl vs. LV-fu, $p<0.0001$; PV-bl vs. LPN-fu, $p<0.0001$).

Measuring from peak to half-max (PV-bl to PV-bl) and half-max to half-max (LNP-fu to PV-fu) for baseline and follow-up, respectively (figure 6), the average strut thickness was 158±11 µm at baseline and 152 ± 20 µm at the 6-month follow-up ($p=0.41$), both of which are similar to the nominal BVS strut thickness (ca. 152 µm for the backbone only and ca. 158 µm for the backbone and coating)

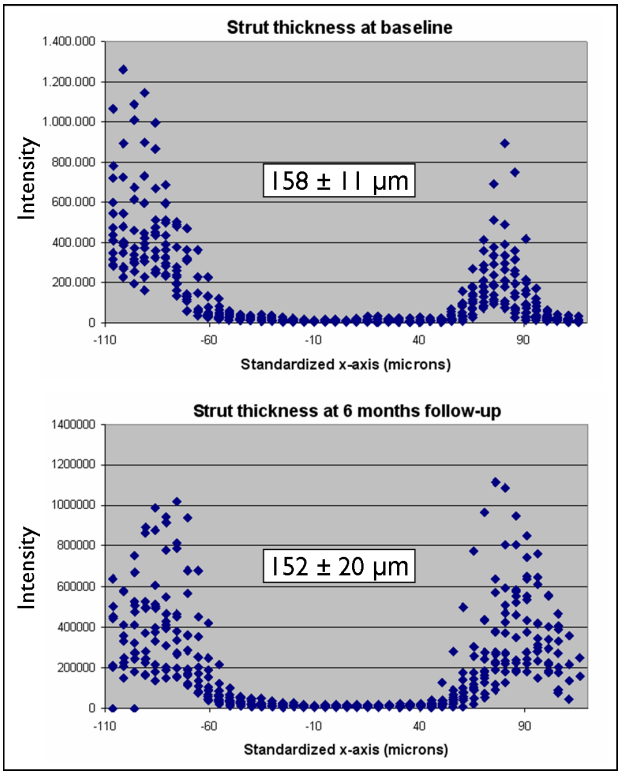

Figure 6: (a) Strut thickness measured from the peak intensity of the fitting curve for the adluminal interface to the half-max of the fitting curve for the abluminal interface at baseline, and (b) Strut thickness measured from the half-max of the fitting curve for the adluminal interface to the half-max of the fitting curve for the abluminal interface at follow-up (human data).

Results in the swine model

Three struts meeting the same selection criteria defined for the clinical sample was randomly selected in each of the four animals (12 at baseline, 12 at follow-up). The curve fit parameters for each interface had absolute values different than the ones reported in humans, but the same trends were observed.

Similar to the clinical samples, the FWHM increased when tissue was present. In swine samples, LNP-fu had the greatest FWHM at 60.71 μm, while LP-bl had the smallest FWHM at 22.24. Table 1 summarizes the curve fit parameters for each interface (figures 4 and 5). Neointimal coverage of struts resulted in an increase of the FWHM when going from LP-bl to LNP-fu ($p<0.0001$, Table 2). Paralleling the human results, the LNP and PV interfaces had similar FHWM at the 28-day follow-up. All other curves were significantly different from each other with p values less than 0.01.

Based upon the previously defined edge detection algorithm, the average strut thickness was 164 ± 14 μm at baseline and 172 ± 16 μm at the 6-month follow-up ($p=0.28$).

DISCUSSION

The main findings of this study are: 1) the different interfaces between lumen, polymer, and vessel can be characterized *in vivo* according to the peak intensity and the FWHM of the Gaussian fit of the raw OCT intensity signal; 2) considering the half-max of the LSF as the strut boundary when it is adjacent to tissue, the strut thickness remains the same at all time points and consistent with the nominal thickness of BVS struts given the resolution intrinsic to the OCT equipment.

To the best of our knowledge, this study is the first attempt to differentiate the interface between a translucent polymer and tissue on the basis of optical properties in vivo. It describes a methodology by which these interfaces may be defined that utilizes LSFs to fit the raw OCT intensity signal and FWHM analysis to compensate for the convolution of polymer and tissue reflectivity.

The intensity of the OCT signal is a measurement of the backscattering intensity of infrared light. The magnitude of changes in the refractive index on length scales greater than the wavelength of that light determines the backscattering intensity. In the case of a polymeric implant like the ABSORB BVS, a signal is produced at the boundary of the BVS strut, but there is no signal in the center of the strut due to the homogeneity of the refractive index of the polymer.[1,12] The FWHM of the axial reflectance at an interface has been reported as the true image resolution[19]. Though methodologies differ slightly from previous reports, the FHWM measurement for LP-bl reported here (22.24 – 25.86) may be consistent with the practical resolution of OCT *in vivo* for measurements of BVS struts. The absolute difference in the mea-

sured FWHM between human and swine is within the resolution of OCT. Additionally, slight variability in imaging catheters and the ability of the edge of the scaffold to be a perfect line could contribute to slight differences in the measured FWHM.

The LSF characterizing the LP-bl interface is significantly different from that for interfaces where polymer is adjacent to tissue, because tissue increases backscattering in proximity to the interface and broadens the resulting backscattering signal. Hence, the FWHM increases. On the abluminal side of struts, the LSF also changes over time, as evidenced by the fact that the FWHM of the PV-bl and PV-fu interfaces differ significantly for both humans and swine. Several factors may contribute to this result, including changes in the optical properties of the BVS near the interface or changes in the optical properties of the tissue due to pharmacological activity or foreign body response. Further bench and animal investigations will be needed to interrogate the mechanisms behind these observations. As expected, the FWHM of the LNP-fu and PV-fu interfaces were not significantly different, suggesting that optical changes at the BVS interface occur consistently in both locations over time.

Quantification of strut dimensions over time has been difficult due to the similarity of OCT backscattering signal from tissue and polymer. Utilization of the LSF to characterize the OCT signal offers an objective tool by which the interface between tissue and polymer may be defined, resulting in a more consistent measurement of strut thickness. According to the results reported here, no significant change in strut thickness is observed between baseline and 6 months, as the baseline measurements (158±11 μm) were similar to the reported thickness of the device (ca. 158μm). The finding that the strut thickness remains stable over this time scale is also consistent with the previous OCT results where a gross estimate of "mean strut core area" did not change significantly between baseline and 6 months in a cohort of 25 patients.[12] Future investigation at longer time points will be required to evaluate changes in optical properties following further degradation and mass loss from the scaffold.

The second potential application of the LSF methodology applies to the objective assessment of tissue coverage of a BVS. Incomplete neointimal coverage of struts and incomplete endothelialization are the morphologic features most strongly associated with stent thrombosis.[20] Although OCT has been validated for the assessment of neointimal coverage after stenting in animal models,[5-8] the inability to discriminate between neointima and fibrin/thrombus and the inability to detect endothelial rims thinner than the axial resolution of the equipment limit the specificity and the sensitivity of this technology, respectively. In metallic stents, the hyper-intense backscattering at the luminal edge of struts caused by the profound refractive index contrast between metal and tissue facilitates identification and accurate measurement of very thin layers of tissue covering the struts. Conversely, the assessment of tissue coverage of BVS is more challenging, because the refractive index contrast is less. For thin layers of tissue, the signal displayed is often indistinguishable from that generated by the LP interface alone, requiring more sophisticated signal processing to detect. In considering this issue, it is important to revisit the various length scales that frame the problem.

Although OCT reflectivity can theoretically be caused by refractive index changes on a length scale as small as that of the wavelength of the OCT light (1.3 μm), the axial resolution of OCT is reported to be 10 – 15 μm[13], and the FWHM of the LP-bl signal was measured at 22 – 26 μm in the current study, The latter may represent the practical resolution of OCT applied to polymeric materials. However, the presence of even thin layers of tissue broadens the FWHM, as reported herein, and consequently the LSF FWHM methodology might permit detection of tissue coverage even when the thickness of that coverage cannot be directly measured. A recent study demonstrated the potential of OCT analysis to discern between tissue and fibrin/thrombus (i.e., specificity) in metallic stents.[10] The LSF FWHM approach may constitute a step forward in improving sensitivity and provide an objective criterion for the assessment of neointimal coverage of BVS struts.

Besides the objective assessment of neointimal coverage and the differential diagnosis between neointima and fibrin[10], the analysis of the raw linear OCT signal has been used to detect inflammation and to quantify the density of macrophages in the vessel wall[21,22]. An ongoing study is using also this technology to evaluate cardiac allograft vasculopathy (NCT01403142). All these fields constitute potential future applications for the hereby described LSF analysis, after adjusting the methodology. However, the diagnostic efficiency of LSF analysis is maximal when there exists a normal reference to compare: this uses to be readily available for study of intracoronary devices (post-implant study), but it can be substantially more problematic for the study of the non-stented vessel wall. Sub-cellular OCT appears as a more attractive alternative for the study of vessel inflammation and atherosclerosis in a near future[23].

Limitations

Contrary to previous optical intensity analysis,[10] the current study does not perform any normalization of the signal intensity due to the lack of a reliable reference in the tissue or polymer. Therefore, the absolute intensity values are not directly comparable. The analysis was focused on the shape of the curves, represented by the LSF curve fit and FWHM calculation, which could explain the differences in absolute peak intensity between the human and swine results.

This study was performed on a random sampling of struts meeting specific inclusion criteria. This was necessary to circumvent challenging *in vivo* problems, such as signal attenuation due to eccentricity of the imaging catheter and differences in interpolation as a function of distance from the light source. The described methodology cannot be directly applied to struts not meeting these criteria, e.g. struts lying oblique to the light beam, which are in fact the majority of struts, but further investigations to adapt this methodology for more general use are underway. The LSF analysis of raw linear OCT signal can be performed on any conventional commercially available OCT system, using simple specific software, but this analysis is still experimental and must be performed offline manually by experienced investigators.

The assessment of oblique struts will require alignment of measurements perpendicularly to the adluminal strut surface, calculation of the angle of this adluminal surface with the light beam, and eventually deriving a correction factor. Automation of the analysis protocol will be essential before it can be used more broadly. Future validation studies to identify cut-off values, sensitivity, specificity, and predictive capability are still unknown.

CONCLUSIONS

Fitting the raw OCT backscattering signal to a Gaussian LSF facilitates identification of the interfaces between BVS struts and lumen or tissue. The resulting analysis enables more precise and consistent measurement of BVS strut thickness, which for the ABSORB Cohort B BVS remains unchanged from baseline to the 6-month follow-up and not different from the nominal value. It may also allow inferential detection of neointimal coverage that might not be detected without the benefit of this more sophisticated signal processing.

REFERENCES

1. Serruys PW, Ormiston JA, Onuma Y, Regar E, Gonzalo N, Garcia-Garcia HM, Nieman K, Bruining N, Dorange C, Miquel-Hebert K, Veldhof S, Webster M, Thuesen L, Dudek D. A bioabsorbable everolimus-eluting coronary stent system (ABSORB): 2-year outcomes and results from multiple imaging methods. *Lancet* 2009;373:897-910.
2. Onuma Y, Serruys PW, Perkins LE, Okamura T, Gonzalo N, Garcia-Garcia HM, Regar E, Kamberi M, Powers JC, Rapoza R, van Beusekom H, van der Giessen WJ, Virmani R. Intracoronary Optical Coherence Tomography and Histology at 1 Month and 2, 3, and 4 Years After Implantation of Everolimus-Eluting Bioresorbable Vascular Scaffolds in a Porcine Coronary Artery Model. An Attempt to Decipher the Human Optical Coherence Tomography Images in the ABSORB Trial. *Circulation* 2010;122:2288-2300.
3. Oberhauser JP, Hossainy S, Rapoza RJ. Design principles and performance of bioresorbable polymeric vascular scaffolds. *EuroIntervention Supplement* 2009;5:F15-F22.
4. Ormiston JA, Serruys PW, Regar E, Dudek D, Thuesen L, Webster MW, Onuma Y, Garcia-Garcia HM, McGreevy R, Veldhof S. A bioabsorbable everolimus-eluting coronary stent system for patients with single de-novo coronary artery lesions (ABSORB): a prospective open-label trial. *Lancet* 2008;371:899-907.
5. Suzuki Y, Ikeno F, Koizumi T, Tio F, Yeung AC, Yock PG, Fitzgerald PJ, Fearon WF. In vivo comparison between optical coherence tomography and intravascular ultrasound for detecting small degrees of in-stent neointima after stent implantation. *JACC Cardiovasc Interv* 2008;1:168-173.
6. Deuse T, Erben RG, Ikeno F, Behnisch B, Boeger R, Connolly AJ, Reichenspurner H, Bergow C, Pelletier MP, Robbins RC, Schrepfer S. Introducing the first polymer-free leflunomide eluting stent. *Atherosclerosis* 2008;200:126-134.
7. Prati F, Zimarino M, Stabile E, Pizzicannella G, Fouad T, Rabozzi R, Filippini A, Pizzicannella J, Cera M, De Caterina R. Does optical coherence tomography identify arterial healing after stenting? An in vivo comparison with histology, in a rabbit carotid model. *Heart* 2008;94:217-221.
8. Murata A, Wallace-Bradley D, Tellez A, Alviar C, Aboodi M, Sheehy A, Coleman L, Perkins L, Nakazawa G, Mintz G, Kaluza GL, Virmani R, Granada JF. Accuracy of optical coherence tomography in the evaluation of neointimal coverage after stent implantation. *JACC Cardiovasc Imaging* 2010;3:76-84.
9. Guagliumi G, Sirbu V. Optical coherence tomography: high resolution intravascular imaging to evaluate vascular healing after coronary stenting. *Catheter Cardiovasc Interv* 2008;72:237-247.
10. Templin C, Meyer M, Muller MF, Djonov V, Hlushchuk R, Dimova I, Flueckiger S, Kronen P, Sidler M, Klein K, Nicholls F, Ghadri JR, Weber K, Paunovic D, Corti R, Hoerstrup SP, Luscher TF, Landmesser U. Coronary optical frequency domain imaging (OFDI) for in vivo evaluation of stent healing: comparison with light and electron microscopy. *Eur Heart J* 2010;31:1792-1801.
11. Rossmann K, LUBBERTS G, Cleare H.M. Measurement of the Line Spread-Function of Radiographic Systems Containing Fluorescent Screens. *J Opt Soc Am* 1964;54:187-189.
12. Serruys PW, Onuma Y, Ormiston JA, De Bruyne B, Regar E, Dudek D, Thuesen L, Smits PC, Chevalier B, McClean D, Koolen J, Windecker S, Whitbourn R, Meredith I, Dorange C, Veldhof S, Hebert KM, Rapoza RJ, Garcia-Garcia HM. Evaluation of the second generation of a bioresorbable everolimus drug-eluting vascular scaffold for treatment of de novo coronary artery stenosis: 6-month clinical and imaging outcomes. *Circulation* 2010;122:2301-2312.

13. Bezerra HG, Costa MA, Guagliumi G, Rollins AM, Simon DI. Intracoronary optical coherence tomography: a comprehensive review clinical and research applications. *JACC Cardiovasc Interv* 2009;2:1035-1046.
14. Prati F, Cera M, Ramazzotti V, Imola F, Giudice R, Giudice M, Propris SD, Albertucci M. From bench to bedside: a novel technique of acquiring OCT images. *Circ J* 2008;72:839-843.
15. Davis CC. Lasers and electro-optics: fundamentals and engineering. New York, N.Y.: Cambridge University Press; 1996.
16. Yang Yr, Wanek J, Shahidi M. Representing the retinal line spread shape with mathematical functions. *Journal of Zhejiang University - Science B* 2008;9:996-1002.
17. Peng Y, Lu R. Modeling multispectral scattering profiles for prediction of apple fruit firmness. *Trans ASAE* 2005;48:235-242.
18. Amirav I, Kramer SS, Grunstein MM, Hoffman EA. Assessment of methacholine-induced airway constriction by ultrafast high-resolution computed tomography. *J Appl Physiol* 1993;75:2239-2250.
19. Jang IK, Bouma BE, Kang DH, Park SJ, Park SW, Seung KB, Choi KB, Shishkov M, Schlendorf K, Pomerantsev E, Houser SL, Aretz HT, Tearney GJ. Visualization of coronary atherosclerotic plaques in patients using optical coherence tomography: comparison with intravascular ultrasound. *Journal of the American College of Cardiology* 2002;39:604-609.
20. Finn AV, Joner M, Nakazawa G, Kolodgie F, Newell J, John MC, Gold HK, Virmani R. Pathological Correlates of Late Drug-Eluting Stent Thrombosis: Strut Coverage as a Marker of Endothelialization. *Circulation* 2007;115:2435-2441.
21. Tearney GJ, Yabushita H, Houser SL, Aretz HT, Jang IK, Schlendorf KH, Kauffman CR, Shishkov M, Halpern EF, Bouma BE. Quantification of Macrophage Content in Atherosclerotic Plaques by Optical Coherence Tomography. *Circulation* 2003;107:113-119.
22. MacNeill BD, Jang IK, Bouma BE, Iftimia N, Takano M, Yabushita H, Shishkov M, Kauffman CR, Houser SL, Aretz HT, DeJoseph D, Halpern EF, Tearney GJ. Focal and multi-focal plaque macrophage distributions in patients with acute and stable presentations of coronary artery disease. *Journal of the American College of Cardiology* 2004;44:972-979.
23. Liu L, Gardecki JA, Nadkarni SK, Toussaint JD, Yagi Y, Bouma BE, Tearney GJ. Imaging the subcellular structure of human coronary atherosclerosis using micro-optical coherence tomography. *Nat Med* 2011;17:1010-1014.

"Cuanto menos se lee, más daño hace lo que se lee".

(The less you read, the more harmful is what you read)

Miguel de Unamuno

PART 8

SPECIAL SCENARIOS

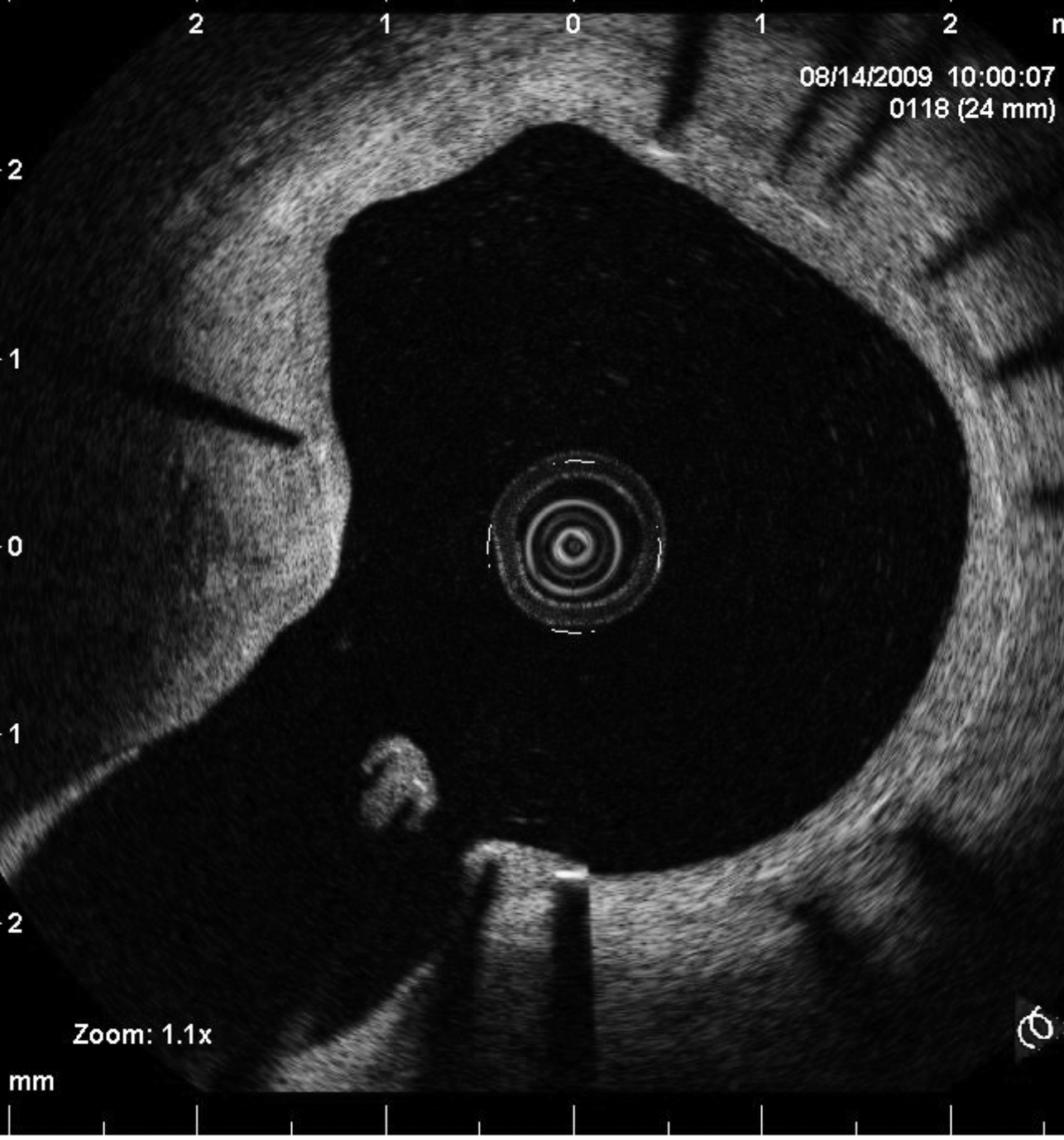
2
1
0
1
2
08/14/2009 10:00:07
0118 (24 mm)
2
1
0
1
2
Zoom: 1.1x
mm

CHAPTER 12

Malapposition and side branches


2
1
0
1
2
mm
08/14/2009 10:00:07
0118 (24 mm)
Zoom: 1.1x

12.1

Delayed coverage in malapposed and side-branch struts with respect to well-apposed struts in drug-eluting stents: in vivo-assessment with optical coherence tomography.

Gutiérrez-Chico JL, Regar E, Nüesch E, Okamura T, Wykrzykowska JJ, di Mario C, Windecker S, van Es GA, Gobbens P, Jüni P, Serruys PW.

Circulation 2011; 124 (5): 612-23.

ABSTRACT

Background: Pathology studies on fatal cases of very late stent thrombosis have described incomplete neointimal coverage as common substrate, in some cases appearing at side branch struts. IVUS studies have described the association between incomplete stent apposition (ISA) and stent thrombosis, but the mechanism explaining this association remains unclear. Whether the neointimal coverage of non-apposed side-branch (NASB) and ISA struts is delayed with respect to well-apposed (WA) struts is unknown.

Methods and results: OCT studies from 178 stents implanted in 99 patients from 2 randomized trials were analyzed at 9-13 months follow-up. The sample included 38 sirolimus-eluting (SES), 33 biolimus-eluting (BES), 57 everolimus-eluting (EES) and 50 zotarolimus-eluting stents (ZES). OCT coverage of NASB and ISA struts was compared vs. WA struts of the same stent, using statistical pooled analysis with a random effects model. 34120 struts were analyzed. The risk-ratio of delayed coverage was 9.00 (95% CI: 6.58 – 12.32) for NASB vs. WA struts, 9.10 (95% CI: 7.34 – 11.28) for ISA vs. WA and 1.73 (95% CI: 1.34 – 2.23) for ISA vs. NASB struts. Heterogeneity of the effect was observed in the comparison ISA vs. WA ($H=1.27$; $I^2=38.40$), but not in the other comparisons.

Conclusions: Coverage of ISA and NASB struts is delayed with respect to WA struts in DES, as assessed by OCT.

Clinical Trial Registration Information: NCT00389220 (http://clinicaltrials.gov/ct2/show/NCT00389220), NCT00617084 (http://clinicaltrials.gov/ct2/show/NCT00617084),

Key words: Coronary vessels; coronary stenosis; angioplasty, transluminal percutaneous coronary; drug-eluting stents; sirolimus; biolimus A9; everolimus; zotarolimus; tomography, optical coherence.

LIST OF ABBREVIATIONS

BES: Biolimus-eluting stent
DES: Drug-eluting stent
EES : Everolimus-eluting stent
ISA: Incomplete stent apposition
LVLST: Late and very late stent thrombosis
NASB: Non-apposed side-branch struts
OCT: Optical coherence tomography
RR: Risk ratio
SES: Sirolimus-eluting stent
WA: Well-apposed struts
ZES: Zotarolimus-eluting stent

INTRODUCTION

The reduction of restenosis rates achieved by drug eluting stents (DES)[1] has been somewhat obscured by concerns about their safety and the incidence of late and very late stent thrombosis (LVLST)[2-5].

Pathology studies have described delayed neointimal healing[6-10] with incomplete endothelialization of the struts[10] as the common morphologic finding in fatal cases of LVLST. Some of these autopsy studies found incomplete neointimal coverage and fibrin deposition in struts lying across the take-off of side branches in bifurcations, also named non-apposed side-branch struts (NASB), thus pointing out NASB struts as potential triggers for LVLST[7,9]. However clinical studies on bifurcation stenting techniques have not confirmed this hypothesis. Jailing side branches is a widespread practice and there is no clinical evidence of an eventual association to higher thrombotic risk[11]. Moreover, some randomized trials failed to prove any clinical advantage of strategies pursuing the apposition of NASB struts compared to the simple "stenting across"[12] .

IVUS studies have described consistently the association between incomplete stent apposition (ISA) and LVLST[13,14]. However the mechanism responsible for this association is still not clear. ISA might represent a handicap per se for a proper endothelialization, but might be just the consequence of a primary process causing both ISA and LVLST, as in the case of delayed hypersensitivity resulting in an inflammatory response, aneurysmatic dilatation of the vessel wall, late-acquired malapposition and thrombosis[8,15,16]. The elucidation of the mechanism linking ISA and thrombosis is relevant for the interventional cardiologist, because it determines how important the optimization of apposition is: spending time and resources in optimization only makes sense if ISA is the primary problem. A recent descriptive sequential optical coherence tomography (OCT) study found that 2/3 of acutely malapposed struts were uncovered at 10 months follow-up, suggesting that neointimal coverage might be hampered in ISA struts[17], but no comparative analysis between ISA and well-apposed struts for the risk of incomplete coverage was performed. No OCT study has addressed hitherto the question whether ISA or NASB struts pose higher risk of incomplete coverage in DES, the latter having been excluded from the analysis in most of the studies published hitherto[18-21].

The aim of this OCT study is evaluating whether the coverage of ISA and NASB struts is delayed with respect to well-apposed (WA) struts of the same stent in DES.

METHODS

Study sample

Data at follow-up from the OCT substudies of two different randomized trials were analyzed: the LEADERS trial[22,23], comparing a biolimus-eluting stent (BES) with biodegradable polymer in abluminal coating (BioMatrix™ Flex, Biosensors International, Morges, CH) vs. a sirolimus-eluting stent (SES) with durable polymer (Cypher™ SELECT, Cordis, Miami Lakes, FL, USA); and the RESOLUTE-All comers trial[24], comparing a zotarolimus-eluting stent (ZES) with hydrophilic-polymer coating (Resolute, Medtronic Inc, Santa Rosa, CA, USA) vs. an everolimus-eluting stent (EES) with fluoropolymer (Xience V, Abbott Vascular, Santa Clara, CA, USA). The design and results of these trials have been published elsewhere[22-24]. Both trials followed an all-comers design, with minimal exclusion criteria. In LEADERS the OCT follow-up was scheduled at 9 months, whereas in RESOLUTE-all comers it was at 13 months.

OCT study and analysis

OCT pullbacks were obtained at follow-up with M2, M3 or C7 systems (Lightlab Imaging, Westford, Massachusetts, USA), according to the availability at the participating sites, using occlusive or non-occlusive technique as appropriate[25]. Table 1 summarizes the technical specifications of each OCT system and optical catheters. Infusion of intracoronary nitroglycerin before the OCT pullback was strongly encouraged.

Table 1: Technical specifications of the different OCT systems in the study.

	M2	M3	C7
Technique	Occlusive	Non-occlusive	Non-occlusive
Domain	Time	Time	Fourier
Catheter	ImageWire	ImageWire	Dragonfly
Rotation speed (frames/s)	15.6	20	100
Pullback speed (mm/s)	2	3	10-20
Patients with SES	0	22	0
Patients with BES	0	19	0
Patients with EES	2	9	17
Patients with ZES	1	9	20
Total nr of patients	3	59	37

All systems and catheters from Lightlab Imaging, Westford, Massachusetts, USA.

OCT pullbacks were analysed offline in a core-laboratory (Cardialysis BV, Rotterdam, NL) by independent staff blinded to stent-type allocation and clinical and procedural characteristics of the patients, using proprietary software (Lightlab Imaging). Cross-sections at 1mm intervals within the stented segment and 5mm proximal and distal to the stent edges were analyzed. A metallic strut typically appears as a bright signal-intense structure with dorsal shadowing. Apposition was assessed strut by strut by measuring the distance between the strut marker and the lumen contour. The marker of each strut was placed at the endoluminal leading edge, in the mid-point of its long-axis, and the distance was measured following a straight line connecting this marker with the centre of gravity of the vessel[26]. Struts were classified as ISA if the distance between the strut marker and the lumen contour was bigger than the specific strut thickness plus the axial resolution of OCT (14μm). This resulted in ISA thresholds of >168μm for SES, >131μm for BES, >99μm for EES, 111μm for ZES and 95μm

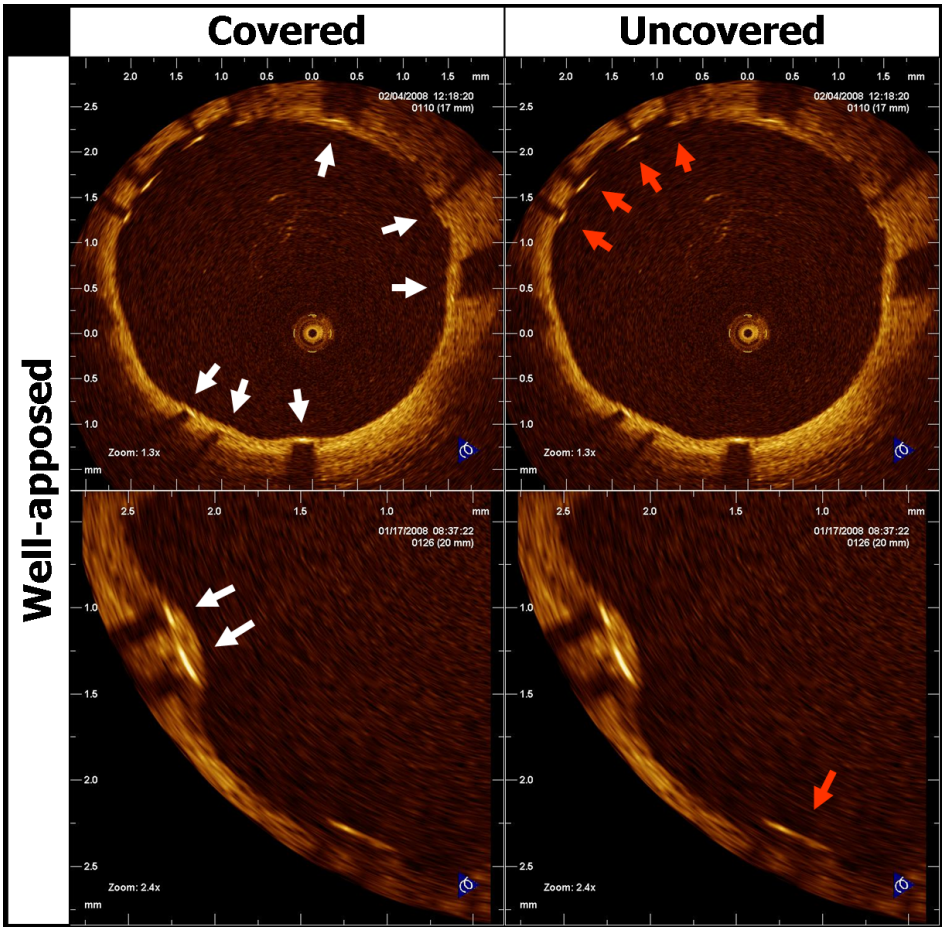

Figure 1: Examples of covered (white arrows) and uncovered (red arrows) well-apposed struts.

for the combination drug-coated balloon (DCB) plus bare-metal stent. Struts located at the ostium of side branches, with no vessel wall behind, were labelled as NASB and excluded from the analysis of apposition.

Struts were classified as uncovered if any part of the strut was visibly exposed to the lumen or as covered if a layer of tissue was visible over all the reflecting surfaces. In covered struts, the thickness of coverage was measured from the marker of each visible strut to the endoluminal edge of the tissue coverage, following a straight line connecting the strut marker with the centre of gravity of the vessel[18-21,23].

Each strut was finally categorized according to apposition as WA, ISA or NASB, and according to coverage as covered or uncovered (Figures 1-2).

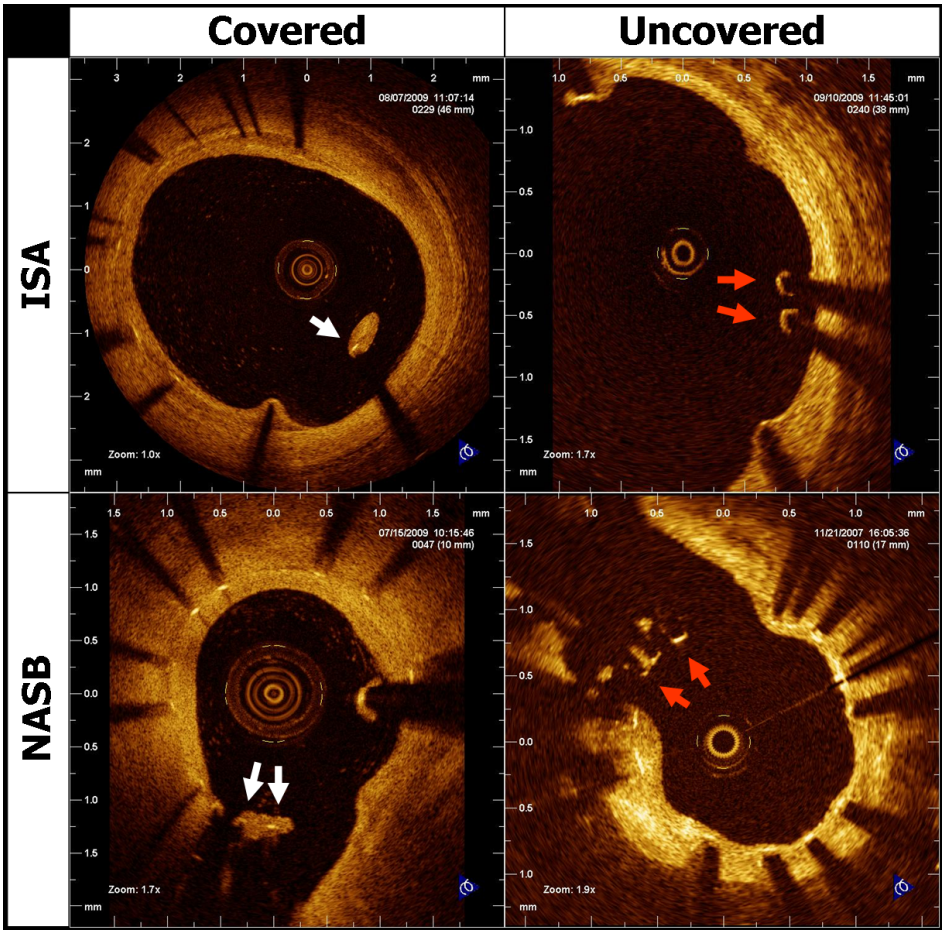

Figure 2: Examples of malapposed (ISA) and side-branch (NASB) struts appearing covered (white arrows) and uncovered (red arrows) at follow-up.

ISA: Incomplete stent apposition

NASB: Non-apposed side-branch (struts).

Statistical analysis

The risk ratio (RR) for non-coverage of ISA and NASB was calculated vs. WA struts by pooled analysis using an inverse variance random effects model, taking into account the between-clusters and within-the-cluster variability, using each stent as independent unit of clustering (see supplemental methods). For each comparison between apposition categories, stents with zero struts in any of the compared apposition categories (no exposition) or zero uncovered struts (no events) were considered not informative to evaluate the RR, and discarded for the analysis. A proportional continuity correction was applied to stents with zero uncovered struts (zero events) in only one of the compared apposition categories[27]. The risk ratio at each individual stent and the pooled risk ratio of the whole sample were graphically represented by mean of forest plots. Analysis of heterogeneity of the effect was performed with the Q, H and I^2 parameters, considering the presence of heterogeneity when the p-value of the test was ≤0.1. Calculations were done with PASW 17.0 software (Chicago, IL, USA), using a specific macro (© Domenech JM)[28]. The RR for non-coverage of ISA vs. NASB struts was calculated following the same method.

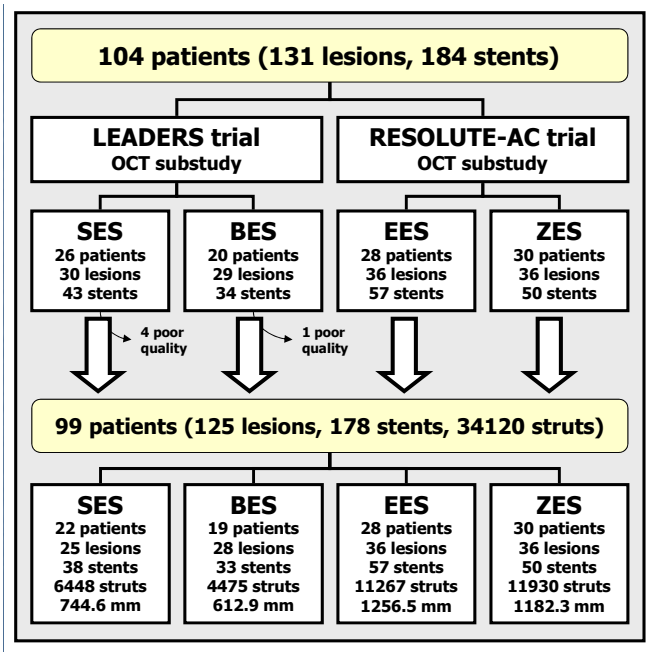

Figure 3:

Flow chart summarizing the patients and stents included in this study, pooled from three different OCT randomized trials.
BES: Biolimus-eluting stent; EES: Everolimus-eluting stent; SES: Sirolimus-eluting stent; ZES: Zotarolimus-eluting stent.

RESULTS

104 patients (131 lesions, 184 stents) were included in this study. Insufficient quality of the OCT pullback, owed to incomplete blood removal, led to exclusion of 5 patients from the analysis: 4 SES, 1 BES. 99 patients (22 SES, 19 BES, 28 EES, 30 ZES), 125 lesions, 178 stents, 34120 struts and 3796mm of stented vessel were finally analyzed (Figure 3, supplemental tables).

Table 2: Patients' and procedural baseline characteristics grouped by type of stent.

	SES (n=22)	BES (n=19)	EES (n=28)	ZES (n=30)	p-val
Age (years)	61.5 (11.3)	64.9 (9.8)	62,6 (8,9)	60,9 (12,5)	0.621
Males	15 (68.2%)	14 (73.7%)	23 (82,1%)	23 (76,7%)	0.849
Cardiovascular risk factors					
Hypertension	13 (59.1)	9 (47.4%)	15 (53,6%)	18 (60,0%)	0.823
DM	4 (18.2%)	4 (21.1%)	7 (25%)	7 (23,3%)	0.947
Insulin-requiring	1 (4.5%)	2 (10.5%)	2 (7,1%)	0 (0,0%)	0.384
Hypercholesterolemia	16 (72.7%)	10 (52.6%)	20 (71,4%)	21 (70,0%)	0.480
Smoking	13 (59.1%)	11 (57.9%)	16 (57,1%)	18 (60,0%)	0.825
Current smoker (<30d)	10 (45.5%)	5 (26.3%)	9 (32,1%)	11 (36,7%)	0.613
Family history of CHD	15 (68.2%)	11 (57.9%)	11 (50,0%)	7 (35,0%)	0.179
Antecedents					
Previous MI	7 (31.8%)	6 (31.6%)	9 (32,1%)	7 (25,0%)	0.929
Previous PCI	6 (27.3%)	4 (21.1%)	4 (14,3%)	8 (26,7%)	0.636
Previous CABG	3 (13.6%)	1 (5.3%)	3 (10,7%)	2 (6,7%)	0.756
Clinical presentation					0.598
Stable angina	14 (63.6%)	11 (57.9%)	11 (39,3%)	16 (53,3%)	0.350
Unstable angina	3 (13.6%)	0 (0.0%)	5 (17,9%)	3 (10,0%)	0.279
Myocardial infarction	5 (22.7%)	7 (36.8%)	10 (35,7%)	9 (30%)	0.729
STEMI	3 (13.6%)	5 (26.3%)	7 (25,0%)	6 (20,0%)	0.725
Silent ischemia	0 (0.0%)	1 (5.3%)	2 (7,1%)	2 (6,7%)	0.661
Procedural characteristics					
Nr vessels treated	1.14 (0.35)	1.26 (0.45)	1,21 (0,42)	1,30 (0,54)	0.615
Nr of lesions treated	1.64 (0.95)	1.89 (0.88)	1,46 (0,64)	1,40 (0,68)	0.149
Nr of stents implanted	1.45 (0.80)	1.32 (0.58)	2,36 (1,22)	2,00 (1,78)	**0.019***
Total stented length (mm)	36.8 (25.7)	39.5 (21.4)	47,9 (29,7)	40,1 (42,6)	0.641
Small vessel (<2.5mm diam)	11 (50%)	7 (36.8%)	15 (68,2%)	12 (48,0%)	0.239
Overlap	9 (40.9%)	5 (26.3%)	9 (32,1%)	3 (10,0%)	0.071

* $p \leq 0,05$

BES: Biolimus-eluting stent; BMS: Bare Metal Stent; CABG: Coronary Artery By-pass Graft; CHD: Coronary Heart Disease; DCB: Drug-coated balloon; DES: Drug-eluting stent; DM: Diabetes Mellitus; EES: Everolimus-eluting stent; LAD: Left anterior descending; LCX: Left Circumflex; LM: Left Main Stem; MI: Myocardial Infarction; PCI: Percutaneous Coronary Intervention; RCA: Right coronary artery; SES: Sirolimus-eluting stent; STEMI: ST elevation myocardial infarction; ZES: Zotarolimus-eluting stent.

Tables 2 and 3 summarize the baseline clinical and procedural characteristics of the patients and angiographic characteristics of the lesions in the sample, respectively, grouped by type of stent. There were significant different between the groups in average number of implanted stents, bifurcation stenting or reference vessel diameter. Table 4 shows the OCT-derived areas and volumes in the stented regions, excluding stent overlaps, averaged per stent. The parameters measuring neointimal hyperplasia were significantly different between the DES subgroups. 65 stents had ≥1 ISA struts (35.3%). In this subgroup, the average in-stent mean lumen area (8.01±2.78 mm^2) was in between the average mean lumen areas of the proximal and distal reference segments (8.61±2.80, 6.90±2.59mm^2, respectively). In 9 cases (13.2% of the ISA stents, 4.9% of total), the mean in-stent lumen area (8.85±1.98

Table 3: Angiographic lesions characteristics grouped by type of stent.

	SES (n=25)	BES (n=28)	EES (n=36)	ZES (n=36)	p-val
Target vessel					0.919
	0 (0.0%)	0 (0.0%)	1 (2.4%)	0 (0.0%)	0.477
	10 (40.0%)	13 (46.4%)	15 (41.7%)	14 (38.9%)	0.939
	5 (20.0&)	3 (10.7%)	6 (16.7%)	5 (13.9%)	0.803
	10 (40.0%)	12 (42.9%)	14 (38.9%)	17 (47.2%)	0.900
TO	2 (8.0%)	2 (7.1%)	6 (16.7%)	6 (16.7%)	0.516
Ostial lesion	0 (0.0%)	0 (0.0%)	1 (2.8%)	1 (2.8%)	0.683
Bifurcation	3 (12.0%)	2 (7.1%)	12 (33.3%)	8 (22.2%)	**0.046***
Mod or severe calcific	2 (8.0%)	1 (3.6%)	5 (13.9%)	8 (22.2%)	0.135
QCA characteristics					
Lesion length (mm)	10.0 (5.2)	14.1 (15.1)	13.8 (10.0)	16.6 (9.9)	0.280
Pre-stenting					
RVD (mm)	2.38 (0.61)	2.81 (0.57)	2.59 (0.54)	2.84 (0.56)	**0.044***
MLD (mm)	0. 59 (0.50)	0.89 (0.64)	0.78 (0.51)	0.88 (0.58)	0.164
% diam stenosis	75 (21)	68 (22)	70 (19)	69(19)	0.609
Post-stenting					
In-stent					
RVD (mm)	2.61 (0.46)	2.76 (0.49)	2.82 (0.45)	2.91 (0.49)	0.094
MLD (mm)	2.21 (0.44)	2.40 (0.46)	2.40 (0.48)	2.44 (0.51)	0.257
% diam stenosis	15 (8)	13 (6)	15 (7)	16 (8)	0.353
In-segment					
RVD (mm)	2.55 (0.50)	2.69 (0.55)	2.66 (0.46)	2.83 (0.47)	0.159
MLD (mm)	1.94 (0.45)	2.11 (0.53)	2.01 (0.39)	2.15 (0.44)	0.277
% diam stenosis	24 (8)	22 (8)	24 (9)	24 (9)	0.692

* p≤0,05

BES: Biolimus-eluting stent; DCB: Drug-coated balloon; EES: Everolimus-eluting stent; LAD: Left anterior descending; LCX: Left Circumflex; LM: Left Main Stem; MLD: Minimal Lumen Diameter; QCA: Quantitative Coronary Angiography; RCA: Right coronary artery; RVD: Reference vessel diameter; SES: Sirolimus-eluting stent; TO: Total occlusion; ZES: Zotarolimus-eluting stent.

Table 4: Areas and volumetric analysis per stent (excluding overlapping segments) grouped by type of stent.

99 patients **125 lesions** **178 stents**	**SES** 22 patients 25 lesions 38 stents	**BES** 19 patients 28 lesions 33 stents	**EES** 28 patients 36 lesions 57 stents	**ZES** 30 patients 36 lesions 50 stents	**p-val**
Stent length (mm)	16.6 (8.2)	20.6 (7.7)	18.6 (8.6)	18.7 (9.3)	0.180
MLA (mm^2)	5.05 (2.16)	5.55 (2.49)	5.35 (2.45)	5.45 (2.39)	0.843
Mean lumen Area (mm^2)	6.63 (2.24)	7.10 (2.49)	6.68 (2.75)	6.89 (2.52)	0.883
Lumen volume (mm^3)	108.9 (74.4)	139.7 (71.6)	123.2 (73.0)	130.1 (80.4)	0.341
Min stent area (mm^2)	5.66 (2.04)	6.13 (2.17)	6.47 (2.42)	6.37 (2.41)	0.386
Mean stent area (mm^2)	6.97 (2.09)	7.66 (2.05)	7.64 (2.59)	7.70 (2.38)	0.476
Stent volume (mm^3)	114.2 (74.4)	152.9 (68.4)	140.8 (77.2)	145.2 (85.1)	0.181
% frames with ISA	4.76 (11.07)	3.83 (8.92)	3.18 (7.00)	5.10 (9.84)	0.734
Max ISA area (mm^2)	0.59 (1.29)	0.21 (0.47)	0.49 (1.56)	0.39 (0.76)	0.662
ISA volume (mm^3)	1.52 (5.58)	0.49 (1.50)	1.08 (3.90)	0.79 (1.80)	0.741
Corrected by stent volume (%)	1.22 (4.25)	0.31 (0.98)	0.66 (2.27)	0.58 (1.39)	0.538
Max NIH area (mm^2)	1.08 (0.77)	1.46 (1.23)	1.88 (0.87)	1.73 (0.82)	**<0.0001***
NIH volume (mm^3)	6.8 (6.8)	13.6 (21.2)	18.7 (14.4)	15.9 (11.6)	**0.002***
In-stent NIH vol obstruction (%)	6.8 (6.0)	10.1 (14.5)	15.0 (10.7)	12.5 (7.9)	**0.001***

* p≤0,05

BES: Biolimus-eluting stent; DCB: Drug-coated balloon; EES: Everolimus-eluting stent; ISA: Incomplete stent apposition; MLA: Minimal lumen area; NIH: Neointimal hyperplasia; SES: Sirolimus-eluting stent; ZES: Zotarolimus-eluting stent.

mm^2) was bigger than the mean lumen areas in both the proximal and distal reference segments (7.32±2.25, 7.27±3.04mm^2, respectively), but not significantly larger than in the whole ISA subgroup (p=0.333) (figure 4); ISA volume was not significantly different between the aneurysmatic and non-aneurysmatic subgroups (1.85±1.58 vs. 2.24±3.00mm^3, p=0.707), respectively; and the total number of ISA struts was significantly lower in the aneurysmatic pattern (3.44 vs. 6.77, p=0.024).

Raw proportions of coverage in the global sample

Table 5 shows the total count of struts in each apposition category in the whole sample, and the raw proportions of coverage without clustering by patient, lesion or stent. 94.9% of well-apposed struts are covered at follow-up, versus only 78.1% of NASB struts and 27.4% of ISA struts.

Risk of non-coverage at the stent level

73 stents (41.0%) had NASB struts; 64 (36.0%) had ≥1 ISA strut and 127 (71.3%) were incompletely covered at follow-up. The presence of NASB struts was significantly associated to incomplete coverage of the stent: 63 (86.3%) stents with NASB struts were incompletely

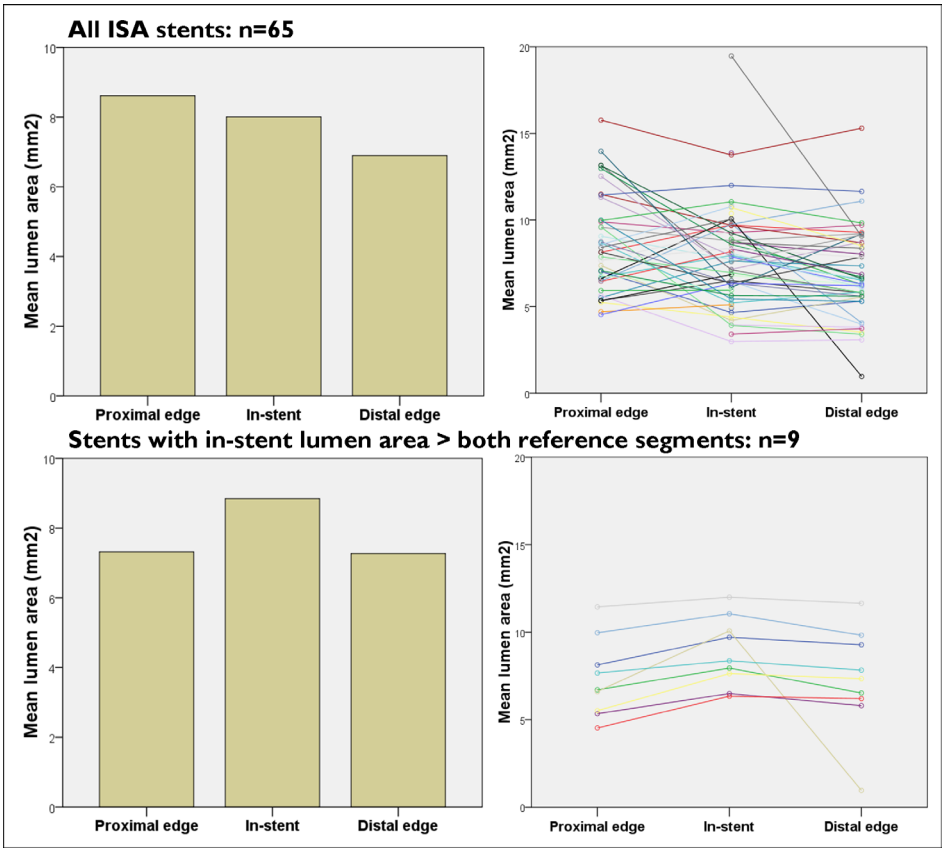

Figure 4:

Mean lumen areas by OCT in the stented segment and in the proximal/distal reference segments. The upper panel represents the mean areas (left) and individual areas (right) of the 73 stents wth ISA. Only in 11 stents (lower panel) the mean in-stent lumen area was bigger than in both the proximal and distal reference segments, typical pattern described in cases of stent thrombosis.

Table 5: Cross-tab with the categories of apposition and the coverage of the struts in the global sample, without clustering by patient or stent. The results are presented as "count (percent)".

			Coverage		Total
			Covered	Uncovered	
DES	**Apposition**	Well-apposed	31722 (94.9%)	1709 (5.1%)	33431
		ISA	115 (27.4%)	304 (72.6%)	419
		NASB	211 (78.1%)	59 (21.9%)	270
	Total		32048 (93.9%)	2072 (6.1%)	34120

covered, compared to 64 (61.0%) without NASB (p=0,008). Likewise, the presence of ISA was significantly associated to incomplete coverage of the stent: 62 (96.9%) stents with ISA were incompletely covered, compared to 65 (57.0%) totally well-apposed stents (p<0.0001).

Coverage of NASB vs. well-apposed struts

105 DES had no NASB struts; 11 DES across side-branches had all NASB and well-apposed struts completely covered. 62 DES (13083 struts) were suitable for the pooled comparison of the risk of non-coverage in NASB (n=216) vs. WA struts (n=12867). NASB struts present a risk ratio for non-coverage of 9.00 (95% CI: 6.58 – 12.32) compared to WA struts (Table 6, figure 5). There was no significant heterogeneity of the effect in any of the subgroups (H<1; I^2=0).

Table 6: Stratified pooled analysis by type of stent of the risk ratio for non-coverage in side-branch vs. well-apposed struts, malapposed vs. well-apposed struts and malapposed vs. side-branch struts.

				Magnitude of effect			Heterogeneity of the effect				
			n	RR	95% CI		Q	p val	H	I^2	τ^2
					Lower	Upper					
NASB vs. WA	DES		62	9.00	6.58	12.32	57.52	0.603	0.97	0.00	0.41
		SES	9	22.69	11.93	43.15	7.03	0.534	0.94	0.00	0.00
		BES	10	6.19	3.27	11.70	1.75	0.995	0.44	0.00	0.00
		EES	18	11.52	6.47	20.51	24.08	0.117	1.19	29.41	0.80
		ZES	25	6.59	4.56	9.52	20.61	0.662	0.93	0.00	0.09
ISA vs. WA	DES		62	9.10	7.34	11.28	99.03	0.001	1.27	38.40	0.48
		SES	14	5.43	3.44	8.57	14.40	0.346	1.05	9.75	0.33
		BES	9	6.67	4.12	10.80	15.02	0.059	1.37	46.75	0.22
		EES	16	12.36	7.76	19.67	23.19	0.080	1.24	35.31	0.66
		ZES	23	10.56	7.51	14.84	36.92	0.024	1.30	40.41	0.53
ISA vs. NASB	DES		33	1.73	1.34	2.23	23.04	0.877	0.85	0.00	0.00
		SES	2	0.65	0.03	16.50	1.00	0.317	1.00	0.00	3.40
		BES	5	1.81	0.55	5.97	2.47	0.650	0.79	0.00	0.00
		EES	8	1.70	1.07	2.69	5.65	0.582	0.90	0.00	0.00
		ZES	18	1.78	1.29	2.45	11.66	0.820	0.83	0.00	0.00

BES: Biolimus-eluting stent; DCB: Drug-coated balloon; DES: Drug-eluting stents; EES: Everolimus-eluting stent; ISA: Incomplete stent apposition; NASB: Non-apposed side-branch struts; SES: Sirolimus-eluting stent; WA: well-apposed struts; ZES: Zotarolimus-eluting stent.

Coverage of ISA vs. well-apposed struts

113 DES had no ISA struts; 3 DES with malapposition had all ISA and well-apposed struts completely covered. 62 DES (12558 struts) were suitable for the pooled comparison of the

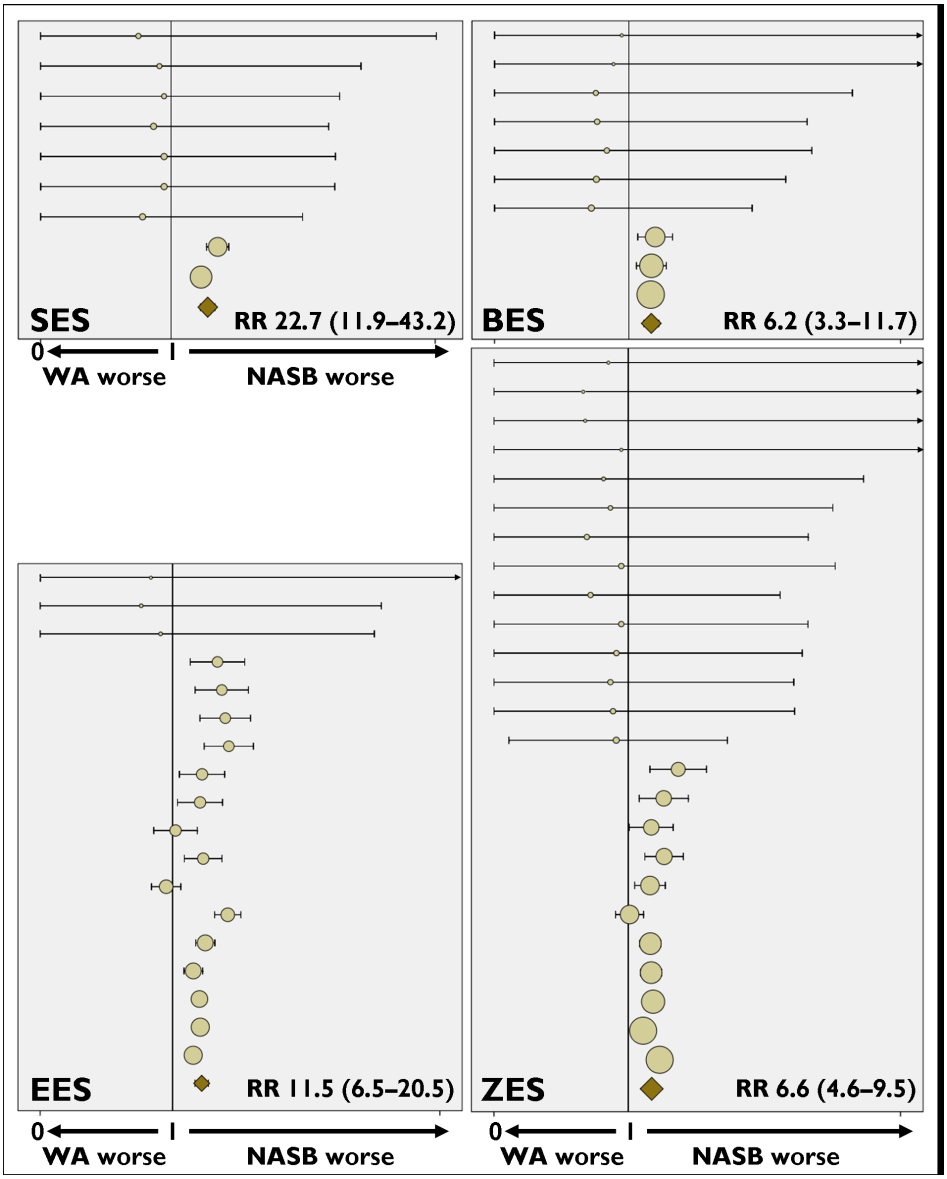

Figure 5:

Forest plot showing the pooled analysis for uncoverage at 6-13 months follow-up in non-apposed side branch (NASB) struts vs. well-apposed (WA) struts. Lines represent the confidence interval for the risk ratio in each analysed stent, with the pooled risk ratio at the bottom.
BES: Biolimus-eluting stent; EES: Everolimus-eluting stent; NASB: Non-apposed side-branch struts; RR: Risk ratio; SES: Sirolimus-eluting stent; WA: Well-apposed struts; ZES: Zotarolimus-eluting stent.

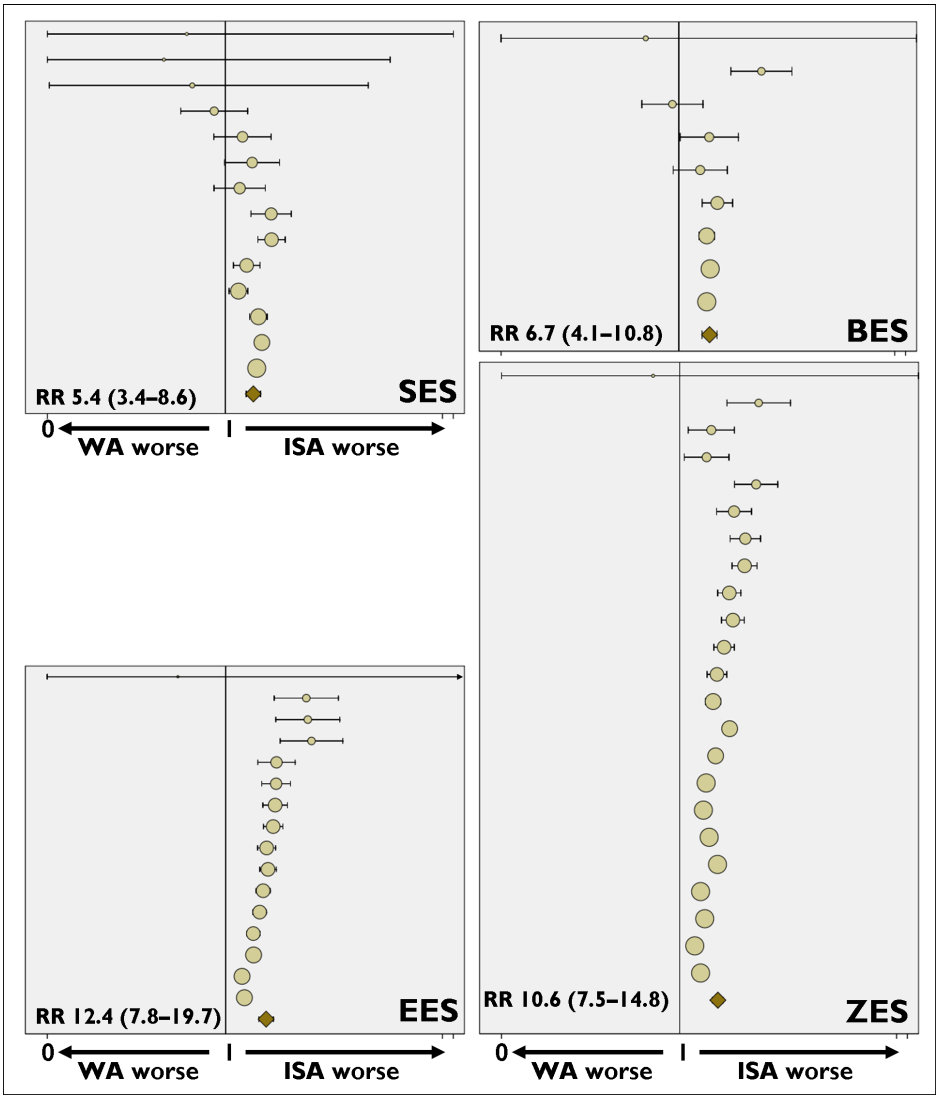

Figure 6:

Forest plot showing the pooled analysis for non-coverage at 6-13 months follow-up in incomplete stent apposition (ISA) struts vs. well-apposed (WA) struts. Lines represent the confidence interval for the risk ratio in each analysed stent, with the pooled risk ratio at the bottom.
BES: Biolimus-eluting stent; EES: Everolimus-eluting stent; ISA: Incomplete stent apposition struts; RR: Risk ratio; SES: Sirolimus-eluting stent; WA: Well-apposed struts; ZES: Zotarolimus-eluting stent.

risk of non-coverage in ISA (n=405) vs. WA struts (n=12153). ISA struts present a risk ratio for non-coverage of 9.10 (95% CI: 7.34 – 11.28) compared to WA struts (Table 6, figure 6). The magnitude of the effect varied substantially between the different types of DES, ranging from 5.43 in SES to 12.36 in EES. There was considerable heterogeneity of the effect, even after stratifying by type of stent.

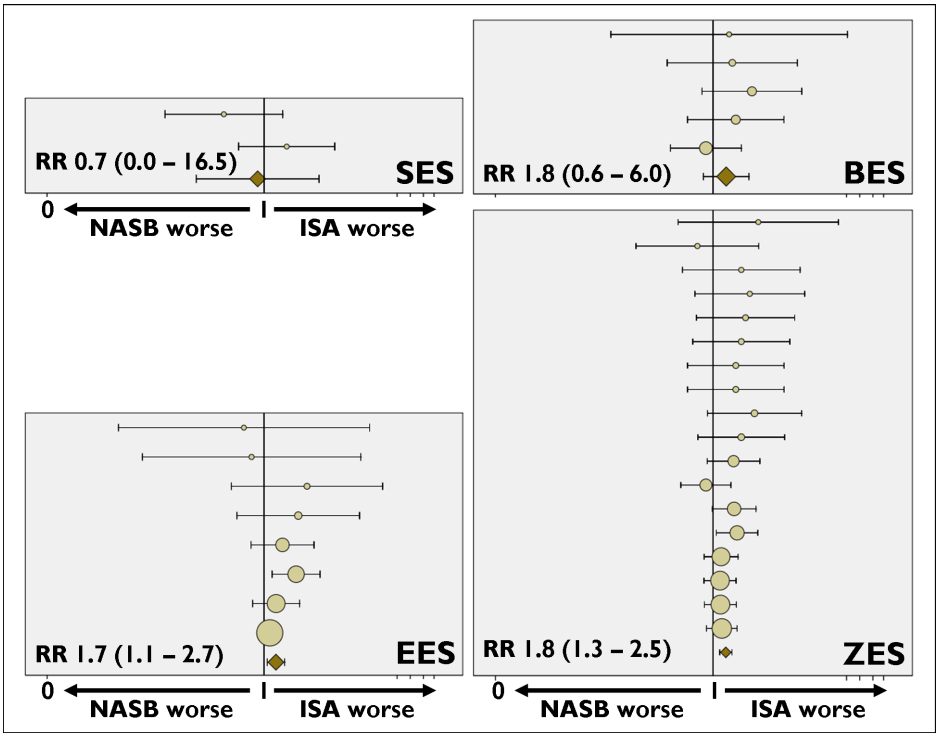

Figure 7:

Forest plot showing the pooled analysis for uncoverage at 6-13 months follow-up in incomplete stent apposition (ISA) struts vs. non-apposed side-branch (NASB) struts. Lines represent the confidence interval for the risk ratio in each analysed stent, with the pooled risk ratio at the bottom.

BES: Biolimus-eluting stent; EES: Everolimus-eluting stent; ISA: Incomplete stent apposition struts; NASB: Non-apposed side-branch struts; RR: Risk ratio; SES: Sirolimus-eluting stent; ZES: Zotarolimus-eluting stent.

Coverage of ISA vs. NASB struts

33 DES (335 struts) were suitable for the pooled comparison of the risk of non-coverage in ISA (n=211) vs. NASB struts (n=124). ISA struts present a risk ratio for non-coverage of 1.73 (95% CI: 1.34 – 2.23) compared to NASB struts (Table 6, figure 7). There was no significant heterogeneity of the effect in any of the subgroups ($H<1$; $I^2=0$).

DISCUSSION

The main findings of this analysis are: 1) Coverage of ISA and NASB struts is delayed with respect to that of WA struts in DES, as assessed by OCT; 2) Coverage of ISA struts is delayed with respect to that of NASB struts in DES, as assessed by OCT. These results suggest that the neointimal coverage of NASB and ISA struts is delayed with respect to WA struts in DES.

Implications for NASB struts

To the best of our knowledge this is the first human in vivo study addressing the coverage of NASB struts. Most of the recently published OCT studies excluded NASB struts from the analysis[18-21], because they were methodologically cumbersome and their meaning was not fully understood. Our results clarify the impact of NASB struts on the coverage of the stent and could explain the apparent discrepancy between pathological and clinical studies in this respect. Although some pathological studies on patients deceased by stent thrombosis found incomplete neointimal coverage in struts at side branches[7,9], "stenting across" continued to be a widespread practice, often the compromise solution for many challenging cases, and LVLST still remained a rare complication[29]. The NORDIC trial did not find any significant difference in clinical outcomes between a simple strategy of "stenting across" and a complex 2-stents technique[11,30]. The NORDIC-III trial compared specifically the strategy of "stenting across" (a NASB-generating technique) vs. systematic final kissing-balloon (a NASB-reducing technique) and also failed to find any clinical advantage for any of the strategies[12]. The inherent selection bias of autopsy studies has been advocated to explain the discrepancy between pathology and clinical data. Our findings might reconcile these apparently contradictory observations: most of NASB struts (78%) appear covered at follow-up, explaining the good results reported in clinical trials; however the neointimal healing is primarily impaired in NASB struts, so the findings in autopsies might reflect a rare but real problem, not properly addressed in trials that were underpowered to detect LVLST. Therefore, although "stenting across" is becoming the default technique for bifurcation stenting, it might pose some disadvantage for a complete neointimal coverage.

Implications for ISA struts

Ozaki et al. have reported a descriptive sequential OCT study in a SES series, showing that 65% of acutely malapposed struts were uncovered at 6 months, in contrast with only 9% of the well-apposed struts[17]. This observation suggests that neointimal coverage of ISA struts might be delayed with respect to well-apposed struts. Our study confirms the hypothesis generated by Ozaki's report, comparing for the first time the risk of incomplete coverage at follow-up between the different apposition categories within the same stent, therefore comparing struts subjected to identical environmental conditions. This approach provides very solid evidence about the effect of apposition on coverage, even though it only analyzes the outcome at follow-up. Albeit it is generally accepted that sequential studies provide more solid evidence about risk estimation, this statement is not totally accurate in the case of OCT due to the impossibility of tracking individual struts between two time points. Sequential OCT studies are based on assumptions and approximations that represent themselves some degree of inaccuracy and bias. Analyzing OCT only at follow-up, we found a similar raw proportion of non-covered ISA struts (72.6%) in the DES group than the one reported by Ozaki in SES[17].

IVUS studies have described the association between ISA and LVLST[13,14], but the mechanism of this association remains unclear. The demonstration that ISA struts have higher risk of non-coverage than well-apposed struts strongly suggests that the underlying mechanism explaining this association might be a deficient re-endothelialization of ISA struts. This means ISA is a risk factor for incomplete coverage in DES, and the effort to optimize apposition might be justified.

Inflammation is an alternative mechanism to explain the association between ISA and thrombosis, described in first-generation DES[8,15]. Vasculitis of the three arterial layers might cause weakening of the vessel wall and aneurysmatic dilatation resulting in late-acquired ISA[31]. IVUS studies have reported larger in-stent mean external elastic membrane area in cases of very late stent thrombosis than in control DES, also larger than in the corresponding proximal and distal reference segments[15]. In the inflammatory mechanism ISA would be the mere consequence of a common primary process causing both thrombosis and ISA and therefore the optimization of acutely malapposed struts would make little sense. However, the inflammatory mechanism cannot explain our results. Firstly, this analysis stems from an asymptomatic cohort of patients who have not suffered thrombotic events to date, conversely to prior case-control designs[13]. Secondly, the analysis of lumen area in the stents with ISA does not fit well with the aneurysmatic pattern described by IVUS in the cases of inflammatory stent thrombosis[13]. Finally and most importantly, the deficient coverage in ISA is also observed in NASB struts, which become NASB at the moment of implantation and certainly not as the consequence of a late hypersensitivity reaction.

A third theoretical mechanism to explain the association between ISA and stent thrombosis is confounding: a severely diseased coronary segment would be more prone to both a suboptimal apposition result and to suffer thrombotic events, resulting in spurious association between ISA and thrombosis. In that case, ISA would be just a marker of poor prognosis, unlikely to change by optimizing the apposition. Although this possibility cannot be strictly ruled out in our study, again the parallelism with the coverage in NASB struts makes this mechanism unlikely to explain the results. Taking altogether these considerations, this study constitutes solid evidence that ISA is a primary risk factor for incomplete neointimal coverage, encouraging the procedural optimization of apposition to the greatest possible extent.

NASB and ISA struts: equivalent or different?

Although both NASB and ISA struts share a higher risk of delayed coverage, they seem to be however slightly different scenarios. Acute ISA is caused by a severely diseased vessel or other underlying condition precluding correct apposition. This scenario might be associated to irregular drug release due to contact of the struts with necrotic core[32], or to severely dysfunctional endothelium with hampered regeneration capabilities, or to more severe structural deformations in the stent platform. These reasons could explain the heterogeneous effect observed in ISA

struts. This heterogeneity is only partially explained by the type of stent and will deserve further clarification in the future. Conversely, NASB struts are not in contact with plaque, necrotic core, or calcium. Presumably they are enshrined in a less severely diseased segment of the vessel, and the stent has suffered less structural distortion at that level. Probably this constitutes a more benign and predictable scenario than the one described for ISA, and could explain the homogeneous effect observed in NASB struts and the higher risk of non-coverage observed in ISA vs. NASB struts.

Pooled analysis as model for inference at the strut level

Research in the field of OCT must face a cumbersome methodological challenge: the level of measurement (the strut) is different from the level of analysis (the patient, or exceptionally the lesion/stent). The clustering of the units of measurement at different levels (patient, lesion, stent) makes the probability of the outcome not independent, thus violating one of the conditions to use conventional statistics. A mathematical model that takes into account between-clusters and within-the-cluster variability is required. Bayesian hierarchical[23] or multilevel regression models have been proposed hitherto. In this study we use a pooled analysis for the first time, which fulfils all the methodological requirements for the analysis of clustered data, with the additional advantage of presenting the results to the biomedical community in a format they are more familiar with. It also allows the representation of the pooled risk ratio as forest plot, where the statistical significance of the result (95% confidence interval not crossing the reference line at RR=1), the contribution of each individual stent to the final result and the heterogeneity of the effect can be easy and intuitively understood.

Limitations

Some caution should be advised about using OCT coverage as surrogate for neointimal healing. Although biologically plausible and intuitively accepted by the scientific community, this approach cannot be fully supported by current evidence. OCT coverage correlates with histological neointimal healing and endothelialization after stenting in animal models[33-35], but its sensitivity and specificity in human atherosclerotic vessels are still unknown. OCT is not able to detect thin layers of endothelium below its 14 microns axial resolution, eventually resulting in an overestimation of the incidence of delayed coverage, and cannot discern between neointima and other material, like fibrin or thrombus. The analysis of optical density might be useful in the future to discern between neointima and thrombus/fibrin[36].

This analysis included OCT studies performed at different follow-up periods, ranging from 9 to 13 months. Although this is a potential limitation, it is not likely to affect significantly the results, because in each case the follow-up was scheduled after healing was estimated to be complete, and no substantial variations were expectable. Moreover the statistical analysis compared the different apposition categories within the same stent, thus minimizing the impact of uneven

follow-up periods in the results. Nonetheless the level of evidence provided by data pooled from different trials might be lower than the level obtained by a homogeneous protocol of study in a randomized fashion. In spite of strict inclusion and exclusion criteria for the OCT substudies, some selection bias of the patients most suitable for imaging cannot be completely ruled out.

Only OCT pullbacks at follow-up were analyzed, under the assumption that the apposition status of each strut remains stable along time. This assumption is acceptable for NASB, but entails some selection bias for ISA struts. It has been described in OCT sequential studies that the proportion of ISA struts drops from baseline to follow-up, due to partial integration in the neointima. The risk of non-coverage might have been hence slightly overestimated in ISA. The choice for risk and risk ratio in the pooled analysis is also based on this assumption, and also because mathematically is a ratio of proportions, which fits better in the analysis performed. Although risk assessment would require strictly the calculation of incidence between 2 time points, in OCT it is not possible to match individual struts between 2 different time points. Acknowledging its limitations, the assumption that apposition remains stable along time might be acceptable in some situations and the complementary solution to sequential studies built upon the assumption that struts can be tracked or their number does not change between two time points.

CONCLUSION

Coverage of ISA and NASB struts is delayed with respect to WA struts in DES, as assessed by OCT.

FUNDING SOURCES

This study pools data from two different randomized trials, sponsored by Medtronic Inc. (Santa Rosa, CA, USA) and Biosensors International (Morges, CH), respectively.

DISCLOSURES

The core-lab and CRO responsible for the analysis (Cardialysis BV, Rotterdam) and the participating centres have received grants from the corresponding sponsors to run the trials, but the content of this manuscript is an investigator-driven post-hoc analysis. Serruys PW, Windecker S and Di Mario C have received speakers' fees from the corresponding sponsors.

REFERENCES

1. Garg S, Serruys PW. Coronary Stents: Current Status. *J Am Coll Cardiol* 2010;56:S1-S42.
2. Iakovou I, Schmidt T, Bonizzoni E, Ge L, Sangiorgi GM, Stankovic G, Airoldi F, Chieffo A, Montorfano M, Carlino M, Michev I, Corvaja N, Briguori C, Gerckens U, Grube E, Colombo A. Incidence, Predictors, and Outcome of Thrombosis After Successful Implantation of Drug-Eluting Stents. *JAMA* 2005;293:2126-2130.
3. Ong AT, McFadden EP, Regar E, de Jaegere PP, van Domburg RT, Serruys PW. Late angiographic stent thrombosis (LAST) events with drug-eluting stents. *J Am Coll Cardiol* 2005;45:2088-2092.
4. Pfisterer M, Brunner-La Rocca HP, Buser PT, Rickenbacher P, Hunziker P, Mueller C, Jeger R, Bader F, Osswald S, Kaiser C. Late clinical events after clopidogrel discontinuation may limit the benefit of drug-eluting stents: an observational study of drug-eluting versus bare-metal stents. *J Am Coll Cardiol* 2006;48:2584-2591.
5. Lagerqvist B, James SK, Stenestrand U, Lindback J, Nilsson T, Wallentin L, the SCAAR Study Group. Long-Term Outcomes with Drug-Eluting Stents versus Bare-Metal Stents in Sweden. *N Engl J Med* 2007;356:1009-1019.
6. Farb A, Heller PF, Shroff S, Cheng L, Kolodgie FD, Carter AJ, Scott DS, Froehlich J, Virmani R. Pathological Analysis of Local Delivery of Paclitaxel Via a Polymer-Coated Stent. *Circulation* 2001;104:473-479.
7. Farb AM, Burke APM, Kolodgie FDP, Virmani RM. Pathological Mechanisms of Fatal Late Coronary Stent Thrombosis in Humans. *Circulation* 2003;108:1701-1706.
8. Virmani R, Guagliumi G, Farb A, Musumeci G, Grieco N, Motta T, Mihalcsik L, Tespili M, Valsecchi O, Kolodgie FD. Localized Hypersensitivity and Late Coronary Thrombosis Secondary to a Sirolimus-Eluting Stent: Should We Be Cautious? *Circulation* 2004;109:701-705.
9. Joner M, Finn AV, Farb A, Mont EK, Kolodgie FD, Ladich E, Kutys R, Skorija K, Gold HK, Virmani R. Pathology of Drug-Eluting Stents in Humans: Delayed Healing and Late Thrombotic Risk. *J Am Coll Cardiol* 2006;48:193-202.
10. Finn AV, Joner M, Nakazawa G, Kolodgie F, Newell J, John MC, Gold HK, Virmani R. Pathological Correlates of Late Drug-Eluting Stent Thrombosis: Strut Coverage as a Marker of Endothelialization. *Circulation* 2007;115:2435-2441.
11. Steigen TK, Maeng M, Wiseth R, Erglis A, Kumsars I, Narbute I, Gunnes P, Mannsverk J, Meyerdierks O, Rotevatn S, Niemela M, Kervinen K, Jensen JS, Galloe A, Nikus K, Vikman S, Ravkilde J, James S, Aaroe J, Ylitalo A, Helqvist S, Sjogren I, Thayssen P, Virtanen K, Puhakka M, Airaksinen J, Lassen JF, Thuesen L. Randomized study on simple versus complex stenting of coronary artery bifurcation lesions: the Nordic bifurcation study. *Circulation* 2006;114:1955-1961.
12. Niemela M, Kervinen K, Erglis A, Holm NR, Maeng M, Christiansen EH, Kumsars I, Jegere S, Dombrovskis A, Gunnes P, Stavnes S, Steigen TK, Trovik T, Eskola M, Vikman S, Romppanen H, Makikallio T, Hansen KN, Thayssen P, Aberge L, Jensen LO, Hervold A, Airaksinen J, Pietila M, Frobert O, Kellerth T, Ravkilde J, Aaroe J, Jensen JS, Helqvist S, Sjogren I, James S, Miettinen H, Lassen JF, Thuesen L. Randomized comparison of final kissing balloon dilatation versus no final kissing balloon dilatation in patients with coronary bifurcation lesions treated with main vessel stenting: the Nordic-Baltic Bifurcation Study III. *Circulation* 2011;123:79-86.
13. Cook S, Wenaweser P, Togni M, Billinger M, Morger C, Seiler C, Vogel R, Hess O, Meier B, Windecker S. Incomplete Stent Apposition and Very Late Stent Thrombosis After Drug-Eluting Stent Implantation. *Circulation* 2007;115:2426-2434.

14. Hassan AKM, Bergheanu SC, Stijnen T, van der Hoeven BL, Snoep JD, Plevier JWM, Schalij MJ, Wouter Jukema J. Late stent malapposition risk is higher after drug-eluting stent compared with bare-metal stent implantation and associates with late stent thrombosis. *Eur Heart J* 2010;31:1172-1180.
15. Cook S, Ladich E, Nakazawa G, Eshtehardi P, Neidhart M, Vogel R, Togni M, Wenaweser P, Billinger M, Seiler C, Gay S, Meier B, Pichler WJ, Juni P, Virmani R, Windecker S. Correlation of Intravascular Ultrasound Findings With Histopathological Analysis of Thrombus Aspirates in Patients With Very Late Drug-Eluting Stent Thrombosis. *Circulation* 2009;120:391-399.
16. Wilson GJ, Nakazawa G, Schwartz RS, Huibregtse B, Poff B, Herbst TJ, Baim DS, Virmani R. Comparison of Inflammatory Response After Implantation of Sirolimus- and Paclitaxel-Eluting Stents in Porcine Coronary Arteries. *Circulation* 2009;120:141-149.
17. Ozaki Y, Okumura M, Ismail TF, Naruse H, Hattori K, Kan S, Ishikawa M, Kawai T, Takagi Y, Ishii J, Prati F, Serruys PW. The fate of incomplete stent apposition with drug-eluting stents: an optical coherence tomography-based natural history study. *Eur Heart J* 2010;31:1470-1476.
18. Guagliumi G, Musumeci G, Sirbu V, Bezerra HG, Suzuki N, Fiocca L, Matiashvili A, Lortkipanidze N, Trivisonno A, Valsecchi O, Biondi-Zoccai G, Costa MA. Optical coherence tomography assessment of in vivo vascular response after implantation of overlapping bare-metal and drug-eluting stents. *JACC Cardiovasc Interv* 2010;3:531-539.
19. Guagliumi G, Sirbu V, Musumeci G, Bezerra HG, Aprile A, Kyono H, Fiocca L, Matiashvili A, Lortkipanidze N, Vassileva A, Popma JJ, Allocco DJ, Dawkins KD, Valsecchi O, Costa MA. Strut coverage and vessel wall response to a new-generation paclitaxel-eluting stent with an ultrathin biodegradable abluminal polymer: Optical Coherence Tomography Drug-Eluting Stent Investigation (OCTDESI). *Circ Cardiovasc Interv* 2010;3:367-375.
20. Guagliumi G, Sirbu V, Bezerra H, Biondi-Zoccai G, Fiocca L, Musumeci G, Matiashvili A, Lortkipanidze N, Tahara S, Valsecchi O, Costa M. Strut coverage and vessel wall response to zotarolimus-eluting and bare-metal stents implanted in patients with ST-segment elevation myocardial infarction: the OCTAMI (Optical Coherence Tomography in Acute Myocardial Infarction) Study. *JACC Cardiovasc Interv* 2010;3:680-687.
21. Guagliumi G, Costa MA, Sirbu V, Musumeci G, Bezerra HG, Suzuki N, Matiashvili A, Lortkipanidze N, Mihalcsik L, Trivisonno A, Valsecchi O, Mintz GS, Dressler O, Parise H, Maehara A, Cristea E, Lansky AJ, Mehran R, Stone GW. Strut Coverage and Late Malapposition With Paclitaxel-Eluting Stents Compared With Bare Metal Stents in Acute Myocardial Infarction: Optical Coherence Tomography Substudy of the Harmonizing Outcomes With Revascularization and Stents in Acute Myocardial Infarction (HORIZONS-AMI) Trial. *Circulation* 2011;123:274-281.
22. Windecker S, Serruys PW, Wandel S, Buszman P, Trznadel S, Linke A, Lenk K, Ischinger T, Klauss V, Eberli F, Corti R, Wijns W, Morice MC, Di MC, Davies S, van Geuns RJ, Eerdmans P, Van Es GA, Meier B, Juni P. Biolimus-eluting stent with biodegradable polymer versus sirolimus-eluting stent with durable polymer for coronary revascularisation (LEADERS): a randomised non-inferiority trial. *Lancet* 2008;372:1163-1173.
23. Barlis P, Regar E, Serruys PW, Dimopoulos K, van der Giessen WJ, van Geuns RJ, Ferrante G, Wandel S, Windecker S, Van Es GA, Eerdmans P, Juni P, di Mario C. An optical coherence tomography study of a biodegradable vs. durable polymer-coated limus-eluting stent: a LEADERS trial sub-study. *Eur Heart J* 2010;31:165-176.
24. Serruys PW, Silber S, Garg S, van Geuns RJ, Richardt G, Buszman PE, Kelbaek H, van Boven AJ, Hofma SH, Linke A, Klauss V, Wijns W, Macaya C, Garot P, DiMario C, Manoharan G, Kornowski R, Ischinger T, Bartorelli A, Ronden J, Bressers M, Gobbens P, Negoita M, van Leeuwen F, Windecker

S. Comparison of Zotarolimus-Eluting and Everolimus-Eluting Coronary Stents. *New Engl J Med* 2010;363:136-146.

25. Gonzalo N, Tearney GJ, Serruys PW, van Soest G, Okamura T, Garcia-Garcia HM, van Geuns RJ, van der Ent M, Ligthart JM, Bouma BE, Regar E. Second-generation optical coherence tomography in clinical practice. High-speed data acquisition is highly reproducible in patients undergoing percutaneous coronary intervention. *Rev Esp Cardiol* 2010;63:893-903.
26. Gonzalo N, Garcia-Garcia HM, Serruys PW, Commissaris KH, Bezerra H, Gobbens P, Costa M, Regar E. Reproducibility of quantitative optical coherence tomography for stent analysis. *EuroIntervention* 2009;5:224-232.
27. Sweeting J, Sutton J, Lambert C. What to add to nothing? Use and avoidance of continuity corrections in meta-analysis of sparse data. *Statist Med* 2004;23:1351-1375.
28. Domenech J. SPSS Macro !MAR. Meta-Analysis OR, RR, RD, IR, ID, B & MD Combined. [V2009.03.30.]. 2009. Bellaterra: Universitat Autònoma de Barcelona.

    Ref Type: Computer Program
29. Daemen J, Wenaweser P, Tsuchida K, Abrecht L, Vaina S, Morger C, Kukreja N, Jüni P, Sianos G, Hellige G, van Domburg RT, Hess OM, Boersma E, Meier B, Windecker S, Serruys PW. Early and late coronary stent thrombosis of sirolimus-eluting and paclitaxel-eluting stents in routine clinical practice: data from a large two-institutional cohort study. *The Lancet* 2007;369:667-678.
30. Jensen JS, Galloe A, Lassen JF, Erglis A, Kumsars I, Steigen TK, Wiseth R, Narbute I, Gunnes P, Mannsverk J, Meyerdierks O, Rotevatn S, Niemela M, Kervinen K, Nikus K, Vikman S, Ravkilde J, James S, Aaroe J, Ylitalo A, Helqvist S, Sjogren I, Thayssen P, Virtanen K, Puhakka M, Airaksinen J, Thuesen L. Safety in simple versus complex stenting of coronary artery bifurcation lesions. The nordic bifurcation study 14-month follow-up results. *EuroIntervention* 2008;4:229-233.
31. Serruys PW, Degertekin M, Tanabe K, Abizaid A, Sousa JE, Colombo A, Guagliumi G, Wijns W, Lindeboom WK, Ligthart J, de Feyter PJ, Morice MC. Intravascular ultrasound findings in the multicenter, randomized, double-blind RAVEL (RAndomized study with the sirolimus-eluting VElocity balloon-expandable stent in the treatment of patients with de novo native coronary artery Lesions) trial. *Circulation* 2002;106:798-803.
32. Hwang C-WMP, Levin ADM, Jonas MM, Li PHB, Edelman ERM. Thrombosis Modulates Arterial Drug Distribution for Drug-Eluting Stents. *Circulation* 2005;111:1619-1626.
33. Suzuki Y, Ikeno F, Koizumi T, Tio F, Yeung AC, Yock PG, Fitzgerald PJ, Fearon WF. In vivo comparison between optical coherence tomography and intravascular ultrasound for detecting small degrees of in-stent neointima after stent implantation. *JACC Cardiovasc Interv* 2008;1:168-173.
34. Prati F, Zimarino M, Stabile E, Pizzicannella G, Fouad T, Rabozzi R, Filippini A, Pizzicannella J, Cera M, De Caterina R. Does optical coherence tomography identify arterial healing after stenting? An in vivo comparison with histology, in a rabbit carotid model. *Heart* 2008;94:217-221.
35. Murata A, Wallace-Bradley D, Tellez A, Alviar C, Aboodi M, Sheehy A, Coleman L, Perkins L, Nakazawa G, Mintz G, Kaluza GL, Virmani R, Granada JF. Accuracy of optical coherence tomography in the evaluation of neointimal coverage after stent implantation. *JACC Cardiovasc Imaging* 2010;3:76-84.
36. Templin C, Meyer M, Muller MF, Djonov V, Hlushchuk R, Dimova I, Flueckiger S, Kronen P, Sidler M, Klein K, Nicholls F, Ghadri JR, Weber K, Paunovic D, Corti R, Hoerstrup SP, Luscher TF, Landmesser U. Coronary optical frequency domain imaging (OFDI) for in vivo evaluation of stent healing: comparison with light and electron microscopy. *Eur Heart J* 2010;31:1792-1801.

SUPPLEMENTAL MATERIAL

Supplemental methods: Detailed explanation of the statistical analysis

Pooled analysis is particularly suitable for the statistical analysis of an effect by combining data from different groups of subjects, each group submitted to slightly different environmental conditions. In this situation it is not acceptable to merge all the individuals together and apply conventional statistics, because one of the requirements for this approach is not accomplished: the individual measurements are not independent from each other, but strongly interdependent within the groups.

The biomedical community is actually very familiar with the methodology of pooled analysis, because it is used in:

- Meta-analysis[1].
- Epidemiology[2].

In this study we propose for the first time to apply a pooled statistical method for the analysis of OCT data, since the clustering of data is an analogous methodological problem to the one faced by meta-analysis or by epidemiologic studies in communities. We can use pooled statistics in meta-analysis (combining different trials or studies), in interventional epidemiology (combining different communities) or in OCT studies (combining the results from different stents), (suppl. figure 1).

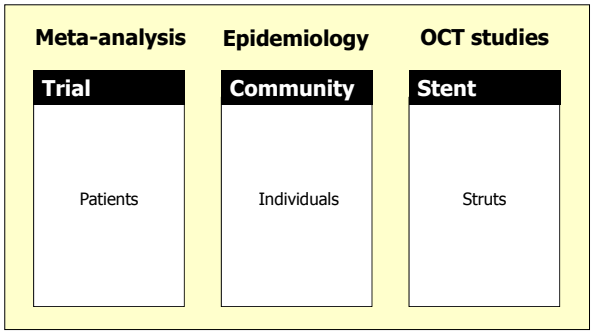

Suppl. figure 1:
Scheme illustrating the parallelism between the units of measurement and units of clustering in different types of studies using pooled analysis. Meta-analysis and epidemiology use pooled analysis, with patients clustered in trials, or individuals clustered in communities, respectively. This justifies the use of this methodology in some OCT studies, considering the struts the unit of measurement and the stent (or the lesion) as unit of clustering.

Number of stents analyzed

The number of stents analyzed depends on the research question, because not all the stents in the sample might be informative for all possible research questions.

In a meta-analysis we select the trials (or studies) addressing our research question, and then we select those which are truly informative to answer the question. To be informative a trial must have:

- Exposition to the study factor
- Events (at least in one of the arms).

In a trial the "exposition" is guaranteed (randomization), but if we performed a meta-analysis of observational studies and we found studies with **no exposition**, they would be discarded (they are not informative for our research question).

Likewise, trials with **no events** (0 events in both arms) should be discarded (they are not informative for our research question).

In OCT studies, taking our manuscript as example (suppl. figure 2), these principles are applied as follows:

- Research question: compare the coverage of NASB vs. WA struts.
  - Stents with no exposition (no NASB struts) are discarded.
  - Stents with no events (complete coverage of NASB and WA struts) are discarded.
- Research question: compare the coverage of ISA vs. WA struts.
  - Stents with no exposition (no ISA struts) are discarded.
  - Stents with no events (complete coverage of ISA and WA struts) are discarded.
- Research question: compare the coverage of ISA vs. NASB struts.
  - In this case we need exposition (ISA) and no exposition (NASB) together in the same stent: therefore stents not meeting this condition are discarded.
  - Stents with no events (complete coverage of ISA and NASB struts) are discarded.

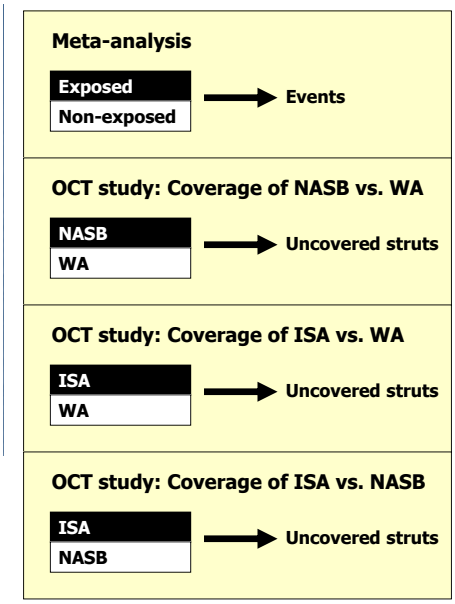

Suppl. figure 2:
Diagram illustrating the parallelism between the terminology used in meta-analysis and how to apply it in pooled analysis for this specific OCT study. Uncovered struts are equivalent to the "events" in meta-analysis, and the treatment vs. control (or exposed vs. non-exposed) categories depend on the research question that we intend to answer, i.e. for calculating the risk of delayed coverage in NASB vs. WA struts, NASB will be the treatment (or exposition) category, whilst WA will be the control (or non-exposed category).

Suppl. table 1: Raw counts, estimated risk ratio (RR) and standard error (SE) of the RR for the comparison of coverage in non-apposed side-branch (NASB) struts vs. well-apposed (WA) struts in drug-eluting stents (DES).

Entry	Stent type	NASB uncovered	NASB covered	WA uncovered	WA covered	RR	SE
1	ZES	0	3	1	192	16,17	1,55
2	SES	0	3	1	180	15,17	1,55
3	SES	0	3	1	170	14,33	1,55
4	ZES	0	2	1	169	19,00	1,53
5	ZES	1	1	0	122	123,00	1,52
6	SES	0	2	1	114	12,89	1,52
7	ZES	0	11	2	240	4,05	1,52
8	EES	2	9	0	232	97,08	1,52
9	ZES	0	4	2	253	10,24	1,48
10	BES	0	1	1	270	45,33	1,47
11	ZES	0	1	1	243	40,83	1,47
12	SES	0	3	2	238	12,05	1,46
13	EES	2	1	0	175	220,00	1,46
14	ZES	0	4	3	241	7,00	1,44
15	EES	0	2	2	174	11,80	1,44
16	ZES	0	4	4	364	8,20	1,42
17	ZES	0	3	4	183	5,22	1,40
18	ZES	0	4	26	241	1,01	1,35
19	SES	0	3	12	139	1,52	1,35
20	BES	0	2	6	151	4,05	1,35
21	BES	0	3	25	119	0,71	1,34
22	BES	0	1	3	193	14,07	1,33
23	ZES	0	2	8	245	4,98	1,33
24	EES	0	2	15	208	2,41	1,31
25	BES	0	2	15	150	1,78	1,31
26	BES	0	2	16	118	1,36	1,31
27	SES	0	1	4	57	3,44	1,31
28	ZES	0	2	36	147	0,84	1,30
29	ZES	0	2	50	475	1,74	1,30
30	ZES	0	1	5	345	15,95	1,30
31	EES	0	1	6	219	8,69	1,28
32	BES	0	1	17	107	1,79	1,24
33	SES	0	1	18	159	2,41	1,24
34	ZES	0	1	42	217	1,53	1,23
35	EES	2	7	1	293	65,33	1,18
36	EES	2	2	1	176	88,50	1,12
37	ZES	1	4	3	272	18,33	1,06
38	EES	1	3	4	186	11,88	1,00

39	EES	1	2	3	87	10,00	0,99
40	EES	1	7	22	190	1,20	0,96
41	ZES	1	3	6	146	6,33	0,95
42	ZES	1	1	5	184	18,90	0,83
43	EES	1	1	5	126	13,10	0,83
44	BES	1	1	13	211	8,62	0,76
45	EES	1	0	2	326	98,70	0,75
46	ZES	2	4	9	145	5,70	0,66
47	BES	2	4	11	196	6,27	0,65
48	EES	2	9	77	150	0,54	0,65
49	ZES	2	5	72	181	1,00	0,61
50	SES	3	0	3	212	54,00	0,56
51	EES	1	0	8	76	7,50	0,52
52	ZES	1	0	13	167	10,06	0,48
53	ZES	2	1	21	165	5,90	0,46
54	ZES	2	1	23	195	6,32	0,45
55	EES	1	0	23	109	4,24	0,45
56	SES	5	3	8	153	12,58	0,44
57	BES	4	6	23	315	5,88	0,44
58	ZES	3	2	17	194	7,45	0,43
59	ZES	2	1	49	184	3,17	0,43
60	EES	3	1	10	200	15,75	0,42
61	EES	3	2	25	208	5,59	0,41
62	EES	2	0	17	166	8,76	0,34

Suppl. table 2: Raw counts, estimated risk ratio (RR) and standard error (SE) of the RR for the comparison of coverage in malapposed (ISA) struts vs. well-apposed (WA) struts in drug-eluting stents (DES).

Entry	Stent type	ISA uncovered	ISA covered	WA uncovered	WA covered	RR	SE
1	BES	1	0	0	186	280,50	1,47
2	EES	3	1	0	233	327,60	1,44
3	EES	3	1	0	211	296,80	1,44
4	EES	6	1	0	256	417,63	1,42
5	SES	0	5	8	153	1,59	1,39
6	SES	0	5	55	215	0,41	1,36
7	BES	0	2	8	187	3,84	1,33
8	SES	0	2	12	139	2,03	1,32
9	ZES	0	1	5	184	8,64	1,29
10	EES	0	1	22	190	2,37	1,24
11	SES	1	29	4	49	0,44	1,09
12	ZES	3	1	1	192	144,75	1,04
13	BES	1	17	15	150	0,61	1,00
14	BES	1	3	6	151	6,54	0,95
15	SES	1	3	7	69	2,71	0,94
16	ZES	1	0	1	243	122,50	0,91
17	SES	1	3	17	326	5,04	0,90
18	BES	1	3	23	315	3,67	0,89
19	SES	1	2	22	127	2,26	0,84
20	ZES	1	1	13	167	6,92	0,76
21	ZES	1	1	26	241	5,13	0,73
22	SES	3	4	4	155	17,04	0,66
23	BES	1	0	3	40	9,43	0,66
24	SES	1	0	4	82	14,50	0,61
25	EES	4	1	3	87	24,00	0,61
26	ZES	1	0	5	345	47,86	0,59
27	ZES	3	1	4	155	29,81	0,57
28	ZES	3	0	3	241	61,25	0,56
29	ZES	1	0	6	146	17,65	0,56
30	SES	1	0	11	78	5,87	0,49
31	EES	3	1	7	212	23,46	0,47
32	BES	1	0	15	73	4,31	0,47
33	BES	1	0	17	107	5,36	0,46
34	ZES	1	0	19	430	17,31	0,46
35	SES	1	0	18	159	7,22	0,46
36	EES	3	0	5	126	21,00	0,46
37	EES	1	0	23	109	4,24	0,45
38	ZES	1	0	36	147	3,78	0,43

39	SES	3	3	40	244	3,55	0,43
40	ZES	7	1	8	245	27,67	0,37
41	EES	2	0	17	166	8,76	0,34
42	ZES	11	1	9	145	15,69	0,33
43	SES	2	0	19	115	5,77	0,33
44	ZES	2	0	23	195	7,77	0,32
45	ZES	4	1	17	194	9,93	0,32
46	EES	12	1	10	200	19,38	0,32
47	SES	3	1	58	104	2,09	0,31
48	ZES	2	0	42	217	5,10	0,29
49	EES	6	1	15	208	12,74	0,29
50	ZES	2	0	50	475	8,68	0,29
51	EES	10	1	15	215	13,94	0,27
52	BES	3	0	25	119	4,98	0,26
53	ZES	7	1	21	165	7,75	0,25
54	EES	23	1	19	143	8,17	0,22
55	EES	17	1	19	90	5,42	0,22
56	EES	4	0	63	133	2,79	0,18
57	ZES	8	0	30	98	3,99	0,18
58	ZES	14	1	55	150	3,48	0,13
59	ZES	46	2	49	184	4,56	0,13
60	EES	17	2	77	150	2,64	0,12
61	ZES	17	1	63	97	2,40	0,11
62	ZES	19	0	72	181	3,42	0,11

Suppl. table 3: Raw counts, estimated risk ratio (RR) and standard error (SE) of the RR for the comparison of coverage in malapposed (ISA) struts vs. non-apposed side-branch (NASB) struts in drug-eluting stents (DES).

Entry	Stent type	ISA uncovered	ISA covered	NASB uncovered	NASB covered	RR	SE
1	2	1	17	0	2	0,47	1,51
2	2	1	3	0	2	1,80	1,46
3	4	1	1	0	4	5,00	1,46
4	3	0	1	1	7	1,50	1,43
5	1	0	5	5	3	0,14	1,38
6	4	3	0	0	4	8,75	1,35
7	4	3	1	0	3	5,60	1,35
8	4	1	0	0	2	4,50	1,35
9	4	0	1	1	1	0,50	1,35
10	3	0	1	2	9	1,20	1,35
11	2	3	0	0	3	7,00	1,34
12	3	3	1	0	2	4,20	1,32
13	4	2	0	0	2	5,00	1,32
14	3	6	1	0	2	4,88	1,30
15	4	7	1	0	2	5,00	1,30
16	2	1	0	0	1	3,00	1,29
17	1	1	0	0	1	3,00	1,29
18	4	1	0	0	1	3,00	1,29
19	4	1	0	0	1	3,00	1,29
20	4	2	0	0	1	3,33	1,25
21	2	1	3	4	6	0,63	0,95
22	3	4	1	1	2	2,40	0,85
23	4	1	0	1	3	2,50	0,80
24	4	1	1	1	0	0,67	0,71
25	3	17	2	2	9	4,92	0,64
26	3	3	0	1	1	1,75	0,61
27	4	11	1	2	4	2,75	0,58
28	4	19	0	2	5	3,12	0,53
29	4	2	0	2	1	1,33	0,47
30	4	7	1	2	1	1,31	0,43
31	4	4	1	3	2	1,33	0,43
32	4	46	2	2	1	1,44	0,41
33	3	12	1	3	1	1,23	0,30

REFERENCES

1. Keeley EC, Boura JA, Grines CL. Primary angioplasty versus intravenous thrombolytic therapy for acute myocardial infarction: a quantitative review of 23 randomised trials. *The Lancet* 2003;361:13-20.
2. Haralabidis AS, Dimakopoulou K, Vigna-Taglianti F, Giampaolo M, Borgini A, Dudley ML, Pershagen G, Bluhm G, Houthuijs D, Babisch W, Velonakis M, Katsouyanni K, Jarup L. Acute effects of night-time noise exposure on blood pressure in populations living near airports. *Eur Heart J* 2008;29:658-664.


2
1
0
1
2
mm
08/14/2009 10:00:07
0118 (24 mm)
Zoom: 1.1x

12.2

Vascular tissue reaction to acute malapposition in human coronary arteries: sequential assessment with optical coherence tomography.

Gutiérrez-Chico JL, Wykrzykowska JJ, Nüesch E, van Geuns RJ, Koch KT, Koolen JJ, di Mario C, Windecker S, van Es GA, Gobbens P, Jüni P, Regar E, Serruys PW.

Circ Cardiovasc Interv 2012;5:20-29.

ABSTRACT

Background: The vascular tissue reaction to acute incomplete stent apposition (ISA) is scarcely known. The aim of this study is characterizing the vascular response to acute ISA in vivo and looking for predictors of incomplete healing.

Methods and results: OCT studies from 66 stents of different design, implanted in 43 patients enrolled in 3 randomized trials, were sequentially analyzed after implantation and at 6-13 month. 78 segments with acute ISA were identified in 36 of the patients and matched with the follow-up study using fiduciary landmarks. The morphologic pattern of healing in the ISA segments was categorized as homogeneous, layered, crenellated, bridged, partially bridged or bare, depending on the persistence of ISA and on the coverage. After 6 months acute ISA volume decreased significantly and 71.5% of the ISA segments were completely integrated into the vessel wall. Segments with acute ISA had higher risk or delayed coverage than well-apposed segments (RR 2.37; 95% CI 2.01 – 2.78). Acute ISA size (estimated as ISA volume or maximal ISA distance per strut) was an independent predictor of ISA persistence and of delayed healing at follow-up.

Conclusions: The neointimal healing tends to reduce ISA, often integrating it completely into the vessel wall and resulting in characteristic morphologic patterns. Coverage of ISA segments is delayed with respect to well-apposed segments. The larger the size of acute ISA, the larger the likelihood of persisting malapposed at follow-up and of delayed healing.

Clinical trial registration: www.clinicaltrials.gov NCT00617084; NCT00934752

Key words: Coronary vessels; coronary stenosis; angioplasty, transluminal percutaneous coronary; angioplasty, balloon; stents; drug-eluting stents; paclitaxel; everolimus; zotarolimus; neointima; tomography, optical coherence.

INTRODUCTION

The vascular tissue reaction to acute incomplete stent apposition (ISA) is barely known. The neointimal healing process after stenting might spontaneously correct ISA to some extent, integrating the malapposed regions into the vessel wall, as suggested by sequential quantitative studies with optical coherence tomography (OCT), reporting ISA volumes and percentage of ISA struts decreasing over time[1-4]. Other qualitative OCT studies have also speculated about some morphologic patterns at follow-up and the hypothesis that they could represent the vascular response to acutely malapposed struts[5]. The reasons why the vascular biology succeeds to cover and even integrate in the vessel wall some ISA regions but not others remain poorly understood.

ISA has been linked to delayed neointimal coverage in two different scenarios: late-acquired ISA and acute ISA. IVUS studies reported the association between ISA and late/very late stent thrombosis[6,7] in a relatively rare clinical context of delayed hypersensitivity to drug-eluting stents, probably triggered by the polymer and recruiting preferentially eosinophils[8,9]. Vasculitis of the three arterial layers resulted in weakening of the vessel wall, aneurysmatic dilatation, late-acquired ISA and thrombosis[6,8,9]. In this context, late-acquired ISA struts presented signs of delayed neointimal coverage[9]. On the other hand, the association between acute ISA and delayed coverage has been only recently demonstrated[1,10]. This association provided some supporting evidence for the optimization of apposition aimed at promoting better coverage of the stent. Nevertheless, regions of minimal acute ISA size appear frequently covered and even totally integrated in the vessel wall at follow-up[2,3]. Thus, the question about which degree of acute ISA is worth to correct remains unanswered for the interventional cardiologist.

The aims of this study are describing the vascular tissue reaction to acute ISA in human coronary arteries after 6 months, characterizing quantitatively different morphologic patterns in terms of apposition and coverage, and looking for predictors at baseline of persisting ISA and delayed coverage.

METHODS

Study sample

OCT images from three different randomized trials were analyzed: the RESOLUTE-All comers trial (NCT00617084)[11,12], the De Novo Pilot Study (NCT00934752)[3] and the SECRITT trial[13].

The RESOLUTE-All comers trial (NCT00617084) compared a zotarolimus-eluting stent (ZES) with hydrophilic-polymer coating (Resolute, Medtronic Cardio Vascular, Santa Rosa, CA, USA) vs. an everolimus-eluting stent (EES) with fluoropolymer (Xience V, Abbott Vascular, Santa

Clara, CA, USA) in a non-selected all-comers population[11]. Twenty percent of the enrolled patients were randomly allocated to angiographic follow-up at 13 months. The patients undergoing angiographic follow-up in selected OCT centres were included in an OCT substudy, with the proportion of covered struts at 13 months as primary endpoint[12]. Sequential OCT study was not mandatory per protocol.

The De Novo Pilot Study (NCT00934752) assessed the performance of a paclitaxel-coated balloon (Moxy, Lutonix Inc, Maple Grove, MN, USA) in combination with a bare-metal stent (Multi-link Vision/MiniVision, Abbott Vascular, Santa Clara, CA, USA) for the treatment of de novo coronary lesions. Myocardial infarction was an exclusion criterion for this study, and a single lesion per patient could be included. The trial randomized the sequence of application (balloon first vs. stent first), with a primary endpoint of percent neointimal volume obstruction assessed by OCT at 6 months[3].

The SECRITT trial studied the efficacy of a nitinol self-expandable bare-metal stent (SE-BMS) with ultra-thin struts (56 µm) and low chronic outward force (vProtect™ Luminal Shield, Prescient Medical Inc, Doylestown, PA, USA) for the treatment of high risk thin-cap fibroatheromas (TCFA)[13]. Patients undergoing catheterization for stable or unstable angina were included if the culprit lesion met the following criteria: 1) intermediate 40-50% diameter stenosis in quantitative coronary angiography (QCA), 2) fractional flow reserve>0.75, 3) morphology of TCFA in the combination of intravascular ultrasound radiofrequency and OCT studies, as previously described[14,15]. Patients were randomized to receive a SE-BMS or medical therapy. OCT follow-up was scheduled after 6 months.

In the three trials the optimization of PCI results was guided by angiography, therefore no additional intervention was performed after stent implantation and OCT acquisition, irrespective of the findings in the OCT images.

OCT study and analysis

OCT pullbacks were obtained with M2, M3 or C7 systems (Lightlab Imaging, Westford, Massachusetts, USA), according to the availability at the participating sites, using occlusive or non-occlusive technique as appropriate[16]. Supplementary table 1 summarizes the patients studied with each system and the corresponding technical specifications. Infusion of intracoronary nitroglycerin before the OCT pullback was strongly encouraged.

OCT pullbacks were analysed offline in a core-laboratory (Cardialysis BV, Rotterdam, NL) by independent staff blinded to stent-type allocation and clinical and procedural characteristics of the patients, using proprietary software (Lightlab Imaging). Cross-sections were analyzed at 1mm longitudinal intervals within the stented segment. A metallic strut typically appears as a bright signal-intense structure with dorsal shadowing. Apposition was assessed strut by strut by measuring the distance between the strut marker and the lumen contour. The marker of each strut was placed at the endoluminal leading edge, in the mid-point of its long-

axis, and the distance was measured following a straight line connecting this marker with the centre of gravity of the vessel[17]. Struts were classified as ISA if the distance between the strut marker and the lumen contour was bigger than the specific strut (plus polymer) thickness[12,18]. This resulted in ISA thresholds of >89µm for EES, >97µm for ZES, >81µm for DCB-BMS and >56µm for SE-BMS. Struts located at the ostium of side branches, with no vessel wall behind, were labelled as non-apposed side-branch struts (NASB) and excluded from the analysis of apposition[3,4,10,12]

Struts were classified as uncovered if any part of the strut was visibly exposed to the lumen or as covered if a layer of tissue was visible over all the reflecting surfaces[3,4,10,12,19-24].

ISA segments, matching and morphologic patterns at follow-up

ISA segments were defined as ≥2 consecutive cross-sections containing ISA struts immediately post-implantation (baseline). ISA segments extended proximal and distally to

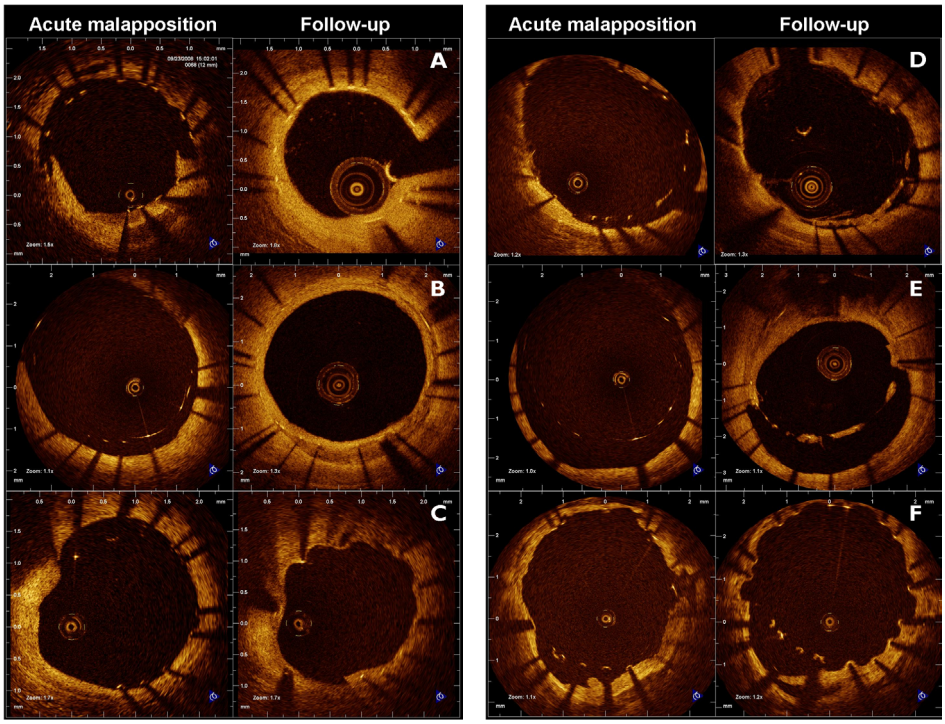

Figure 1 (left panel A): Vascular reaction to acute malapposition, categorized according to the morphologic pattern at follow-up: homogeneous (A), layered (B) or crenellated (C). In these patterns the regions of acute malapposition have been integrated into the arterial wall.

Figure 1 (right panel B): Vascular reaction to acute malapposition, categorized according to the morphologic pattern at follow-up: bridged (D), partially bridged (E) or bare (F). In these patterns the regions of acute malapposition remain malapposed at follow-up.

fiduciary landmarks in the vicinity of the most proximal and distal ISA cross-sections. These fiduciary landmarks enabled the matching of the ISA segments with the follow-up studies. The vascular reaction to acute malapposition was categorized according to the morphologic pattern at follow-up as: 1) homogeneous (ISA integrated into the vessel wall, covered with a homogeneous density and keeping a smooth lumen contour), 2) layered (ISA integrated into the vessel wall, covered with a double or triple density, often with layered appearance, and keeping a smooth lumen contour), 3) crenellated (ISA integrated into the vessel wall and grossly covered, but presenting indentations that give the lumen contour a scalloped appearance) (figure 1, panel A), 4) bridged (persisting ISA, entirely covered by a rim of tissue linking the vessel intima with the malapposed struts), 5) partially bridged (persisting ISA; a rim of tissue linking the vessel intima with the malapposed struts can be seen, but does not cover all the ISA struts), 6) bare (ISA uncovered struts, with scarce tissue reaction, showing a morphologic pattern very similar to the one observed at baseline) (figure 1, panel B). Delayed healing was defined by patterns 3 to 6; persistent ISA was defined by patterns 4 to 6; grossly delayed healing was defined by patterns 5 to 6. Two independent operators classified qualitatively the ISA segments at follow-up as the worst morphologic pattern present in the segment. In case of disagreement, the final category was obtained upon consensus after joint review.

Statistical analysis

Interobserver agreement regarding the classification of the patterns was measured with quadratic weighted kappa. Continuous variables in the volumetric analysis were compared with multilevel linear regression for paired measurements (baseline vs. follow-up), using linear mixed models with the time sequence as fixed effect and the hierarchical modelling of the measurements as random effect. Differences in apposition and coverage between the different morphologic patterns were analyzed with Kruskal-Wallis test, and a linear trend among the ranked categories was explored with the Jonckheere-Terpstra test. The relative risk (RR) for delayed coverage of ISA vs. well-apposed segments was calculated using pooled analysis with an inverse variance random effects model, taking into account the between-clusters and within-the-cluster variability, and considering each stent as independent unit of clustering[10]. Predictors of persistent ISA, grossly delayed coverage, percent of ISA and of uncovered struts were studied by multilevel regression, using the generalized estimating equations to correct for clustering of data. The goodness of fit of the model containing the significant predictors of the effect was estimated by the corrected quasi-likelihood under independence model criterion (QICC); the lower the QICC values, the better the fit of the model. Calculations were done with PASW 17.0 (Chicago, IL, USA) and CMA version 2 (Biostat Inc., Englewood, NJ, USA) software packages.

RESULTS

48 lesions and 66 stents implanted in 43 patients were finally available for sequential analysis among the population included in this study (Figure 2). Tables 1 and 2 summarize the baseline clinical and procedural characteristics of the patients and angiographic characteristics of the lesions, respectively. 78 segments with acute ISA were identified in 36 patients at baseline. Matching with the OCT at follow-up was not possible in 8 segments, due to lack of fiduciary landmarks (3 cases), out-of-image artifact (3 cases), or to incomplete follow-up pullbacks not-including the ISA segment (2 cases). The following results correspond to the 70 matched segments (32 patients).

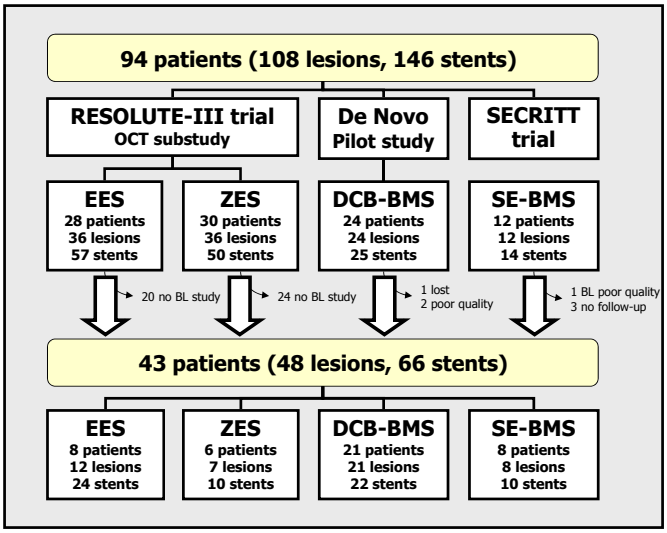

Figure 2: Flow chart summarizing the patients and stents included in this study, pooled from three different OCT randomized trials.
BL: Baseline study post-stent implantation; DCB-BMS: Drug-coated balloon in combination with BMS; EES: Everolimus-eluting stent; SE-BMS: Self-expandable bare-metal stent; ZES: Zotarolimus-eluting stent.

Analysis of the morphologic patterns at follow-up

The distribution of the morphologic patterns at follow-up in the ISA segments is provided in supplementary table 2. The agreement between the initial classifications of the two observers was very high (weighted kappa 0.96, 95% CI 0.94 – 0.98). The most frequent pattern was the homogeneous (32.9%), with decreasing proportions in the subsequent ordered patterns, up to the bare pattern (2.9%). 71.5% of the analysed segments had a pattern of spontaneous re-apposition onto the vessel wall. The proportion of uncovered, ISA and ISA-uncovered struts in the quantitative analysis varied significantly between the patterns ($p<0.0001$), following a significant lineal trend in the ranked categories ($p<0.0001$), (table 3 and figure 3).

Table 1: Patients' and procedural baseline characteristics.

	Patients (n=43)
Age (years)	60.4 (10.8)
Males	35 (81.4%)
Cardiovascular risk factors	
Hypertension	23 (53.5%)
DM	8 (18.6%)
Insulin-requiring	1 (2.3%)
Hypercholesterolemia	33 (76.7%)
Smoking	20 (46.5%)
Current smoker (<30d)	10 (23.3%)
Family history of CHD	17 (39.5%)
Antecedents	
Previous MI	15 (34.9%)
Previous PCI	9 (20.9%)
Previous CABG	2 (4.7%)
Clinical presentation	
TCFA	8 (18.6%)
Silent ischemia	1 (2.3%)
Stable angina	19 (44.2%)
Unstable angina	12 (27.9%)
Myocardial infarction	3 (7.0%)
STEMI	2 (4.7%)
Procedural characteristics	
Nr vessels treated	1.43 (0.63)
Nr of lesions treated	1.62 (0.79)
Nr of stents implanted	1.67 (1.27)
Total stented length (mm)	30.4 (29.9)
Small vessel (<2.5mm diam)	20 (46.5%)
Overlap	7 (16.3%)
Type of stent	
EES	8 (18.6%)
ZES	6 (14.0%)
DCB-BMS	21 (48.8%)
SE-BMS	8 (18.6%)

CABG: Coronary Artery By-pass Graft; CHD: Coronary Heart Disease; DCB-BMS: Combination of drug-coated balloon with bare metal stent; DM: Diabetes Mellitus; EES: Everolimus-eluting stent; MI: Myocardial Infarction; PCI: Percutaneous Coronary Intervention; SE-BMS: Self-expandable bare metal stent; STEMI: ST elevation myocardial infarction; ZES: Zotarolimus-eluting stent.

Table 2: Angiographic characteristics of the lesions.

	Lesions (n=48)
Target vessel	
LAD	19 (39.6%)
LCX	5 (10.4%)
RCA	23 (47.9%)
TO	3 (6.3%)
Ostial lesion	1 (2.1%)
Bifurcation	12 (25.0%)
Mod or severe calcific	9 (18.8%)
QCA characteristics	
Lesion length (mm)	12.7 (7.7)
Pre-stenting	
RVD (mm)	2.62 (0.46)
MLD (mm)	1.04 (0.60)
% diam stenosis	61.03 (20.35)
Post-stenting in-stent	
RVD (mm)	2.74 (0.39)
MLD (mm)	2.29 (0.42)
% diam stenosis	13.97 (8.11)

DCB-BMS: Combination of drug-coated balloon with bare metal stent; EES: Everolimus-eluting stent; LAD: Left anterior descending; LCX: Left Circumflex; LM: Left Main Stem; MLD: Minimal Lumen Diameter; QCA: Quantitative Coronary Angiography; RCA: Right coronary artery; RVD: Reference vessel diameter; SE-BMS: Self-expandable bare metal stent; TO: Total occlusion; ZES: Zotarolimus-eluting stent.

Table 3: Percentage of uncovered, ISA and ISA-uncovered struts in the segments with acute malapposition, according to the morphologic pattern at follow-up.

n=70 segments 32 patients		% of struts		
		Uncovered	ISA	ISA-uncovered
Pattern	**Homogeneous**	0.0 (0.0 -0.0)	0.0 (0.0 -0.0)	0.0 (0.0 -0.0)
	Layered	0.0 (0.0 -0.0)	0.0 (0.0 -0.0)	0.0 (0.0 -0.0)
	Crenellated	10.0 (0.0 – 24.0)	0.0 (0.0 – 7.8)	0.0 (0.0 – 4.2)
	Bridged	8.2 (6.0 – 23.5)	13.7 (0.0 – 18.8)	1.3 (0.0 – 8.3)
	Partially bridged	21.0 (9.8 – 32.0)	17.4 (13.5 – 24.1)	10.3 (5.5 – 15.9)
	Bare	17.1 (12.5 – 21.7)	10.7 (8.3 – 13.0)	7.5 (6.3 – 8.7)

Values are median (percentile 25 – percentile 75)

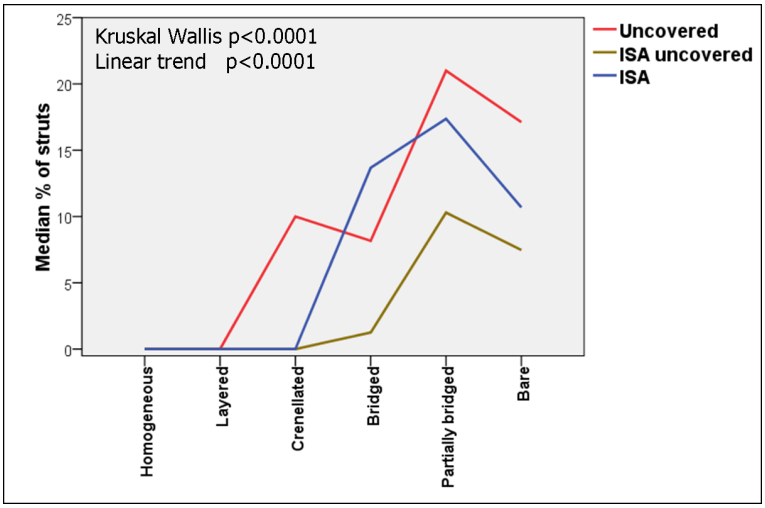

Figure 3: Graphic showing the median percentage of uncovered, ISA and ISA uncovered struts in the segments with acute malapposition according to the morphologic pattern at follow-up.
ISA: Incomplete stent apposition.

The most significant step-up for delayed coverage was observed between the layered and crenellated categories (median percentage of uncovered struts 0.0 and 10.0, respectively), whilst the most significant step-up for ISA was observed between crenellated and bridged (median percentage of ISA struts 0.0 and 13.7, respectively).

Quantitative analysis of the ISA segments

Three segments were excluded from the quantitative analysis because ISA was located at one of the stent edges, with very different vessel-catheter coaxiality between baseline and follow-up studies, thus making the sequential volumetric calculations unreliable. Table 4 shows the volumetric analysis of the ISA segments. A significant reduction in lumen and ISA areas was observed (Supplement Figure 1).

Raw per strut analysis of apposition and coverage is provided in supplementary table 3. The raw proportion of ISA struts in ISA segments was reduced from 37.7% at baseline to 11.8% at follow-up. The incidence of delayed coverage in the ISA segments was 15.4%, vs. 5.9% in the corresponding well-apposed segments of the same stents (pooled relative risk 2.37; 95% CI 2.01 – 2.78) (supplementary table 4, figure 4).

Predictors of persistence of ISA and of delayed coverage

Type of stent and one estimator of the ISA size at baseline (either ISA volume, or maximal distance to the vessel wall per strut) were tested as predictors of the vascular healing reac-

Table 4: Areas and volumetric analysis of the ISA segments, comparing the baseline vs. follow-up results.

n=67 segments 30 patients	Baseline	Follow-up	Mean diff	95% CI		p-val
				Lower	Upper	
Length (mm)	2.0 (0.3)	1.9 (0.3)	-0.1 (0.5)	-1.1	0.8	0.780
MLA (mm^2)	8.05 (0.32)	6.71 (0.32)	-1.34 (0.45)	-2.23	-0.45	**0.003**
Mean lumen Area (mm^2)	8.47 (0.33)	7.14 (0.33)	-1.33 (0.47)	-2.25	-0.42	**0.005**
Mean stent area (mm^2)	8.09 (0.31)	7.99 (0.31)	-0.10 (0.44)	-0.97	0.77	0.819
Max ISA area (mm^2)	0.79 (0.11)	0.29 (0.11)	-0.50 (0.16)	-0.82	-0.19	**0.002**
Mean ISA area (mm^2)	0.60 (0.08)	0.19 (0.08)	-0.41 (0.11)	-0.62	-0.20	**<0.0001**
ISA volume (mm^3)	1.44 (0.40)	0.68 (0.40)	-0.76 (0.57)	-1.89	0.37	**0.184**

Values are mean (SE).

CI: Confidence interval; ISA: Incomplete stent apposition; MLA: Minimal lumen area.

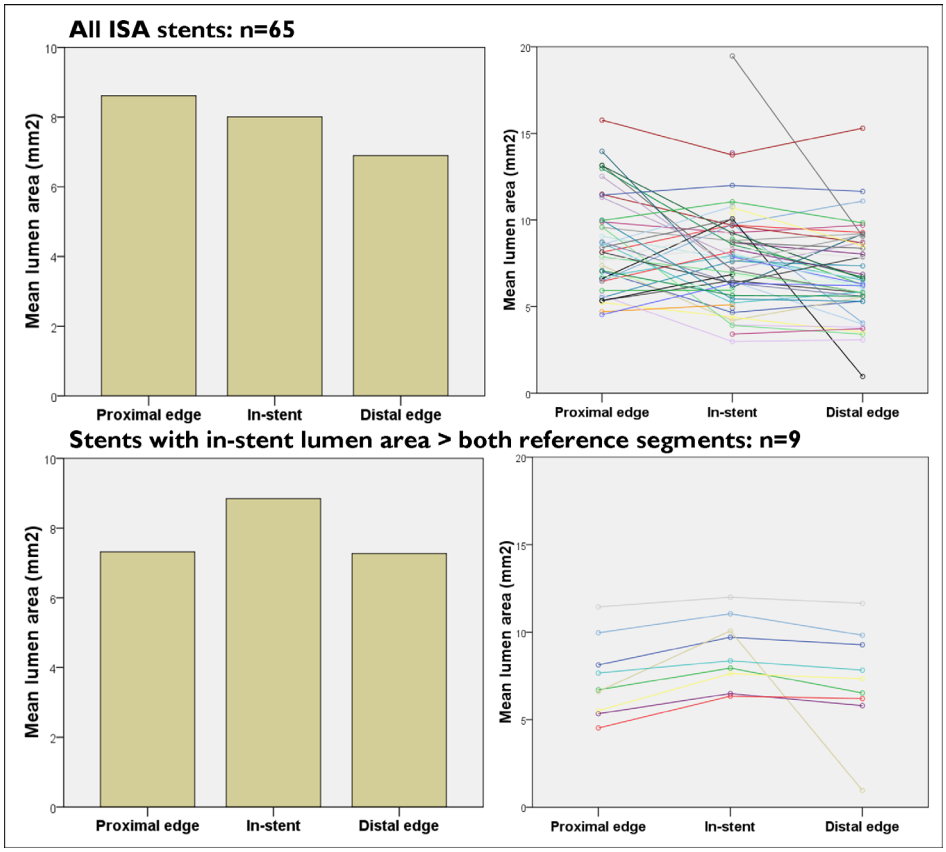

Figure 4: Forest plot showing the pooled relative risk of delayed coverage at 6-13 months in malapposed vs. well-apposed segments, stratified by type of stent.

Lines represent the 95% confidence interval for the relative risk in each stent, with the pooled relative risk at the bottom.

DCB-BMS: Drug-coated balloon in combination with bare metal stent; EES: Everolimus-eluting stent; ISA: Incomplete stent apposition struts; SE-BMS: Self-expandable bare metal stent; ZES: Zotarolimus-eluting stent.

tion at follow-up. ISA size was the only independent predictor of a pattern of persistent ISA or grossly delayed coverage at follow-up, with similar predictive value when ISA size was estimated by ISA volume, as when it was estimated by the maximal ISA distance per strut (supplementary figure 2). ISA size and the type of stent were both independent predictors of a pattern of delayed coverage, with similar predictive values for the models with ISA volume or with maximal ISA distance per strut as estimators of ISA size. The percentage of ISA struts in the segment at follow-up could be predicted by the ISA volume after implant ($p \leq 0.0001$, QICC 336.87) or by the maximal ISA distance per strut ($p \leq 0.0001$, QICC 342.64) alone, whereas the percentage of uncovered struts at follow-up was predicted by the ISA size after implant ($p=0.02$ for ISA volume, $p=0.04$ for maximal ISA distance per strut) and by the type of stent ($p=0.045$; QICC 5056.30 for the model with ISA volume, QICC 5389.10 for the model with maximal ISA distance per strut).

Table 5 shows an estimation of the likelihood at follow-up of resolved vs. persistent ISA and of grossly covered vs. grossly delayed pattern of healing, based on the analysis of this sample. Maximal ISA distances <270 μm post stent implantation appear grossly covered and spontaneously re-apposed in 100% of cases at follow-up; whilst maximal ISA distances ≥850 μm) result in persisting ISA and grossly delayed coverage in 100% of cases.

Table 5: Predictive values for resolved vs. persistent ISA and for grossly covered vs. grossly delayed healing patterns at follow-up of different thresholds of ISA size at baseline.

n=67 segments 30 patients			Likelihood at follow-up of				
			Resolved ISA (%)	Grossly covered (%)		Persistent ISA (%)	Grossly delayed healing (%)
ISA size at baseline	ISA volume (mm^3)	**< 0.1**	100	100	**≥ 0.1**	34.6	18.6
		< 0.2	96.9	100	**≥ 0.2**	47.2	22.9
		< 2.5	84.5	93.4	**≥ 2.5**	100	44.4
		< 4.4	79.0	93.1	**≥ 4.4**	100	66.7
		< 12.5	74.2	89.4	**≥ 12.5**	100	100
	Max ISA distance (μm)	**< 270**	100	100	**≥ 270**	46.15	20.5
		< 350	94.9	100	**≥ 350**	57.1	26.9
		< 400	92.7	97.6	**≥ 400**	57.7	28.6
		< 520	83.3	92.6	**≥ 520**	69.2	30.8
		< 850	75.4	87.9	**≥ 850**	100	100

ISA: Incomplete stent apposition.

Clinical outcomes

At the moment of OCT follow-up, 6 patients had suffered major adverse cardiovascular events, all of them in the DCB-BMS group: 1 peri-procedural non-Q wave MI, 1 target-vessel

related non-Q wave MI at follow-up and 4 clinically-driven TVR due to stable angina. No case of stent thrombosis occurred in any of the subgroups.

DISCUSSION

The main findings of this study are: 1) The vascular tissue reaction to acute ISA can be described by OCT according to simple morphologic patterns, that represent different degrees of persisting malapposition and coverage; 2) The neointimal response tends to reduce ISA size, often integrating it completely into the vessel wall; 3) Within the same stent, coverage of ISA segments is delayed with respect to that of well-apposed segments; 4) The size of acute ISA is directly associated with its persistence at follow-up and with delayed coverage.

To the best of our knowledge this is the first sequential OCT study describing the healing process of acute ISA both qualitative and quantitatively, and the first to link simple morphologic qualitative patterns of healing with specific malapposition and coverage rates in the subsequent quantitative analysis. This observation might allow semi-quantitative estimations of coverage and apposition, that could be potentially useful for in situ clinical decision-making.

The vascular tissue reaction ends up with the complete integration of ISA into the vessel wall in most of cases (71.5%)., but 2 out of 3 cases of acute ISA have a morphologic healing pattern other than homogeneous. This might represent the in vivo correlate of some experimental observations: 1) Re-endothelialization ensuing a vessel injury happens by proliferation of endothelial and smooth muscle cells, starting from the non-injured margins until the endothelial continuity is restored[25-29]. At this point the confluence of endothelial cells inhibits their own proliferation and stimulates the secretion of heparin-sulfates, inhibiting in turn the proliferation of smooth muscle cells[30]. According to this confluent model, endothelial cells would spread on the malapposed struts surface, resulting in conformal coverage of the detached mesh. The bridged pattern might represent the maturation of this neointimal conformal coverage. 2) This re-endothelialization process is limited in time[26-28]: it stops after 2 weeks (in the rabbit) or after 6 weeks (in the rat), regardless the endothelial continuity has been restored or not[25,29]. The partially-bridged and bare patterns (grouped as "grossly delayed coverage") might represent the failure of neointima to cover large ISA regions before the vascular healing response ceases. This is consistent with our finding of large acute ISA volumes associated to patterns of grossly delayed coverage at follow-up. Likewise, small ISA volumes could induce a conformal bridged pattern of healing that ends up connecting the ISA struts with the vessel wall (homogeneous pattern) or that creates a false lumen undergoing subsequent low-flow and thrombosis phenomena (layered pattern). The layered pattern might be also due to cytotoxicity of specific drugs or stents[31], or to increased presence of fibrinoid or proteoglycans[32,33]. Finally, the crenellated pattern has been previously proposed

as the result of a vascular reaction to acute ISA[5]. Our findings confirm the hypothesis that the crenellated pattern appears as one of the possible vascular reactions to acute ISA and is associated to delayed coverage. The abnormally hyporeactive neointima leading to a bare pattern might reflect something else than the mere failure to restore a too large ISA region and deserves further investigation in the future.

The quantitative results constitute additional and definite evidence about the higher risk of delayed coverage associated to acute ISA, already suggested and demonstrated by previous OCT studies[1,10]. This is a truly sequential study with the finest level of matching possible (segments), thus complementing the limitations of previous analytical studies[10]. Although the level of evidence provided by this approach is only at an ecological level (i.e. the uncovered struts could theoretically be the well-apposed struts in the segment), the consistency with previous studies following different approaches[1,10] should constitute definite evidence of the association between acute ISA and delayed coverage.

The larger the ISA, the more likely to persist at follow-up and to present a pattern of grossly delayed coverage. The size of acute ISA can be estimated by different parameters. The estimation by ISA volume is very accurate but cannot be done straightforward, hence this parameter is of limited utility to take decisions in the cathlab. Conversely, maximal ISA distance per strut can be directly measured in situ and has a predictive value equivalent to that of ISA volume for the persistence of ISA and for coverage, therefore it might be preferable as objective criterion for the optimization of acute ISA in the cathlab. Although our study can provide some rationale for the optimization of apposition, the clinical benefit of such approach remains still unproven. Interestingly, the coverage rate cannot be predicted by ISA size alone, (except in cases of grossly delayed coverage), depending also on the type of stent.

Limitations

OCT coverage correlates with histological neointimal healing and endothelialization after stenting in animal models[21,34], but its sensitivity and specificity in human atherosclerotic vessels are unknown.

For the 14 patients in the RESOLUTE-all comers trial the follow-up period was 13 instead of 6 months, due to the sustained kinetics of release of the device and in order to warrant that OCT were performed after the neointimal healing process had achieved its maximum. The heterogeneity of devices and follow-up periods compels to take our results as preliminary and to replicate this analysis in more specific scenarios and larger samples.

Primary stenting in STEMI predisposes to acute ISA[35]. Our sample included only 2 cases with STEMI. Thus, the role of the clinical indication on the healing of ISA would deserve clarification in larger samples including more STEMI patients[23,24,35].

CONCLUSION

The neointimal healing process tends to reduce ISA size, often integrating it completely into the vessel wall, and resulting in characteristic morphologic patterns. The coverage of ISA segments is delayed with respect to well-apposed segments. The larger the size of acute ISA, the larger the likelihood of persisting malapposed at follow-up and of delayed healing.

FUNDING SOURCES / DISCLOSURES

This study pools data from three different randomized trials, sponsored by Medtronic Cardio Vascular (Santa Rosa, CA, USA), Lutonix Inc (Maple Grove, MA, USA) and Prescient Medical Inc (Doylestown, PA, USA). The core-lab and CRO responsible for the analysis (Cardialysis BV, Rotterdam) have received grants from the corresponding sponsors to run the trials. The Research extraclinical activities pertaining to the study protocols have been reimbursed to the participating sites by the sponsors, according to the corresponding Health Service reimbursement. Windecker S and Di Mario C have received speakers' fees from the corresponding sponsors.

REFERENCES

1. Ozaki Y, Okumura M, Ismail TF, Naruse H, Hattori K, Kan S, Ishikawa M, Kawai T, Takagi Y, Ishii J, Prati F, Serruys PW. The fate of incomplete stent apposition with drug-eluting stents: an optical coherence tomography-based natural history study. *Eur Heart J* 2010;31:1470-1476.
2. Kim WH, Lee BK, Lee S, Shim JM, Kim JS, Kim BK, Ko YG, Choi D, Jang Y, Hong MK. Serial changes of minimal stent malapposition not detected by intravascular ultrasound: follow-up optical coherence tomography study. *Clin Res Cardiol* 2010;99:639-644.
3. Gutiérrez-Chico J, van Geuns RJ, Koch K, Koolen J, Duckers HJ, Regar E, Serruys PW. Paclitaxel-coated balloon in combination with bare metal stent for treatment of de novo coronary lesions: an optical coherence tomography first-in-human randomized trial balloon-first vs. stent first. *EuroIntervention* 2011;7:711-722.
4. Gutiérrez-Chico J, Jüni P, García-García HM, Regar E, Nüesch E, Borgia F, van der Giessen WJ, Davies S, van Geuns RJ, Secco GG, Meis S, Windecker S, Serruys PW, di Mario C. Long term tissue coverage of a biodegradable polylactide polymer-coated biolimus-eluting stent: comparative sequential assessment with optical coherence tomography until complete resorption of the polymer. *Am Heart J* 2011;162:922-931.
5. Radu M, Jørgensen E, Kelbæk H, Helqvist S, Skovgaard L, Saunamäki K. Strut apposition after coronary stent implantation visualised with optical coherence tomography. *EuroIntervention* 2010;6:86-93.
6. Cook S, Wenaweser P, Togni M, Billinger M, Morger C, Seiler C, Vogel R, Hess O, Meier B, Windecker S. Incomplete Stent Apposition and Very Late Stent Thrombosis After Drug-Eluting Stent Implantation. *Circulation* 2007;115:2426-2434.
7. Hassan AKM, Bergheanu SC, Stijnen T, van der Hoeven BL, Snoep JD, Plevier JWM, Schalij MJ, Wouter Jukema J. Late stent malapposition risk is higher after drug-eluting stent compared with bare-metal stent implantation and associates with late stent thrombosis. *Eur Heart J* 2010;31:1172-1180.
8. Cook S, Ladich E, Nakazawa G, Eshtehardi P, Neidhart M, Vogel R, Togni M, Wenaweser P, Billinger M, Seiler C, Gay S, Meier B, Pichler WJ, Juni P, Virmani R, Windecker S. Correlation of Intravascular Ultrasound Findings With Histopathological Analysis of Thrombus Aspirates in Patients With Very Late Drug-Eluting Stent Thrombosis. *Circulation* 2009;120:391-399.
9. Virmani R, Guagliumi G, Farb A, Musumeci G, Grieco N, Motta T, Mihalcsik L, Tespili M, Valsecchi O, Kolodgie FD. Localized Hypersensitivity and Late Coronary Thrombosis Secondary to a Sirolimus-Eluting Stent: Should We Be Cautious? *Circulation* 2004;109:701-705.
10. Gutiérrez-Chico JL, Regar E, Nüesch E, Okamura T, Wykrzykowska J, di Mario C, Windecker S, van Es GA, Gobbens P, Jüni P, Serruys PW. Delayed Coverage in Malapposed and Side-Branch Struts With Respect to Well-Apposed Struts in Drug-Eluting Stents. *Circulation* 2011;124:612-623.
11. Serruys PW, Silber S, Garg S, van Geuns RJ, Richardt G, Buszman PE, Kelbaek H, van Boven AJ, Hofma SH, Linke A, Klauss V, Wijns W, Macaya C, Garot P, DiMario C, Manoharan G, Kornowski R, Ischinger T, Bartorelli A, Ronden J, Bressers M, Gobbens P, Negoita M, van Leeuwen F, Windecker S. Comparison of Zotarolimus-Eluting and Everolimus-Eluting Coronary Stents. *New Engl J Med* 2010;363:136-146.
12. Gutierrez-Chico JL, van Geuns RJ, Regar E, van der Giessen WJ, Kelbaek H, Saunamaki K, Escaned J, Gonzalo N, Di MC, Borgia F, Nuesch E, Garcia-Garcia HM, Silber S, Windecker S, Serruys PW. Tissue coverage of a hydrophilic polymer-coated zotarolimus-eluting stent vs. a fluoropolymer-coated

everolimus-eluting stent at 13-month follow-up: an optical coherence tomography substudy from the RESOLUTE All Comers trial. *Eur Heart J* 2011;32:2454-2463.

13. Shin ES, Garcia-Garcia HM, Okamura T, Wykrzykowska JJ, Gonzalo N, Shen ZJ, van Geuns RJ, Regar E, Serruys PW. Comparison of acute vessel wall injury after self-expanding stent and conventional balloon-expandable stent implantation: a study with optical coherence tomography. *J Invasive Cardiol* 2010;22:435-439.
14. Sawada T, Shite J, Garcia-Garcia HM, Shinke T, Watanabe S, Otake H, Matsumoto D, Tanino Y, Ogasawara D, Kawamori H, Kato H, Miyoshi N, Yokoyama M, Serruys PW, Hirata K. Feasibility of combined use of intravascular ultrasound radiofrequency data analysis and optical coherence tomography for detecting thin-cap fibroatheroma. *Eur Heart J* 2008;29:1136-1146.
15. Gonzalo N, Garcia-Garcia HM, Regar E, Barlis P, Wentzel J, Onuma Y, Ligthart J, Serruys PW. In vivo assessment of high-risk coronary plaques at bifurcations with combined intravascular ultrasound and optical coherence tomography. *JACC Cardiovasc Imaging* 2009;2:473-482.
16. Gonzalo N, Tearney GJ, Serruys PW, van Soest G, Okamura T, Garcia-Garcia HM, van Geuns RJ, van der Ent M, Ligthart JM, Bouma BE, Regar E. Second-generation optical coherence tomography in clinical practice. High-speed data acquisition is highly reproducible in patients undergoing percutaneous coronary intervention. *Rev Esp Cardiol* 2010;63:893-903.
17. Gonzalo N, Garcia-Garcia HM, Serruys PW, Commissaris KH, Bezerra H, Gobbens P, Costa M, Regar E. Reproducibility of quantitative optical coherence tomography for stent analysis. *EuroIntervention* 2009;5:224-232.
18. Tanigawa J, Barlis P, di Mario C. Intravascular optical coherence tomography: optimisation of image acquisition and quantitative assessment of stent strut apposition. *EuroIntervention* 2007;3:128-136.
19. Barlis P, Regar E, Serruys PW, Dimopoulos K, van der Giessen WJ, van Geuns RJ, Ferrante G, Wandel S, Windecker S, Van Es GA, Eerdmans P, Juni P, di Mario C. An optical coherence tomography study of a biodegradable vs. durable polymer-coated limus-eluting stent: a LEADERS trial sub-study. *Eur Heart J* 2010;31:165-176.
20. Guagliumi G, Musumeci G, Sirbu V, Bezerra HG, Suzuki N, Fiocca L, Matiashvili A, Lortkipanidze N, Trivisonno A, Valsecchi O, Biondi-Zoccai G, Costa MA. Optical coherence tomography assessment of in vivo vascular response after implantation of overlapping bare-metal and drug-eluting stents. *JACC Cardiovasc Interv* 2010;3:531-539.
21. Templin C, Meyer M, Muller MF, Djonov V, Hlushchuk R, Dimova I, Flueckiger S, Kronen P, Sidler M, Klein K, Nicholls F, Ghadri JR, Weber K, Paunovic D, Corti R, Hoerstrup SP, Luscher TF, Landmesser U. Coronary optical frequency domain imaging (OFDI) for in vivo evaluation of stent healing: comparison with light and electron microscopy. *Eur Heart J* 2010;31:1792-1801.
22. Guagliumi G, Sirbu V, Musumeci G, Bezerra HG, Aprile A, Kyono H, Fiocca L, Matiashvili A, Lortkipanidze N, Vassileva A, Popma JJ, Allocco DJ, Dawkins KD, Valsecchi O, Costa MA. Strut coverage and vessel wall response to a new-generation paclitaxel-eluting stent with an ultrathin biodegradable abluminal polymer: Optical Coherence Tomography Drug-Eluting Stent Investigation (OCTDESI). *Circ Cardiovasc Interv* 2010;3:367-375.
23. Guagliumi G, Sirbu V, Bezerra H, Biondi-Zoccai G, Fiocca L, Musumeci G, Matiashvili A, Lortkipanidze N, Tahara S, Valsecchi O, Costa M. Strut coverage and vessel wall response to zotarolimus-eluting and bare-metal stents implanted in patients with ST-segment elevation myocardial infarction: the OCTAMI (Optical Coherence Tomography in Acute Myocardial Infarction) Study. *JACC Cardiovasc Interv* 2010;3:680-687.

24. Guagliumi G, Costa MA, Sirbu V, Musumeci G, Bezerra HG, Suzuki N, Matiashvili A, Lortkipanidze N, Mihalcsik L, Trivisonno A, Valsecchi O, Mintz GS, Dressler O, Parise H, Maehara A, Cristea E, Lansky AJ, Mehran R, Stone GW. Strut Coverage and Late Malapposition With Paclitaxel-Eluting Stents Compared With Bare Metal Stents in Acute Myocardial Infarction: Optical Coherence Tomography Substudy of the Harmonizing Outcomes With Revascularization and Stents in Acute Myocardial Infarction (HORIZONS-AMI) Trial. *Circulation* 2011;123:274-281.
25. Reidy MA, Standaert D, Schwartz SM. Inhibition of endothelial cell regrowth. Cessation of aortic endothelial cell replication after balloon catheter denudation. *Arteriosclerosis* 1982;2:216-220.
26. Haudenschild CC, Schwartz SM. Endothelial regeneration. II. Restitution of endothelial continuity. *Lab Invest* 1979;41:407-418.
27. Reidy MA, Schwartz SM. Endothelial regeneration. III. Time course of intimal changes after small defined injury to rat aortic endothelium. *Lab Invest* 1981;44:301-308.
28. Bjorkerud S, Bondjers G. Arterial repair and atherosclerosis after mechanical injury. 5. Tissue response after induction of a large superficial transverse injury. *Atherosclerosis* 1973;18:235-255.
29. Reidy MA, Clowes AW, Schwartz SM. Endothelial regeneration. V. Inhibition of endothelial regrowth in arteries of rat and rabbit. *Lab Invest* 1983;49:569-575.
30. Clowes AW, Karnowsky MJ. Suppression by heparin of smooth muscle cell proliferation in injured arteries. *Nature* 1977;265:625-626.
31. Tanimoto S, Aoki J, Serruys PW, Regar E. Paclitaxel-eluting stent restenosis shows three-layer appearance by optical coherence tomography. *EuroIntervention* 2006;1:484.
32. Teramoto T, Ikeno F, Otake H, Lyons JK, van Beusekom HM, Fearon WF, Yeung AC. Intriguing peri-strut low-intensity area detected by optical coherence tomography after coronary stent deployment. *Circ J* 2010;74:1257-1259.
33. van Beusekom HM, Saia F, Zindler JD, Lemos PA, Swager-Ten Hoor SL, van Leeuwen MA, de Feijter PJ, Serruys PW, van der Giessen WJ. Drug-eluting stents show delayed healing: paclitaxel more pronounced than sirolimus. *Eur Heart J* 2007;28:974-979.
34. Murata A, Wallace-Bradley D, Tellez A, Alviar C, Aboodi M, Sheehy A, Coleman L, Perkins L, Nakazawa G, Mintz G, Kaluza GL, Virmani R, Granada JF. Accuracy of optical coherence tomography in the evaluation of neointimal coverage after stent implantation. *JACC Cardiovasc Imaging* 2010;3:76-84.
35. Gonzalo N, Barlis P, Serruys PW, Garcia-Garcia HM, Onuma Y, Ligthart J, Regar E. Incomplete stent apposition and delayed tissue coverage are more frequent in drug-eluting stents implanted during primary percutaneous coronary intervention for ST-segment elevation myocardial infarction than in drug-eluting stents implanted for stable/unstable angina: insights from optical coherence tomography. *JACC Cardiovasc Interv* 2009;2:445-452.

Suppl table 1: Technical specifications of the different OCT systems and number of patients studied with each model at baseline and follow-up.

		M2	M3	C7
Technique		Occlusive	Non-occlusive	Non-occlusive
Domain		Time	Time	Fourier
Catheter		ImageWire	ImageWire	Dragonfly
Rotation speed (frames/s)		15.6	20	100
Pullback speed (mm/s)		2	3	10-20
Post-stent implantation	**EES**	1	7	0
	ZES	0	6	0
	DCB-BMS	0	0	21
	SE-BMS	0	6	2
Total nr of patients		**1**	**19**	**22**
Follow-up	**EES**	0	7	1
	ZES	0	6	0
	DCB-BMS	0	0	21
	SE-BMS	0	3	5
Total nr of patients		**0**	**16**	**27**

All systems and catheters from Lightlab Imaging, Westford, Massachusetts, USA.

Suppl. table 2: Morphologic patterns at follow-up in the regions with acute malapposition at baseline, stratified by type of stent.

	Homogeneous	**Layered**	**Crenellated**	**Bridged**	**Partially bridged**	**Bare**
EES (n=14)	9 (64.3%)	0 (0.0%)	0 (0.0%)	4 (28.6%)	0 (0.0%)	1 (7.1%)
ZES (n=13)	5 (38.5%)	0 (0.0%)	4 (30.8%)	2 (15.4%)	2 (15.4%)	0 (0.0%)
DCB-BMS (n=31)	9 (29.0%)	11(35.5%)	5 (16.1%)	4 (12.9%)	1 (3.2%)	1 (3.2%)
SE-BMS (n=12)	0 (0.0%)	3 (25.0%)	4 (33.3%)	1 (8.3%)	4 (33.3%)	0 (0.0%)
Total (n=70)	23 (32.9%)	14 (20.0%)	13 (18.6%)	11 (15.7%)	7 (10.0%)	2 (2.9%)

DCB-BMS: Combination of drug-coated balloon with bare metal stent; EES: Everolimus-eluting stent; SE-BMS: Self-expandable bare metal stent; ZES: Zotarolimus-eluting stent.

Suppl. table 3: Analysis per strut of apposition and coverage in the matched stents.

n=66 stents 43 patients		Malapposed stents				Well-apposed stents	
		ISA segments		Well-apposed segments			
		BL	FU	BL	FU	BL	FU
Apposition	Well-apposed	1345 (62.2%)	2164 (87.9%)	5002 (94.4%)	4870 (98.8%)	5347 (99.3%)	5563 (99.7%)
	ISA	815 (37.7%)	290 (11.8%)	237 (4.5%)	19 (0.4%)	6 (0.1%)	3 (0.1%)
	NASB	3 (0.1%)	7 (0.3%)	55 (1.0%)	39 (0.8%)	30 (0.6%)	11 (0.2%)
Uncovered		2163 (100%)	379 (15.4%)	5924 (100%)	289 (5.9%)	5383 (100%)	251 (5.3%)
	ISA-uncovered	815 (37.7 %)	146 (5.9%)	237 (4.5%)	16 (0.3%)	6 (0.1%)	3 (0.1%)
TOTAL		2163	2461	5294	4928	5383	5577

Values are count (%) of struts.

BL: Baseline; DCB-BMS: Drug-coated balloon in combination with bare metal stent; EES: Everolimus-eluting stent; FU: Follow-up; ISA: Incomplete stent apposition; NASB: Non-apposed side-branch strut; SE-BMS: Self-expandable bare metal stent; ZES: Zotarolimus-eluting stent.

Suppl. table 4: Relative risk for delayed coverage in ISA vs. non-ISA segments pooled by stent, and stratified by the type of stent.

	n	Magnitude of effect			Heterogeneity of the effect		
		RR	95% CI		p val	I^2	τ^2
			Lower	Upper			
All	52	2.34	2.01	2.78	<0.0001	50.20	0.38
EES	9	4.10	2.52	6.65	0.005	63.92	1.21
ZES	11	2.57	1.98	3.34	0.110	36.15	0.12
DCB+BMS	26	2.01	1.56	2.60	0.010	43.62	0.44
SE-BMS	6	1.68	0.96	2.95	0.036	58.06	0.86

DCB-BMS: Drug-coated balloon in combination with bare metal stent; EES: Everolimus-eluting stent; RR: Relative risk; SE-BMS: Self-expandable bare metal stent; ZES: Zotarolimus-eluting stent.

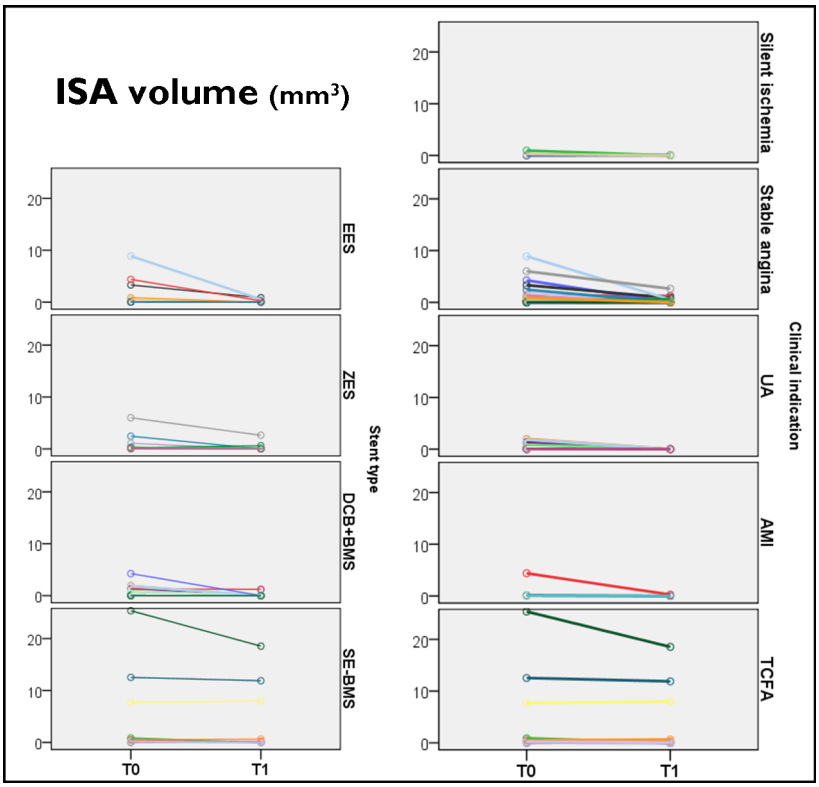

Suppl figure 1:

ISA volume immediately after stent implantation (T0) and at follow-up (T1), stratified by type of stent (left panel) and by clinical indication (right panel).

AMI: Acute myocardial infarction; DCB-BMS: Drug-coated balloon in combination with BMS; EES: Everolimus-eluting stent; ISA: Incomplete stent apposition struts; SE-BMS: Self-expandable bare-metal stent; TCFA: Thin cap fibroatheroma; UA: Unstable angina; ZES: Zotarolimus-eluting stent.

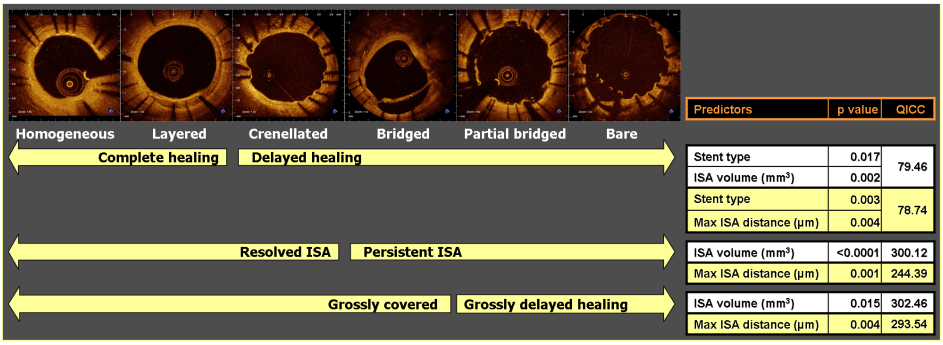

Suppl figure 2:

Predictors of complete vs. delayed healing, resolved vs. persistent ISA and grossly covered vs. grossly delayed healing patterns. Stent type and ISA size at baseline were both predictors of delayed healing, with similar predictive value of the model using either ISA volume (white cells) or maximal ISA distance per strut (yellow cells). ISA size at baseline was the only independent predictor of persistent ISA or grossly delayed coverage.


2
1
0
1
2
mm
08/14/2009 10:00:07
0118 (24 mm)
Zoom: 1.1x

12.3

Differences in neointimal thickness between the adluminal and the abluminal sides of malapposed and side-branch struts: evidence in vivo about the abluminal healing process.

Gutiérrez-Chico JL, Gijsen FJH, Regar E, Wentzel JJ, De Bruyne B, Thuesen L, Ormiston JA, McClean D, Windecker S, Chévalier B, Dudek D, Whitbourn R, Brugaletta S, Serruys PW.

JACC Cardiovasc Interv 2012; 5: 428-435.

STRUCTURED ABSTRACT

Objectives: Describing the neointimal healing on the abluminal side (ABL) of the struts in terms of coverage by optical coherence tomography (OCT) and compared with the adluminal side (ADL).

Background: The neointimal healing on the ABL of malapposed (ISA) and non-apposed side-branch (NASB) struts has been never explored in vivo and could be involved in the correction of acute malapposition. The bioresorbable vascular scaffold (BVS) is made of a translucent polymer that enables imaging of the ABL with OCT.

Methods: Patients enrolled in the ABSORB cohort B study (NCT00856856) were treated with implantation of a BVS and imaged with OCT at 6 months. Thickness of coverage on the ADL and ABL of ISA and NASB struts was measured by OCT.

Results: 28 patients were analyzed. 114 (2.4%) struts were malapposed or at side-branches. In 76 ISA struts (89.4%) and 29 NASB struts (100%) the thickness of ABL coverage was >30 μm. Coverage was thicker on the ABL than on the ADL side (101 μm vs. 71 μm; 95% CI of the difference 20-40 μm). In 70 struts (60.7%, 95% CI 50.6-70.0%) the neointimal coverage was thicker on the ABL, vs. only 20 struts (18.5%, 95% CI 11.6-28.1%) with thicker neointimal coverage on the ADL (OR=3.35, 95% CI 2.22 – 5.07).

Conclusion: Most of malapposed and side-branch struts are covered on the abluminal side 6 months after BVS implantation, with thicker neointimal coverage than on the adluminal side. The physiologic correction of acute malapposition involves neointimal growth from the strut to the vessel wall or bidirectional.

Clinical trial registration: NCT00856856; URL: http://clinicaltrials.gov

Keywords: Tomography, Optical Coherence; poly(lactide); neointima; drug-eluting stents.

CONDENSED ABSTRACT

Neointimal healing on the abluminal side (ABL) of malapposed (ISA) and non-apposed side-branch (NASB) struts has been never explored in vivo. The bioresorbable vascular scaffold (BVS) is translucent and enables OCT imaging of the ABL. In 28 patients with BVS, 114 (2.4%) struts were ISA or NASB at 6 months. In 76 ISA (89.4%) and 29 NASB struts (100%) ABL coverage was >30 μm. Thickness was higher in the ABL than in the ADL (92 vs. 62μm; $p<0.0001$). Most of ISA and NASB struts are covered on the ABL at 6 months, with thicker neointimal coverage than on the ADL.

ABBREVIATIONS

ABL: Abluminal side
ADL: Adluminal side
BMS: Bare metal stent
BVS: Bioresorbable Vascular scaffold
DES: Drug-eluting stent
ISA: Incomplete stent apposition
IVUS: Intravascular ultrasound
NASB: Non-apposed side-branch struts
OCT: Optical Coherence Tomography
QCA: Quantitative coronary angiography

INTRODUCTION

The neointimal healing process after stenting has been extensively studied in the bare-metal stent (BMS) era, in order to understand the mechanisms of restenosis. Experimental studies have described proliferation of endothelial and smooth muscle cells after endothelial denudation,(1-4) starting from the non-injured segments, until the endothelial continuity is restored.(5-9) At this point the confluence of endothelial cells inhibits their own proliferation and stimulates the secretion of heparin-sulfates, inhibiting in turn the proliferation of smooth muscle cells.(10) According to this confluent model, in case of detachment of struts from the vessel wall, the endothelial cells can spread on the surface of the stent until the contact with other endothelial cells stops the process, thus resulting in conformal coverage of the whole detached mesh. As an additional mechanism, circulating endothelial progenitor cells enhance reendothelialization.(11;12)

The interest to study the neointimal healing has grown exponentially in the drug-eluting stent (DES) era. Pathology studies described the association between delayed neointimal healing and very late stent thrombosis in DES.(13-16) As a consequence, imaging techniques like angioscopy(17-19) or optical coherence tomography (OCT)(20-24) have tried to estimate the degree of neointimal coverage in clinical series, exploring its value as potential surrogate for thrombotic events. However our knowledge about the healing process is limited to the adluminal (ADL) side of the struts. Pathology studies have paid little attention to the abluminal (ABL) side of malapposed or side-branch struts, probably due to the scarce information available about these specific categories and to methodological challenges for an accurate assessment. The ABL side has remained inaccessible in vivo also for angioscopy and OCT. OCT has become an experimental tool for the assessment of coverage due to 10-fold higher axial resolution (14μm) than IVUS, but the intense optical backscattering at the surface of metallic struts casts a dorsal shadow that prevents ABL visualization. The healing process on the ABL side might play a relevant role in the spontaneous resolution of acute incomplete stent apposition (ISA), as described in recent sequential OCT studies.(24-26)

Conversely to DES, the Bioresorbable Vascular Scaffold (BVS) (Abbott Vascular, Santa Clara, CA, USA) is made of a translucent polymer, resulting in significant backscattering of the optical radiation only at the strut boundaries and no dorsal shadowing, thus enabling for the first time quantification of the neointimal thickness on the ABL side of those struts detached from the vessel wall. In this study we compare the neointimal thickness on the ABL vs. ADL sides of ISA and non-apposed side-branch (NASB) struts in the BVS.

METHODS

BVS technical specifications

BVS (Abbott Vascular, Santa Clara, CA, USA) is a fully bioresorbable scaffold, consisting of a semi-crystalline poly-L-lactide (PLLA) backbone, coated by a thin amorphous layer of poly-D,L-lactide (PDLLA) containing the antiproliferative agent everolimus. BVS struts have a total thickness of 150 μm and are fully resorbed 2 years after implantation,(27) following a process in which the long chains of PLLA and PDLLA are progressively cleaved as ester bonds between lactide repeating units are hydrolysed. Eventually small particles less than 2 μm in diameter are phagocytosed by macrophages. Ultimately, PLLA and PDLLA degrade to lactate, which is metabolised via the Krebs cycle. The whole scaffold is translucent to optical radiation, with the exception of two radiopaque platinum markers embedded into the proximal and distal edges, to ease fluoroscopic visualization. BVS has proven excellent clinical and angiographic results up to 2 years follow-up, at which time the scaffold is resorbed.(27;28)

Study sample

The ABSORB Cohort B registry (NCT00856856) enrolled patients older than 18 years, with diagnosis of stable or unstable angina pectoris or silent ischemia, and *de novo* lesions in native coronary arteries amenable for percutaneous treatment with the BVS: % diameter stenosis ≥50% by visual estimation and reference vessel diameter of 2.5-3.5mm. Major exclusion criteria were: acute myocardial infarction, unstable arrhythmias, left ventricular ejection fraction ≤ 30%, restenotic lesions, lesions located in the left main coronary artery or in bifurcations involving a side branch >2 mm, a second clinically or hemodynamically significant lesion in the target vessel, documentation of intracoronary thrombus, or initial TIMI 0 flow. For invasive follow-up purposes, the cohort was subdivided into two groups: cohort B1, undergoing multimodality invasive imaging (QCA, IVUS, virtual histology, palpography and OCT) at 6 and 24 months; and cohort B2, with identical imaging follow-up protocol scheduled at 12 and 24 months. All the study lesions were treated with the BVS device revision 1.1 (3.0 x 18 mm). The registry was approved by the ethics committee at each participating institution and each patient gave written informed consent before inclusion.

The present study analyses the OCT images obtained 6 months after implantation from cohort B1, when the structural integrity of the device is still preserved.

OCT study

OCT pullbacks were obtained with M2, M3 or C7 systems (Lightlab Imaging, Westford, Massachusetts, USA), depending on the site, using occlusive or non-occlusive technique, as appropriate (Table 1).

Table 1: Characteristics of the different OCT systems* in the study, with the corresponding number of patients imaged by each of them.

	M2	M3	C7
Technique	Occlusive	Non-occlusive	Non-occlusive
Domain	Time	Time	Fourier
Catheter*	ImageWire	ImageWire	Dragonfly
Rotation speed (frames/s)	15.6	20	100
Pullback speed (mm/s)	2	3	20
Nr of patients	5	5	18

* All systems and catheters from Lightlab Imaging, Westford, Massachusetts, USA.

OCT images were analysed offline in a core-laboratory (Cardialysis BV, Rotterdam, the Netherlands) by independent investigators, using proprietary software (Lightlab Imaging, Westford, Massachusetts, USA). Cross-sections at 1mm longitudinal intervals within the scaffolded segment and 5mm proximal and distal to the scaffold edges were analyzed. Apposition was visually assessed strut by strut. Malapposition or incomplete stent apposition (ISA) was defined as a break in continuity between the backscattering frame of the translucent strut and the vessel wall, appearing as a contrast-filled gap between these two structures (Figure 1). In the regions where ISA was found, cross sections every 0.2 mm longitudinal intervals were analyzed. Struts located at the ostium of side branches, with no vessel wall behind, were labelled as non-apposed side-branch (NASB) struts and considered an independent category of apposition (Figure 1).

Neointimal thickness was measured on both the ADL and ABL sides of each ISA or NASB strut as the distance from the black-box boundary to the neointima-lumen interface, following a straight line connecting the mid point of the longitudinal axis of the strut with the centre of gravity of the vessel (Figure 2). Well-apposed struts were disregarded for this study. Previous analysis of 400 BVS struts immediately post-implantation reported an average thickness of 30.1 ± 5.7 μm for the ADL interface of the strut frame and 30.4 ± 5.7 μm for the ABL interface (the latter only accessible in 80 ISA or NASB struts).(29) On this basis, ABL neointimal thickness >30 μm or thicker than in the ADL side were both considered as highly suggestive of neointimal coverage.

Two independent analysts (JLGC and YO) measured the thickness of coverage in the selected struts following the method described and blinded to one another's results, in order to assess interobserver reproducibility.

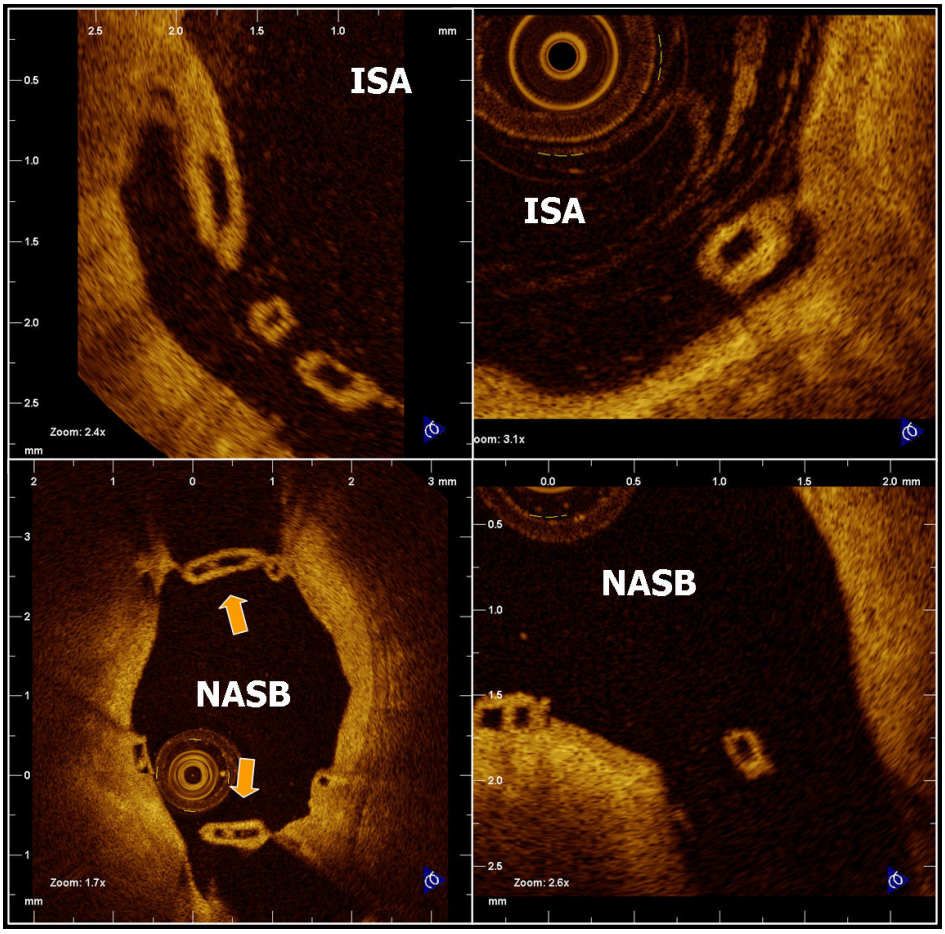

Figure 1:

ISA and NASB struts. Incomplete stent apposition (ISA) or malapposed struts are those separated from the vessel wall by a contrast-filled gap (upper part). The underlying vessel wall needs to be visible in the cross-section to properly classify a strut as ISA. Non-apposed side-branch (NASB) struts are those located at the ostium of side branches, with no vessel wall behind (lower part). In NASB struts apposition cannot be assessed by OCT.

Statistical analysis

Coverage thickness on the ADL vs. the ABL side of each strut was compared by multilevel linear regression with struts clustered at the patient level. The pooled percentages of struts with thicker ABL coverage and with thicker ADL coverage were calculated and compared by pooled analysis with the use of an inverse variance random effects model for paired measurements, taking into account the between-clusters and within-the-cluster variability, using each stent as independent unit of clustering.(30) The odds ratio at each individual stent and the pooled odds ratio of the whole sample were graphically represented by means of

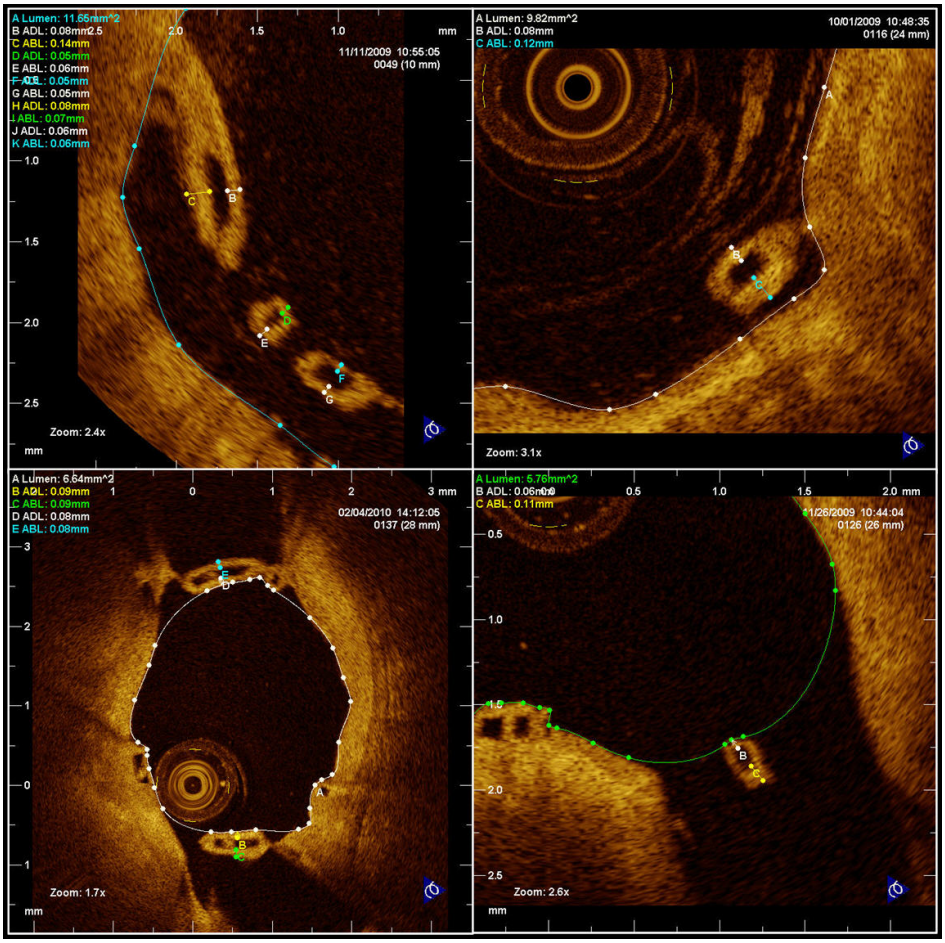

Figure 2:

Measurement of neointimal thickness at the adluminal (ADL) and abluminal (ABL) sides of ISA (upper part) and NASB (lower part) struts. Thickness was measured as the distance from the inner contour of the polymer-neointima interface to the neointima-lumen interface, following a straight line connecting the mid point of the longitudinal axis of the strut with the gravitational centre of the vessel. The correct alignment is achieved using a tool of Lightlab's (Westford, Massachusetts, USA) proprietary software named "thickness ruler". This guiding line has been however erased from the image to ease its comprehension.

forest plots. Results for the whole sample of struts and for the ISA and NASB subgroups were reported. Interobserver variability for measurements at each side of the struts was estimated by intraclass correlation coefficients for the absolute agreement (ICCa).

All the analyses and graphics were performed with the PASW 17.0.2 (SPSS Inc., Chicago, IL, USA) and CMA version 2 (Biostat Inc., Englewood, NJ, USA) software packages.

RESULTS

The average follow-up period for cohort B1 was 183 ± 9 days. A total of 28 patients (28 lesions and scaffolds, 4670 struts) were analyzed with OCT. Table 2 shows the baseline clinical characteristics of the patients. 16 out of 28 analysed scaffolds presented ISA or NASB struts suitable for the planned comparison: 114 struts (2.4%, 85 ISA and 29 NASB). The reproducibility of the measurements was excellent (ICCa=0.908, 95% CI: 0.869 – 0.935 for the ADL side; ICCa= 0.982, 95% CI: 0.975 – 0.988 for the ABL side; with no significant bias detected).

Coverage was significantly thicker on the ABL than on the ADL side in the whole sample (101 µm; 95% CI: 87-116 µm vs. 71 µm; 95% CI: 59-83 µm; mean difference 30 µm, 95% CI: 20-40 µm; p<0.0001) and in the subgroups of ISA (95 µm; 95% CI: 80-111 µm vs. 65 µm; 95% CI: 53-76 µm; mean difference 31 µm, 95% CI: 19-43 µm; p<0.0001) and NASB struts (110 µm; 95% CI: 83-139 µm vs. 83 µm; 95% CI: 58-108 µm; mean difference 30 µm, 95% CI: 20-40 µm; p=0.008). (Table 3).

In 70 struts (60.7%, 95% CI: 50.6-70.0%) the neointimal coverage was thicker on the ABL side. Conversely, only 20 of struts (17.5%) had thicker neointimal coverage on the ADL side

Table 2: Baseline clinical characteristics of the patients.

n=28	n	%
Sex (male)	23	82.1%
Age (years)	64.5 (56.0 – 70.4)*	
Hypertension	15	53.6
DM	2	7.1
Insulin-requiring	1	3.6
Hypercholesterolemia	27	96.4
Smoking	5	17.9
Family histoty of CHD	13	46.4
Prior		
MI	13	46.4
PCI	7	25.0
Of the target vessel	2	7.1
Clinical indication		
Stable angina	21	75.0
Unstable angina	4	14.3
Nr of diseased vessels		
1	22	78.6
2	3	10.7
3	3	10.7

*Median (percentile 25 - percentile 75)

CHD: Coronary heart disease; DM: Diabetes Mellitus; MI: Myocardial infarction; PCI: Percutaneous coronary intervention.

Table 3: Thickness of neointimal coverage at the adluminal and abluminal sides of the struts: weighted average values and paired comparisons (multilevel linear regression for paired measurements).

Neointimal thickness (µm)		Mean	95% CI		p-value
			Lower	Upper	
All detached struts n=114 (16 stents)	ADL	71	59	83	
	ABL	101	87	116	
	(ABL – ADL) diff	30	20	40	<0.0001
ISA struts n=85 (12 stents)	ADL	65	53	76	
	ABL	95	80	111	
	(ABL – ADL) diff	31	19	43	<0.0001
NASB struts n=29 (6 stents)	ADL	83	58	108	
	ABL	110	83	139	
	(ABL – ADL) diff	28	8	47	0.008

ABL: Abluminal side; ADL: Adluminal side; CI: Confidence Interval; ISA: Incomplete Stent Apposition; NASB: Non-apposed Side Branch (struts); SD: Standard Deviation.

(p<0.0001). Similar results were observed in the ISA and NASB subgroups, although in the latter the difference in percentages did not reach statistical significance (Table 4, figure 3). In 105 struts (92.1%) the thickness of ABL coverage was >30 µm: 76 (89.4%) ISA struts and 29 (100%) NASB struts, compared with 98 struts (86.0%) in which the ADL thickness was >30 µm: 71 (83.5%) ISA and 27 (93.1%) NASB struts.

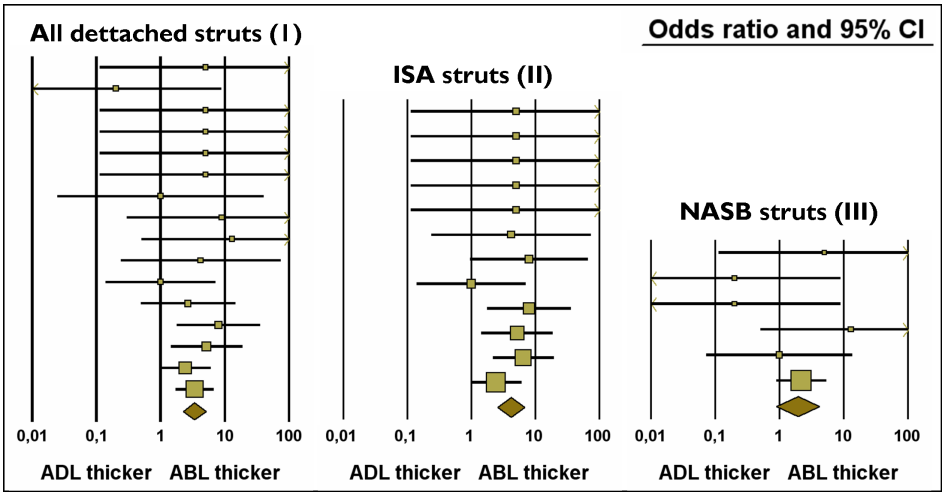

Figure 3:

Paired pooled comparison of the percentages of struts with thicker coverage on the abluminal (ABL) than on the adluminal (ADL) side vs. the opposite. Forest plot representing the odds ratio and 95% confidence interval for each stent and the pooled odds ratio at the bottom.

ABL: Abluminal side; ADL: Adluminal side; ISA: Incomplete Stent Apposition; NASB: Non-apposed Side Branch (struts).

ISA: Incomplete stent apposition; NASB: Non-apposed side-branch struts.